

UNIVERSITA' DEGLI STUDI  
DI MILANO-BICOCCA

*Facolta' di scienze Matematiche, Fisiche e Naturali  
Dipartimento di Biotecnologie e Bioscienze*

*Dottorato di ricerca in Biotecnologie Industriali  
XXII ciclo*

Synthesis and biological  
characterization of novel TLR4  
ligands

Dott. Matteo Piazza

Anno Accademico 2008/2009

# 1. INTRODUCTION

## *1.1. Innate immunity*

The immune system has been traditionally divided into innate and adaptive compartments, each with a different function and role<sup>1</sup>. The adaptive system is organized around T and B cells. Since each lymphocyte display a different kind of unique receptor, the repertoire of antigen receptors is very large and diverse. This extreme recognition diversity increase the probability that an individual lymphocyte will encounter a suitable antigen thereby triggering activation and proliferation of the cells. This process of clonal expansion is absolutely necessary to elicit a correct and efficient immune response. Despite the primary importance of this process it require three or five days to rise an appropriate response, which allow more than enough time for most pathogens to damage the host. The innate immunity compartment fulfill the necessity of a fast response against microbial, fungal or viral infections and directs a correct response of the adaptive compartment against non-self<sup>2</sup>.

Innate immunity system use a specific set of cells that in some case almost overlap with the one used from the adaptive immunity compartment. Innate immunity is largely dependent upon myeloid cells able to engulf and destroy pathogens. These cells have stand alone capabilities but evolution biased their properties to better perform in conjunction with components of the adaptive immune system. Amongst myeloid cells some are noteworthy for innate immunity: macrophages, dendritic cells, mast cells, Natural Killer cells, eosinophils, basophils<sup>2</sup>.

## 1. Introduction

Mammals body surface is mainly defended by epithelia, a physical barrier against the external environment that contain pathogens. Epithelia is more than a passive barrier but provide a wide array of chemical substances that could kill bacteria or inhibit their growth. An infection is raised when a pathogen cross epithelia and colonize some suitable internal niches in the body. When the infection happened the pathogen is usually quickly recognized by tissues resident macrophages. Blood circulating Neutrophils are also recruited to site of infection helping macrophage to engulf pathogens and raise the so-called inflammation process.

### ***1.2. Inflammation***

Four stages of inflammation have been described<sup>3</sup>: destruction and removal of injurious agent, containment of the harmful agents, stimulation and amplification of the immune response, promotion of healing. On the onset of infection, stimulus-dependent chemokines, like IL-8, are released by macrophages and attract to the site previously cited innate immunity effectors cells and promote leucocytes extravasation to the involved tissue. Innate immunity effectors cells thus release chemical substances responsible for the inflammation related effects. Most important amongst those acute-inflammation substances are cytokines and vasoactive compounds<sup>4</sup>.

At the site of injury there is immediate vasoconstriction followed rapidly by dilatation of the blood vessels, in particular the postcapillary veinules. Substances involved in the immediate inflammatory response include the vasoactive amines, histamine, and 5-hydroxytryptamine (serotonin), released

## 1. Introduction

from basophils and platelets, respectively. These substances cause smooth muscle constriction of the bronchi, dilatation of the blood vessels, local hyperemia, redness, and heat.

Slow-reacting inflammatory mediators include prostaglandins (eg, PGE<sub>2</sub>), thromboxanes (eg, TxA<sub>2</sub>), and leukotrienes (eg, Leukotrienes C<sub>4</sub>, D<sub>4</sub> and E<sub>4</sub>). PGE<sub>2</sub> causes both vasodilatation and bronchodilatation. Platelets manufacture thromboxane which a powerful vasoconstrictor and causes platelets to aggregate. The leukotrienes, derived from basophils and mast cells, have a similar action on vessels as histamine. In addition they are chemotactic for neutrophils and monocytes. Leukotrienes C<sub>4</sub>, D<sub>4</sub>, and E<sub>4</sub> are synthesized in response to inflammation or tissue injury. Leukotrienes are involved in the inflammatory response in conditions such as asthma, psoriasis, rheumatoid arthritis, and inflammatory bowel disease<sup>5</sup>. They are extremely powerful bronchoconstrictors and vasodilators. Cytokines are small soluble glycoproteins (8 to 80 kilodaltons [kDa]) produced by a wide variety of nonimmune and immune cells that have proinflammatory and anti-inflammatory functions.

In addition to cytokines autocrine and paracrine activity also exhibit some endocrine function; for example, interleukin-1 (IL-1) can stimulate the hypothalamus and cause fever. An example of enhanced production of cytokines such as tumor necrosis factor alpha (TNF ) and IL-1 occurs in the inflamed synovial tissue of patients with rheumatoid arthritis.

Cytokines bind to cell membrane receptor sites and can induce, enhance, or inhibit cytokine-regulated genes. For example, cytokines such as interferon gamma (IFN ) and TNF have been shown to stimulate mononuclear phagocytes to be up regulated and produce nitric oxide (NO). In the setting of inflammation, NO derived from NO synthase (type III) in the vascular endothelium is a powerful

## 1. Introduction

vasodilator. There are several important cytokine characteristics including:

- different cells of the body can produce the same type of cytokine,
- cytokines can act upon different cell types under different circumstances. (ie, pleiotropism).
- different cytokines can have the same activity depending on the situation (ie, redundancy).
- cytokines can act in combination with each other producing synergistic effects on target cells.

Chemotaxis is the phenomenon responsible for attracting cells of the immune system to the site of injury or inflammation. Chemotaxis is the attraction and movement of cells (eg, neutrophils) along a concentration gradient of the chemotactic molecule. There is a super-family of approximately 30 chemoattractant cytokines (chemokines) responsible for initiating cellular activities that occur during the inflammatory response. Many chemokines are produced by leucocytes and endothelial cells.

Several aspects of the molecular structure of chemokines are similar. The chemokines are divided into two subgroups; C-C and C-X-C depending on the presence of a residue between the two cysteine. Briefly, C-C chemokines attract monocytes, basophils, eosinophils, and lymphocytes but do not attract neutrophils, whereas the majority of C-X-C chemokines are chemotactic for neutrophils but not monocytes.

### ***1.3. Receptors***

Main distinction between the innate and adaptive immunity lies in mechanisms and receptors used. The adaptive system use T and B-Cells receptors generated somatically. Since these receptors are not germ-line encoded they are not predestined to recognize any particular antigen. Rather lymphocytes bearing useful receptors are selected for clonally expansion by encountering the correct antigen. Since binding sites of antigens receptors arise as a results of random genetic mechanism the generated repertoire contains binding sites that can react also with innocuous environmental antigens and self antigens. The innate immune system has a major role in directing a correct, non-self, adaptive immune response. Innate immune recognition is mediated by germ-line-encoded receptors<sup>6</sup>, so the specificity of each receptor is genetically predetermined. The strategy of the innate immune response is to focus on a few, highly conserved structures present in large groups of microorganisms. These structures are referred to as Pathogen Associated Molecular Patterns (PAMPS) and the receptors evolved to recognize them are called Pattern Recognition Receptors (PRRs).

PAMPS share some common features: first they are produced only by microbial pathogens and not by their hosts. Second, structures recognized are usually essential for the survival or pathogenicity of invading microorganisms and are usually invariant features shared by entire classes of pathogens.

Bacteria are often recognize from PRRs trough some common components of the cell wall, such as lipopolysaccharide, peptidoglycan, lipoteichoic acids and cell-wall lipoproteins.

A wide recognize fungal PAMP is Beta-glucan, an important component

## 1. Introduction

of fungal cell wall. Because all viral components are synthesized from host cells the main target of innate immunity receptors are viral nucleic acids. Discrimination between host and viral DNA is based on specific chemical modifications and structural features unique to viral RNA or DNAs well as cellular compartments where viral, but not host-derived, nucleic acids are found<sup>7</sup>.

There are several distinct classes of PRRs. Best characterized are the Toll Like Receptors (TLRs)<sup>8</sup>.

Another well studied receptor of this class is the mannan-binding lectin<sup>9</sup>, a member of the calcium-dependent lectin family that binds to microbial carbohydrates to initiate the lectin pathway of complement activation. Mannan-binding lectin and surfactant proteins form a structurally related family of collectins, so named because they consist of a collagenous domain linked to the calcium-dependent lectin domain. Mannan-binding lectin is synthesized in the liver and is secreted into the serum as a component of the acute-phase response. It can bind to carbohydrates on gram-positive and gram-negative bacteria and yeast, as well as some viruses and parasites. Mannan-binding lectin is associated with two serine proteases<sup>10</sup> (mannan-binding lectin-associated proteases 1 and 2). These proteases are related to C1r and C1s, the serine proteases of the classic complement pathway. Similar to C1r and C1s, mannan-binding lectin-associated protease, once activated, ultimately leads to the cleavage of the third component of complement (C3) and to the activation of C3 convertase, which results in an amplified cascade of complement activation. However, unlike C1 proteases, which require antigen-antibody complexes for their activation, mannan-binding lectin-associated proteases are activated by the binding of microbial ligands to mannan-binding lectin. In addition to transmembrane receptors on the cell surface and in endosomal

## 1. Introduction

compartments, there are intracellular (cytosolic) receptors that function in the pattern recognition of bacterial and viral pathogens. These include NLRs<sup>11</sup> and the intracellular sensors of viral nucleic acids RIG-I (retinoic-acid-inducible gene I; also known as DDX58), MDA5 (melanoma differentiation-associated gene 5; also known as IFIH1) and DAI (DNA-dependent activator of interferon-regulatory factors; also known as ZBP1). NLRs are a large family of about 20 intracellular proteins with a common protein-domain organization but diverse functions. All NLRs contain a nucleotide-binding oligomerization domain (NOD) followed by a leucine-rich-repeat domain at the carboxy terminus. At the amino terminus, NLRs are thereby categorized into three subfamilies: a caspase-recruitment domain (CARD), a pyrin domain, or a BIR domain, in the NAIP subfamily. The N-terminal domains engage distinct signaling pathways, which define the functional properties of the family members.

The proteins of the NOD subfamily — NOD1 and NOD2 — are both involved in sensing bacterial peptidoglycans. The sensing of peptidoglycan by NOD1 or NOD2 triggers the production of pro-inflammatory cytokines and chemokines and the recruitment of neutrophils to the site of infection. In addition, these NOD proteins contribute to the initiation of the adaptive immune response, and mutations in NOD2 have been implicated in the pathogenesis of Crohn's disease. NOD2 is also crucial for the production of antimicrobial peptides known as defensins by Paneth cells (which are present in the small intestine), and NOD proteins can presumably activate antimicrobial responses in other cell types<sup>23</sup>.

The NALP subfamily of NLRs has 14 members, and at least some of these are involved in the induction of the inflammatory response mediated by the IL-1 family of cytokines, which includes IL-1 $\beta$ , IL-18 and IL-33.



## 1. Introduction

These cytokines are synthesized as inactive precursors that need to be cleaved by the pro-inflammatory caspases: that is, caspase 1, caspase 4 and caspase 5 in humans, and caspase 1, caspase 11 and caspase 12 in mice. These caspases are activated in a multisubunit complex called the inflammasome. There are several types of inflammasome, categorized according to their composition and the involvement of a particular NALP or NAIP. The individual inflammasomes are activated in response to a variety of bacterial infections, by mechanisms that have been poorly defined. Why IL-1-family members are activated by such an elaborate mechanism is puzzling. Unlike other pro-inflammatory cytokines, IL-1 $\beta$  production is regulated by two distinct signals: TLR-induced transcription and inflammasome-mediated processing of the precursor protein. It is possible that, in addition to IL-1-family members, the inflammasomes process antimicrobial peptides or proteins that have not yet been characterized. NALPs might also contribute to antimicrobial defence by inducing the apoptosis of infected cells. Whether they can also directly induce the expression of antimicrobial genes is unknown. Intracellular recognition of viral infections is mediated by two types of viral nucleic-acid sensor. Viral RNA in the cytosol is detected by the RNA-helicase-family proteins RIG-I and MDA5, whereas viral DNA is detected by the recently identified protein DAI. RIG-I and MDA5 recognize different types of viral RNA: single-stranded RNA containing 5' triphosphate and double-stranded RNA, respectively. These structural features are absent from cellular (host) RNAs, which contain either short hairpin structures, in the case of transfer RNAs and ribosomal RNAs, or a 5'-cap structure, in the case of messenger RNA. These structural differences allow discrimination between viral and self RNAs. Activation of RIG-I or MDA5 results in the production of type I interferons (IFNs; IFN- $\alpha$  and IFN- $\beta$ ) and thereby the induction of

## 1. Introduction

antiviral immunity. Interestingly, a crucial adaptor involved in RIG-I and MDA5 signalling is associated with the mitochondrial membrane, but the reason for this is unclear at present. The details of how viral DNA is recognized in the cytosol, and the signaling pathways induced by the engagement of DAI, are not yet known. It is, however, clear that the RNA-sensing pathway and the DNA-sensing pathway converge on the protein kinase TBK1 (TANK-binding kinase 1) and the transcription factor IFN-regulatory factor 3. Type I IFNs are therefore elicited by the engagement of either type of sensor. This results in antiviral immune responses in both cases, through inducing the expression of numerous IFN-inducible genes, the products of which have a broad range of antiviral activities.

### ***1.3.1. TLRs***

Toll-like receptors are one of the most studied pattern recognition receptors and key components of the innate immune defense. As a response of the innate immune system TLRs play a key role in the innate immunity against various infectious agents<sup>12</sup>.

To date, at least 11 TLRs in humans and 13 in mice have been identified which are fundamental in recognition of pathogen associated molecular patterns (PAMPs). Toll-like receptors are type I transmembrane proteins that are expressed in various immune cells such as B cells, DCs, macrophages and specific types of T-cells and are evolutionary conserved between insects and vertebrates<sup>13</sup>. Toll was first described in *Drosophila*<sup>1</sup>.

## 1. Introduction

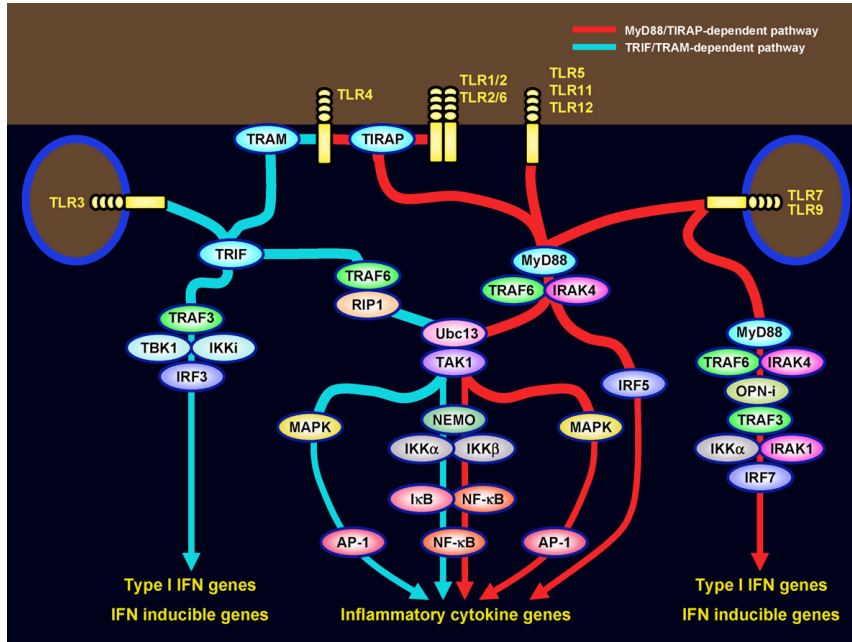


**Figure 1.** Schematic diagram of TLRs intracellular signaling pathway

There are four reported Toll-family members in *Drosophila*: Toll, 18-wheeler, MstProx and STSDm2245. Toll was originally identified and described in the fruit fly as a receptor required for dorso-ventral patterning development but lately was shown to control an immune response to fungal infection in adult flies<sup>14,15</sup>.

Several (TLRs) have been identified in mammals<sup>16</sup> (Fig. 1). The family of TLRs have the ability to recognize various PAMPs from different pathogenic origins such as bacteria, viruses, fungi or protozoan parasites. The TLR subfamily members including TLR 3, 7, 8 and 9, show intracellular localization in the endoplasmic reticulum, endosomes or lysosomes where these receptors recognize nucleic acid components that are normally found in bacteria or viruses<sup>17</sup>. Upon activation by pathogens, the TLR

## 1. Introduction

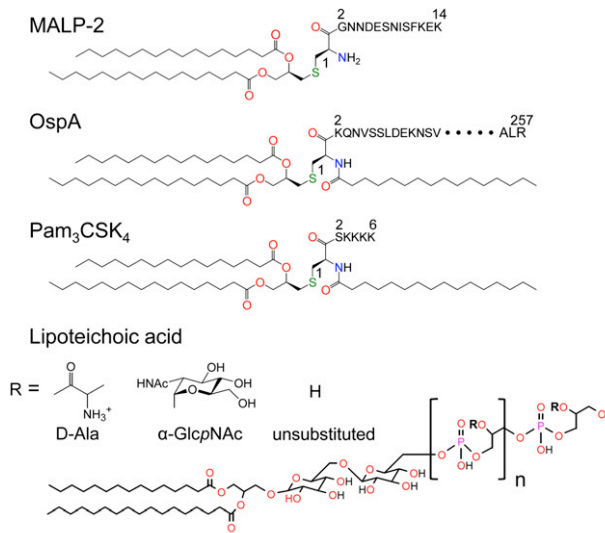
signaling pathway via interactions with 5 different adaptor proteins including MyD88 and Toll/IL-1 receptor domain-containing adaptor inducing IFN-beta (TRIF) triggers a signalling cascade which results in the production several proinflammatory cytokines and immunomodulatory factors subsequently inducing an adaptive immune response<sup>18</sup>. Although the described TLR mediated activation can initiate rapid and effective control of infection it may also be involved in the induction of chronic inflammation and autoimmune reactions<sup>19,20</sup>.

### ***1.3.1.1. TLR1, TLR2, and TLR6***

LPS was originally considered to be the ligand for TLR2, but subsequent studies revealed that contaminating bacterial lipoprotein in LPS preparations is the actual ligand<sup>21</sup>. In agreement with these later findings, TLR2-deficient macrophages were found to be hyporesponsive to several Gram-positive bacterial cell wall components as well as *Staphylococcus aureus* peptidoglycan<sup>22</sup>. Additional work has shown that TLR2 is involved in the recognition of a wide range of microbial products and generally functions as a heterodimer with either TLR1 or TLR6<sup>23</sup> (Fig. 2).

## 1. Introduction

The TLR2/TLR1 heterodimer recognizes a variety of lipoproteins, including those from mycobacteria and meningococci<sup>24</sup>, whereas the TLR2/TLR6 complex recognizes mycoplasma lipoproteins and peptidoglycan<sup>25</sup> (Fig. 2). Recent reports have demonstrated that



triacylated lipoproteins from bacteria are preferentially recognized by the TLR1/TLR2 complex, whereas diacylated lipoproteins are recognized by the TLR2/TLR6

complex<sup>22</sup>. However, additional TLR2 ligands do not appear to require TLR1 or TLR6 for signaling, implying that TLR2 may recognize some ligands as homodimers or heterodimers with other non-TLR

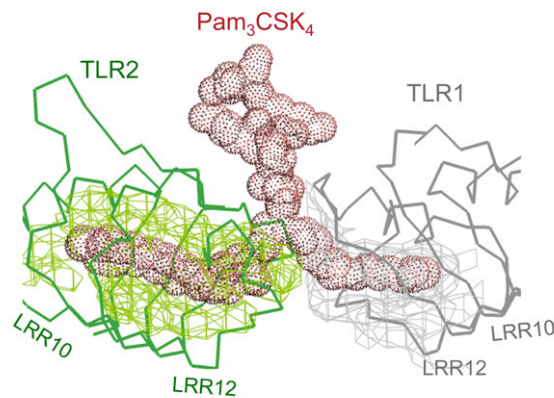


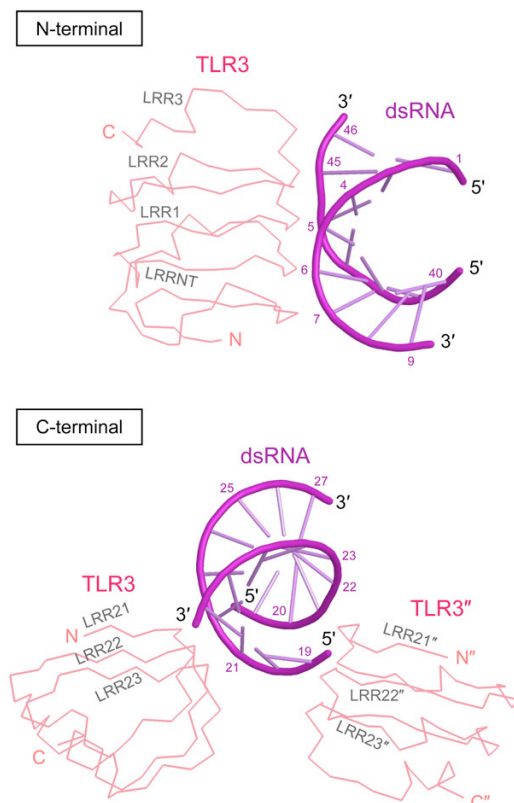
**Figure 2.** TLR1/2 heterodimer and known ligands for TLR1 and TLR2.

Such TLR2 ligands include the Gram-positive cell wall component lipoteichoic acid; the mycobacterial cell wall component lipoarabinomannan; atypical LPS produced by Legionella, Leptospira interrogans, Porphyromonas gingivitis, and Bordetella, and porins

## 1. Introduction

present in the outer membrane of *Neisseria*<sup>26</sup>. In addition to bacterial PAMPs, TLR2hetero/homodimers recognize fungal and protozoan molecules. Zymosan (a crude mixture of glucans, mannan, proteins, chitin, and glycolipids extracted from the cell membrane of fungi) induces signaling through TLR2/6<sup>27</sup>. In addition, glycosylphosphatidylinositol (GPI) anchors and glycoinositol phospholipids from the parasitic protozoa *Trypanosoma cruzi* induce signaling through TLR2.

### 1.3.1.2. TLR3



Double-stranded RNA (dsRNA) was long Hypothesized to be a viral PAMP, as it is produced during the course of many viral infections. Expression of human TLR3 confers responsiveness to purified dsRNA and polyinosinic-polycytidylic acid [poly(I:C)] in HEK293 cells, and TLR3-deficient mice display impaired responses to these ligands. TLR3 signaling results in the activation of

NF- $\kappa$ B and interferon

**Figure 3.** TLR3 in complex with dsRNA

## 1. Introduction

regulatory factor 3 (IRF3), ultimately leading to the production of antiviral molecules, such as type I interferons (IFN- $\alpha/\beta$ )<sup>28</sup> (Fig. 3).

Recent research, however, has demonstrated TLR3-independent recognition of viral dsRNA via the helicases RIG-I (retinoic acid-inducible gene 1) and MDA5 (melanoma-differentiation-associated gene 5), which are cytoplasmic PRRs expressed abundantly in multiple cell types<sup>29</sup>. RIG-I and MDA5 differentially recognize different groups of RNA viruses and are thus critical for a robust antiviral response. These receptors contain a helicase domain for RNA binding and two caspase recruitment domains (CARDs) for signal transduction. Upon ligand binding, RIG-I and MDA5 bind and activate the adaptor IPS-1 (interferon- $\beta$  promoter stimulator 1; also termed CARDIF, MAVS, and VISA) for NF- $\kappa$ B and IRF3 activation and subsequent production of IFN- $\beta$ <sup>30</sup>. The importance of RIG-I- and MDA5-mediated viral recognition is further supported by gene-targeting experiments demonstrating that TLR3 and its adaptor TRIF are not required for type I IFN production in some virally infected cells, such as fibroblasts and conventional DCs. However, plasmacytoid dendritic cells exclusively utilize TLR3/TRIF signaling for type I IFN production in response to RNA viruses and poly(I:C).

### **1.3.1.3. TLR5**

Flagellin, a protein component of Gram-negative bacterial flagella, is the cognate ligand for TLR5<sup>31</sup>. TLR5 recognizes a highly conserved, central core structure of flagellin that is essential for protofilament assembly and bacterial motility. Interestingly, the TLR5 recognition site is masked in the filamentous flagellar structure, thus indicating that TLR5

## 1. Introduction

recognizes only monomeric flagellin. Furthermore, flagellin appears to bind directly to TLR5 at residues 386–407 of the extracellular domain (ED), as TLR5-ED mutants lacking this domain are unable to interact with flagellin in biochemical assays<sup>32</sup>. Recent articles have demonstrated TLR5-independent recognition of cytosolic *Salmonella typhimurium* flagellin via Ipaf, a member of the nucleotide-binding oligomerization domain (NOD)-LRR<sup>33</sup>. Ipaf-mediated recognition of cytosolic flagellin is critical for caspase-1 activation and subsequent IL-1 $\beta$  secretion by macrophages, further highlighting the significance of TLR-independent pattern recognition in the overall complexity of the innate immune response.

### **1.3.1.4. TLR7 and TLR8**

Mouse TLR7 recognizes a class of synthetic antiviral compounds, such as imidazoquinolines and loxoribine<sup>34</sup>. Furthermore, TLR7 and human TLR8 detect the antiviral azoquinoline compound R-848. These synthetic compounds are structurally related to nucleic acids; TLR7 and human TLR8 recognize guanosine- or uridine-rich single-stranded RNA (ssRNA) derived from RNA viruses<sup>35</sup>. Interestingly, mammalian RNA, which contains many modified nucleosides, is significantly less stimulatory via TLRs 7 and 8 than bacterial RNA, suggesting that the mammalian host utilizes nucleoside modification as a means to distinguish between endogenous and pathogen-derived RNA. Similar to the function of TLR3, engagement of these receptors leads to the production of type I IFNs, which are obligate components of antiviral innate immunity.



### **1.3.1.5. TLR9**

TLR9 recognizes bacterial DNA containing unmethylated CpG motifs, and TLR9-deficient mice are not responsive to CpG DNA challenge<sup>35</sup>. TLR9 expressed in plasmacytoid DCs recognizes virally derived CpG sequences for the induction of IFN- $\alpha$ <sup>36</sup>. The low frequency and high rate of methylation of CpG motifs prevent recognition of mammalian DNA by TLR9 under physiological circumstances. In certain autoimmune disorders, however, IgG2a/chromatin complexes containing CpG DNA can engage the B cell receptor and TLR9 concomitantly, leading to the production of rheumatoid factor and other autoreactive molecules. A recent report indicated that the intracellular, endosomal restriction of TLR9 is critical for discriminating between self and nonself DNA, as host DNA, unlike microbial DNA, does not usually enter the endosomal compartment<sup>37</sup>. Finally it was reported that TLR9 recognizes a novel non-DNA ligand called hemozoin, which is a hydrophobic heme polymer produced by malaria parasites as they digest host hemoglobin. In addition to TLR9-mediated detection of CpG DNA in the endosomal compartment, the mammalian innate immune system also responds to foreign DNA in the cytosol. This response is important for type I IFN production in response to viruses and intracellular pathogens, such as *Listeria monocytogenes* and *Shigella flexneri*, that replicate in the cytoplasm. As membrane restriction prevents TLRs from sampling the cytosol for PAMPs, cytosolic PRRs have evolved to provide comprehensive innate immune recognition that offsets TLR restriction.

## 1. Introduction

### **1.3.1.6. TLR11**

Gene-targeting studies revealed that TLR11-deficient mice are susceptible to uropathogenic *Escherichia coli* infection<sup>38</sup>. Although the bacterial ligand for TLR11 remains undiscovered, the stimulatory activity of uropathogenic bacteria can be destroyed by proteinase K treatment, suggesting that TLR11 recognizes a protein ligand. TLR11 also recognizes a class of profilin-like molecules expressed by apicomplexan protozoans, including *Toxoplasma gondii*.

### **1.3.1.7. TLR4**

Prototypic ligand for TLR4 receptor complex is Lipopolysaccharides (LPS) derived from the outer membrane of gram negative bacteria<sup>39</sup>. TLR4 recognition is mainly targeted against the conserved lipid A moiety, which is the minimal fragment that triggers the cellular response. Variability in the LPS core and O-antigen can, however, significantly affect the response as well as the type of the signaling pathway<sup>40</sup>. So far TLR4 is the only known TLR that do not directly bind his ligand. The current view for LPS recognition is that LBP (Lipid Binding Protein, mainly present in a free form in the serum) binds to LPS aggregates helping an endotoxin monomer to be loaded on CD14. Free or membrane bound CD14 then transfer the LPS monomer to MD2 thus allowing the formation of the active trimeric complex (TLR4:MD2:LPS)<sub>2</sub> that trigger the intracellular signaling pathway.

## 1. Introduction

### 1.3.1.7.1. *LBP*

Lipid Binding Protein (LBP) is a glycoprotein of around 60 kDa and is mainly synthesized by hepatocytes<sup>41</sup>. The tertiary structure of LBP is composed of two barrel domains connected by a proline rich linker. Each domain is composed of an antiparallel  $\beta$ -stranded layer twisted around the long  $\alpha$ -helix. The N-terminal domain of LBP contains a cluster of cationic residues essential for LPS binding<sup>42</sup>.

LPS aggregates generated by bacterial lysis is a weak immunostimulator because aggregates are hardly recognized by MD2 and CD14. LBP thus binds to LPS aggregates loosen their interaction between LPS monomers and facilitating endotoxin transfer to CD14<sup>43</sup>. C-terminal domain of LBP present a region that promote interaction with CD14 thus facilitating the transfer of the endotoxin.

### 1.3.1.7.2. *CD14*

The cluster differentiation antigen, CD14, has been shown to be a key high-affinity cellular receptor for these bacterial endotoxins and plays an important role in endotoxin-induced activation of innate immune cells<sup>44-46</sup>. In humans, CD14 is constitutively expressed on cell surfaces of monocytes/macrophages as a 55 kDa membrane-bound protein and also exists in a soluble form (sCD14) (Fig. 4), in serum and bodily fluids in concentrations of 2–6  $\mu\text{g/ml}$  [2,3]. Recognition and binding of different microbial endotoxins to both mCD14 and sCD14 initiates a signaling cascade-mediated by Toll-like receptors (TLRs) that promotes the synthesis and secretion of multiple host-derived inflammatory mediators<sup>47</sup>.

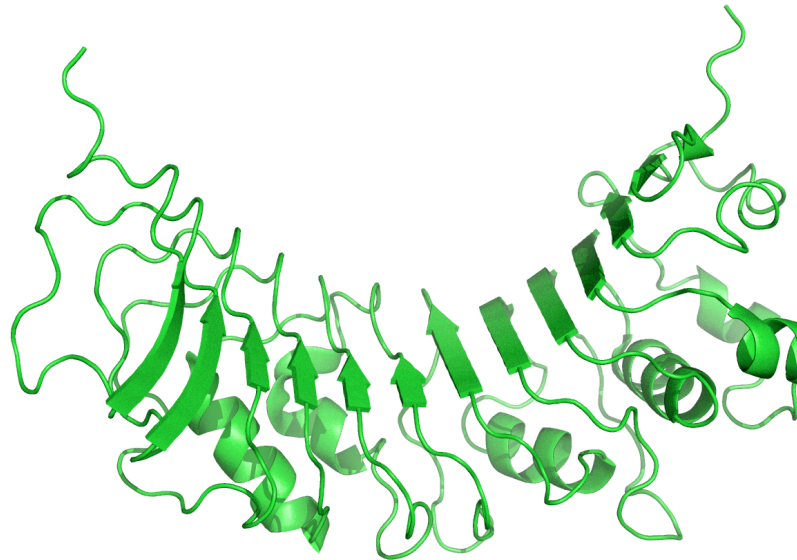


**Figure 4. Soluble form of CD14 (sCD14)**

The monomeric subunit of CD14 contains thirteen strands, and 11 of them, from 3 to 13, overlap with conserved leucine-rich repeats (LRRs) (Fig. 4). The concave surface of the horseshoe-shaped structure consists of a large  $\beta$ -sheet of 11 parallel and two antiparallel beta strands. The convex surface of CD14 contains both helices and loops, in no regular pattern. As a result, it is rough rather than smooth and contains several grooves and pockets that are crucial for ligand binding. The most striking feature of the structure of CD14 is the NH<sub>2</sub>-terminal pocket. The pocket is located near the NH<sub>2</sub> terminus, and it is entirely hydrophobic except for the perimeter (Fig. 5).

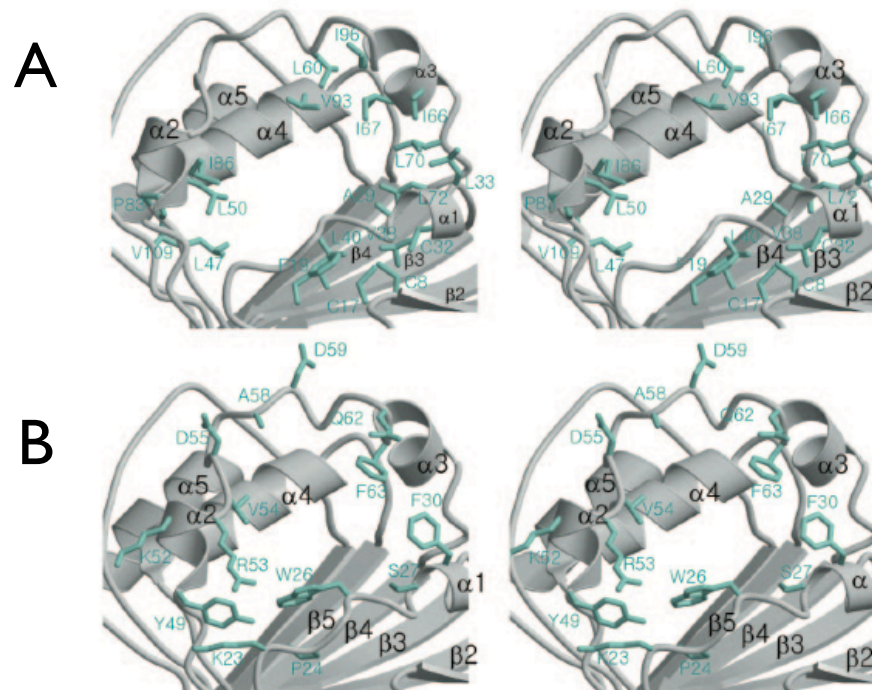


**Figure 5.** Structure of the NH<sub>2</sub>-terminal pocket. (A) Wall and base of the n-terminal subpocket (B) the rim of the main pocket.

## 1. Introduction

The main pocket contains a smaller subpocket at the bottom (Fig. 5).

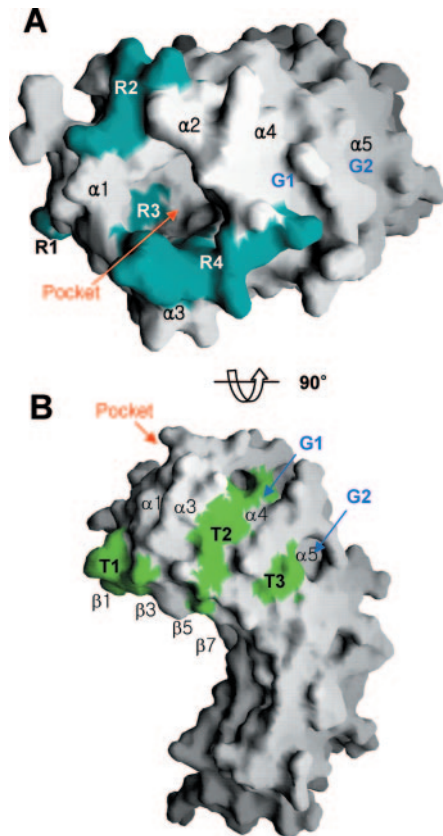


**Figure 6.** Regions involved in LPS binding and signaling. (A) The four LPS-binding regions, R1–R4 (B), regions that interfere with LPS transfer labeled T1–T3 (Fig. 1A).

This sub-pocket is narrow and deep and formed by hydrophobic residues from 4 – 6, 4, 5, and connecting loops. The bottom and walls of the main pocket are lined with residues from 1–3, 1– 4, and their connecting loops. The main pocket is both wide and deep with dimensions, 8 Å wide, 13 Å long, and 10 Å deep. Overall, the pocket including the sub-pocket has a total volume of 820 Å<sup>3</sup> and hence is large enough to accommodate at least part of the lipid chains of LPS. The residues

on the hydrophilic rim of the main pocket are highly flexible. The Pocket Area Is Responsible for LPS Binding—The-binding sites for LPS in CD14 have been intensively studied by mutagenesis and by epitope mapping of antibodies that block LPS binding, and four regions have been identified within the NH<sub>2</sub>-terminal 65 residues of CD14<sup>48,49</sup>. Deletion or missense mutations of these regions significantly reduce LPS binding or responsiveness<sup>50,51</sup>. All of these regions (Fig. 6) are clustered around the pocket; region 1 is located close to the wall and region 3 is at the bottom of the pocket, whereas regions 2 and 4 are

## 1. Introduction

located on the rim of the pocket.

Residues from the turn between the 1 and 2 strands constitute region 1. Region 2 is the loop between the 2 strand and the 1 helix. Monoclonal antibodies that recognize this area inhibited LPS binding. Region 3 consists of residues from the 3 strand. Region 3 is the most frequent target of LPS blocking antibodies. At least nine monoclonal antibodies that recognize the 2 and 3 strands reduce binding of LPS by soluble CD14. Region 4 includes residues from the loop connecting 2 and 3 helices. This area is labile to proteolysis in the absence of bound LPS but becomes resistant when LPS is bound. Furthermore, the antibodies MEM18, CRIS-6, and 6C8 that block LPS binding bind to the same region. Collectively, these mutagenesis and epitope mapping data strongly suggest that the NH<sub>2</sub>-terminal pocket is the principal component of the LPS-binding site in CD14. Based on structural findings it was proposed that the lipid portion of LPS binds to the NH<sub>2</sub>-terminal pocket. It is unlikely that binding of LPS induces a global structural change of CD14, since many residues making up the hydrophobic pocket are in conserved LRR motifs, and the overall shape of LRR proteins displays limited variability. Besides, it has been reported that binding of LPS induces only minor changes in the tryptophan fluorescence and CD spectrum of CD14. However, LPS binding can induce local structural especially within the highly mobile 2 and 3 helices and the connecting loops. The long carbohydrate chain of LPS is hydrophilic and negatively charged and must have its own binding site, as previous research has shown that LPS that has been enzymatically delipidized retains some affinity for CD14<sup>52</sup>. Previous studies of the binding of PGN to CD14 in vitro provide clues to the binding site of the carbohydrate portion of LPS, although the biological importance of PGN binding to CD14/TLR2 is under debate<sup>53</sup>. The hydrophobic NH<sub>2</sub>-terminal pocket of CD14 is

## 1. Introduction

unlikely to be involved in PGN binding, since PGN is a completely hydrophilic molecule. However, the LPS- and PGN-binding sites must overlap, at least in part, because PGN competes with LPS for binding to CD14. The binding site of PGN appears to be shifted to the COOH-terminal side of the pocket, since deletion mutants of regions 1 and 2 that have a profound effect on LPS binding have only minor effects on PGN binding. On the other hand, deletion of region 4 reduces binding of LPS as well as of PGN, and region 4 is on the COOH-terminal side of the pocket. Furthermore, it was reported<sup>54</sup> that a monoclonal antibody, Leu\_M3, specifically reduced the affinity for peptidoglycan without affecting that for LPS. The epitope of this antibody maps to the upper side of the G2 groove formed by the  $\alpha$ 5 helix and loops on the far COOH-terminal side of the pocket. Collectively, the LPS-binding site of CD14 appears to extend further beyond the NH<sub>2</sub>-terminal pocket and includes grooves in the neighboring area. The structural characteristics of the binding site may explain the broad ligand specificity of CD14. Although the hydrophobic bottom and walls of the pocket are rigid, the generous size of the pocket may allow structural variation in the hydrophobic portion of the ligand. Structural diversity in the hydrophilic part of the ligands could be explained by the considerable flexibility of the hydrophilic rim combined with the multiplicity of grooves available for ligand binding. To initiate signaling, LPS bound to CD14 should be transferred to the TLR4/MD-2 complex on the cell membrane. Several laboratories have reported CD14 mutants that have only minor defects in LPS binding but have virtually no signaling activity<sup>55</sup>. They are alanine mutations of Glu7-Asp10, Asp9-Phe13, or Leu91-Glu101 in human CD14 or Pro151-Leu153 in mouse CD14. It is noteworthy that they are clustered on the same side of CD14, although most of them are far apart in the primary sequence. The sequences of



## 1. Introduction

Glu7–Asp10 and Asp9–Phe13 overlap with region 1 of the LPS blocking mutations.

Therefore region 1 appears to play a role in both LPS binding and transfer because some mutations in this area block LPS binding and others LPS transfer. The sequences Leu91–Glu101 and Pro151– Leu153 are the lower parts of the two grooves, G1 and G2. As shown in Fig. 3B, all these mutations are located in the same area near the NH<sub>2</sub>-terminal pocket. These data suggest that the area close to the pocket plays an important role in the transfer of LPS from CD14 to the TLR4/MD-2 complex.

### 1.3.1.7.3. *MD2*

MD-2 is a 160–amino acid glycoprotein with a 16–amino acid secretion signal at the N terminus (Fig. 7) and represents a class of MD-2–related lipid recognition (ML) proteins<sup>56</sup> that also include mite allergen proteins. MD-2 forms a stable complex with TLR4 on the cell surface<sup>57</sup>, and MD-2 alone as well as in the complex directly binds to LPS with nanomolar affinity<sup>58</sup>.

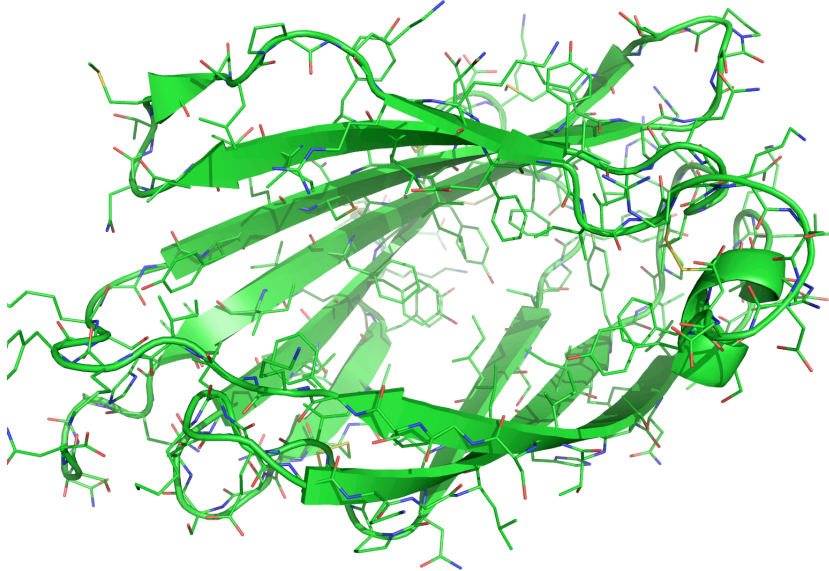


**Figure 7.** Myeloid differentiation protein 2 (MD2)

MD-2 is folded into a single domain consisting of two  $\beta$  sheets in the immunoglobulin fold conserved among the ML proteins: One sheet consists of three antiparallel  $\beta$  strands, and the other consists of six antiparallel strands. Between these sheets is a large and deep hydrophobic cavity (Fig. 8). It has a volume of  $1710 \text{ \AA}^3$  with approximate dimensions of  $15 \text{ \AA}$  by  $8 \text{ \AA}$  by  $10 \text{ \AA}$ . The b6 and b7 strands line the entrance to the cavity<sup>59</sup>. Three disulfide bridges are located between Cys25 and Cys51, between Cys37 and Cys148, and between Cys95 and Cys105, in contrast to the predicted bridges between Cys25 and Cys148 and between Cys37 and Cys51. The glycosylation sites of both Asn26 and Asn114 are distant from the cavity region, indicating that the glycosylation plays a role not in ligand binding, but (presumably) in the secretion and protection of MD-2<sup>59</sup>.

## 1. Introduction

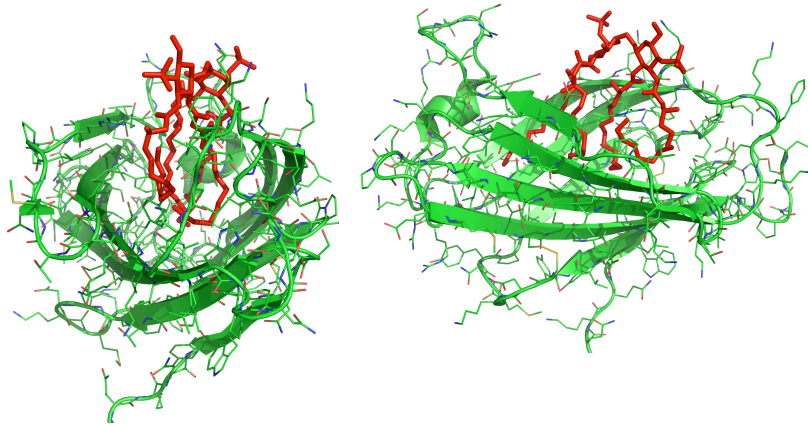


**Figure 8.** MD2 in complex with lipid IVA, front and side view

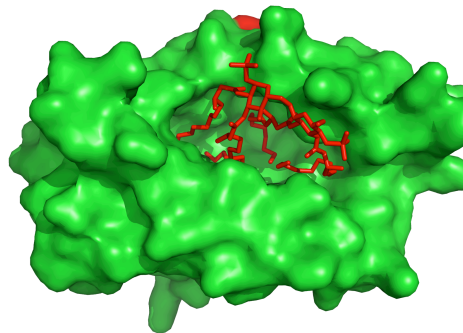


**Figure 9.** MD2 binding site in complex with lipid IVA

The phosphate and sugar groups of Lipid IVA (a natural ligand) are aligned in parallel with b7 in the order XP1, XG1, XG2, and XP2, with an XP1-XP2 distance of 12.5 Å (Fig. 10). Residues Phe119 to Gly123 are important for the LPS recognition, and these residues, with the exception of Lys122, are conserved in all the species of MD-2. Three hydrogen bonds to lipid IVA are noticed: Ser120 N to XA1 O1' (distance of 2.87 Å), Lys122 N to XA3 O1' (3.07 Å), and Ser120 O to XA3 O3' (2.66 Å). Water atoms mediating lipid IVA and MD-2 are located at the cavity entrance<sup>60</sup>.

## 1. Introduction

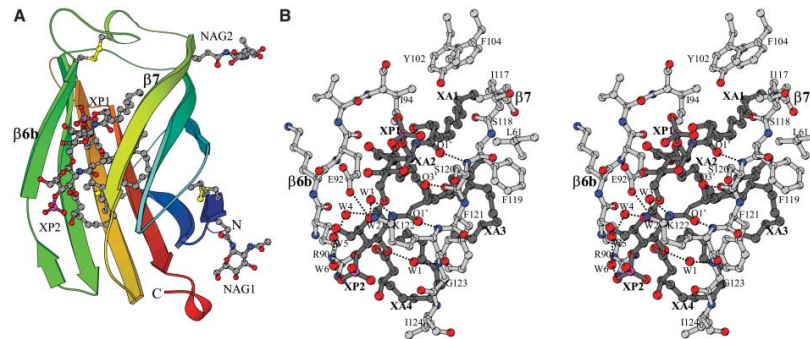


**Figure 10.** Binding interface to lipid IVa. (A) Ribbon representation of the MD2-lipid IVa complex (B) Stereo close-up view of the binding interface. Amino acid residues located in the vicinities of the entrance are drawn as ball-and-stick models with their residue labels. The structure of the lipid IVa moiety is similarly drawn in darker gray, O atoms in red, N in blue, C in gray, and P in pink. Water O atoms involved in hydrogen bonds (broken lines) are also depicted: W1 between Gly123 N and XG2 O3, as well as a group of W2, W3, W4, W5, and W6, in which W2 is hydrogen-bonded to Glu92 Oe1, W2 to W3, and W3 to XG2 N2.

Among a total of 18 lysine and arginine residues of human MD-2 (Fig. 11), which is highly basic with an isoelectric point value of 8.7, only Lys122 and Arg90 are located in the vicinities of the entrance, and their side chains cover XG2 and XP2. These interactions tether the hydrophilic moiety of lipid IVa to the cavity. Hydrophobic and electrostatic surface potentials in the vicinities of the entrance indicate that the entrance is positively charged and the inside of the cavity is highly hydrophobic.

## 1. Introduction

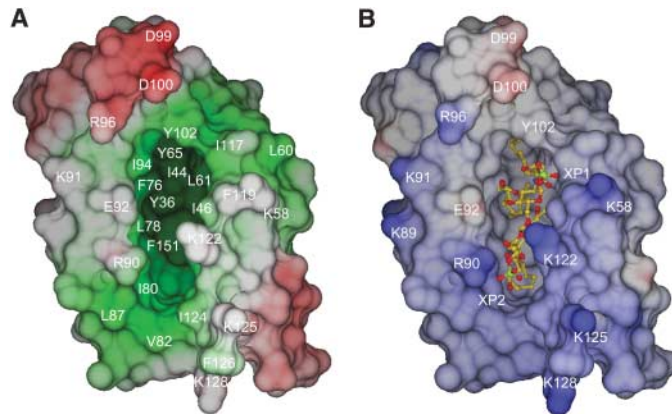


**Figure 11.** Binding pocket and surface properties of MD-2. (A) Protein surface showing hydrophobic and hydrophilic properties. Green and red represent hydrophobicity and hydrophilicity, respectively, and the extent is indicated by color darkness. (B) Electrostatic potential surface. Positive and negative potentials are shown in blue and red, respectively. Bound lipid IVa is drawn as a ball-and-stick representation: O in red, N in blue, C in yellow, and P in green.

None of the phosphate groups of lipid IVa, which are reported to be essential to the activation of immune responses<sup>61</sup>, are involved in direct hydrogen bonds to MD-2 atoms. The lysine and arginine residues mainly contribute to the attraction of negatively charged lipid IVa. Four fatty acid chains of lipid IVa are all deeply confined in the cavity. The XA1 chain (Fig. 10) is in an extended linear conformation and is stuck deeply into the cavity: Three of its four sides are surrounded by hydrophobic MD-2 side chains. The XA2 chain is also in the cavity and lined up with XA1. The XA3 and XA4 chains are curved, and the regions of XA3 C10'-11' and XA4 C11'-13' atoms are loosely packed in the cavity. The tip end of XA4 folds back toward the XG2 moiety, and that of XA3 hangs over XA4. The fatty acid chains in the cavity are packed next to each other through van der Waals contacts, as exemplified in the lipid molecules bound to the GM2 activator protein. The packed and confined

## 1. Introduction

fatty acid structures are distinct from the extended structures of the fatty acid chains of LPS associated with the membrane-embedded region of the FhuA ferrichrome ion receptor. The cavity of MD-2 is divided into four sites on the basis of their interactions to the fatty acid chains: L1 through L4 respectively correspond to XA1 through XA4. In the L1, L2, and L3 sites of the native structure, the fatty acid molecules assigned as myristic acids exist in nearly identical configurations to those of XA1, XA2, and XA3, respectively. It was suggested that the L1, L2, and L3 sites have higher affinities to fatty acid chains. The surface area accommodating lipid IVa is very wide, 890 Å<sup>2</sup>. This large value is comparable to that of ligands bound to the antibodies and explains the nanomolar affinity of MD-2 toward LPS. The MD-2 residues essential to the interaction with TLR4 are reported to be Arg90, Lys91, Asp100, Tyr102, Cys95, and Cys105 in the absence of the ligands. A synthetic peptide from Cys95 to Cys105, in the oxidized form, exhibits a decrease in LPS-induced activation and is supposed to compete with MD-2 through the interaction with TLR4. These residues are located at the cavity entrance. The structure of CD14, which transfers LPS to MD-2, also has a hydrophobic cavity of dimensions nearly equal to those of MD-2; hence, it is presumed to recognize acyl chains of LPS. The only differences between the structures of the antagonist lipid IVa and of the agonist lipid A are two additional acyl chains, XA3' and XA4'. The MD-2 cavity likely could not accommodate more than four acyl chains. When the additional XA3' chain ester-linked to the XA3 O3' atom is directed toward the inside of the cavity, the hydrogen bonds of the XA3 O3' atom to both Ser120 O and to XA1 O1' are disrupted, and hence the XA3 and XA4 portions are rearranged. This rearrangement would displace some portions of XA3 and XA4 toward the region near Val82, Leu87, and Phe126, which is reported to affect ligand-stimulated TLR4 clustering.

## 1. Introduction

Binding sites other than L1 through L4 for the additional acyl chains or conformational changes enlarging the cavity are conceivable for lipid A. The additional lipid A acyl chains displaced from the hydrophobic cavity might be involved inactivation upon MD-2 complexation with TLR4, and they may induce the reported oligomerization of TLR4. This activation scheme is consistent with the increased MD-2 affinity to lipid A upon association with TLR4. Recombinant human MD-2 in which Ser57, Leu61, and Lys122 are replaced with the corresponding mouse residues (Thr57, Val61, and Glu122) is reported to be activated by lipid IVa and lipid A. The hydroxy atom of Ser57 in the b4 strand is hydrogen-bonded to Glu53 N, Leu61 is located deep in the cavity, and Lys122 is on the surface of the cavity entrance. The former two replacements would bring subtle changes in the construction of the cavity, and the replacement with the glutamate side chain would change the electrostatic properties of the cavity entrance.

### 1.3.1.7.4. *TLR4*

TLR4 is composed of a 608 residue extracellular domain, a single transmembrane domain, and a 187 residue intracellular domain<sup>62</sup> (Fig. 12). The crystal structure shows that TLR4 is an unusual member of the “typical” subfamily of the LRR superfamily. Typical subfamily LRR proteins have characteristic horse-shoe-like structures whose concave surface is formed by parallel b strands and whose convex surface is formed by loops and 310 helices<sup>63</sup>. The parallel b sheet of the typical subfamily has uniform twist angles and radii throughout the entire protein. Unlike other typical family members including TLR3, analysis of the b sheet conformation of TLR4 demonstrates that it can be divided

## 1. Introduction

into N-, central, and C-terminal domains and undergoes sharp structural transitions at the domain boundaries. The N-terminal domain starts from amino acid residue 26 and ends at residue 201 and contains the LRRNT module and LRR modules 1 to 6. The LRRNT module has no sequence homology with the LRR modules and protects the otherwise exposed hydrophobic cores of the LRR modules. The sequences of the six LRR modules in the N-terminal domain agree well with the conserved pattern of LRR modules of the typical subfamily.

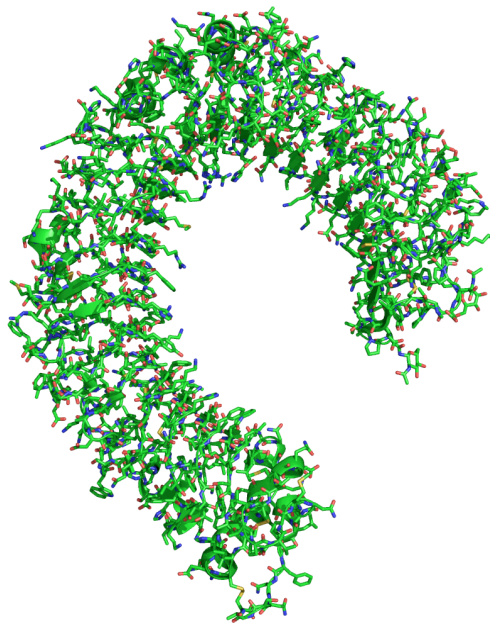


**Figure 12.** Toll Like Receptor 4 (TLR4) ectodomain

The radius and twist angle of the N-terminal domain also agree well with those of typical LRR subfamily members. The C-terminal domain of TLR4 contains the LRRCT module and LRR modules 13 to 22. The radius of the  $\beta$  sheet of the C-terminal domain is 28% larger than that of the N-



## 1. Introduction

terminal domain. Like LRRNT, the LRRCT module contains two disulfide bonds and covers the hydrophobic core of the LRR modules at the C terminus. The central domain is composed of LRR modules 7 to 12 and has a 35% smaller radius and three times greater twist angles than those of TLR3. It includes the “hypervariable” region that is essential for recognition of an LPS variant from *P. aeruginosa*<sup>64</sup>. The conformational variation of the central domain appears to originate from three changes in its sequence conservation pattern. The standard LRR module contains two variable amino acids between the first and second conserved leucines. However, the LRR modules of the central domain have only one variable residue. Signature residues important in the structure of the “typical” subfamily LRR proteins are missing from the central domain<sup>65</sup>. In the typical subfamily, the conserved asparagines form a continuous hydrogen-bonding ladder and the phenylalanines form a hydrophobic spine<sup>66</sup>. In TLR4, the asparagine ladder is absent from LRR modules 9–12 and the phenylalanine spine is broken at the border between the central and the C-terminal domain. The lengths of the LRR modules of the central domain vary considerably, ranging from 20 to 30 amino acid residues<sup>67</sup>. The length of the LRR module is strongly correlated with the overall shape of the horse-shoe-like structure. The LRR superfamily consists of six subfamilies, within which the lengths of the LRR modules are conserved. Subfamilies with shorter LRR modules have loops in their convex regions, and those with longer ones have a-helical structures. Since an a-helix requires more space than loops, the horseshoe-like structures with longer LRR modules have smaller radii. Thus the large variation in the length of the LRR modules appears to affect the radius and shape of the horseshoe-like structure of the central domain.

## 1.4. TLR4 ligands

### 1.4.1. Natural ligands

#### 1.4.1.1. LPS

lipopolysaccharide (LPS) (Fig. 13) is the best characterized and widespread ligand of TLR4 receptor complex. LPS is a major component of the outer membrane of Gram-negative bacteria, contributing greatly to the structural integrity of the bacteria, and protecting the membrane from certain kinds of chemical attack. LPS also increases the negative charge of the cell membrane and helps stabilize the overall membrane structure. It is of crucial importance to gram negative bacteria, whose death results if it is mutated or removed<sup>68</sup>.

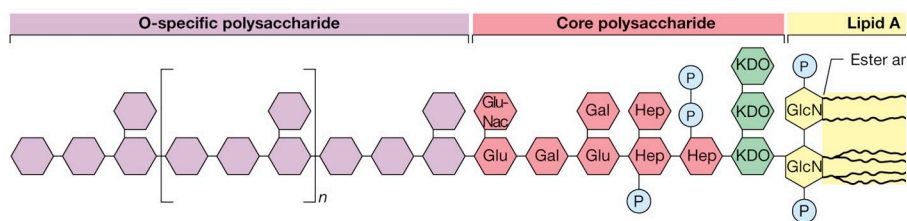


**Figure 13.** Schematic structure of lipopolysaccharide (LPS) from E.Coli

LPS consist of a glycerophospholipid dimer (LipidA) and of a ramificated polysaccharide chain commonly divided in O-chain and core oligosaccharide.

The LipidA (Fig. 14) constitute the so called endotoxin center of LPS thus providing the minimal structure responsible for toxicity in vertebrates. Chemically all LipidA are constituted of D-glucosamine

## 1. Introduction

disaccharide  $\beta(1-6)$  linked. The disaccharide carries two phosphate ester groups linked to the 1 and 4' positions. Four (R)-3-hydroxy fatty acids are linked ester (position 3 and 3') and amide (position 2 and 2') linkages to the disaccharide. In general two fatty acids are acylated at their 3-hydroxyl group. Despite this common architecture, lipid A of different bacterial origin may vary in their fine structure. Variations in structure result from the type of hexosamine present, the degree of phosphorylation, the presence of phosphate substituents and, most notably, the nature, chain length, number and location of lipid chains. *E. Coli* is considered the classical prototype and presents 14 carbon length fatty acids (3-hydroxytetradecanoic acid). The hydroxy groups of the two (R)-3-hydroxy fatty acids of the distal GlcN-residue (GlcN II) are acylated by non-hydroxylated fatty acids whereas those at the GlcN-residue at the reducing site (GlcN I) are free.

Thus the overall acylation pattern is asymmetric (4+2). In contrast, in a second group of lipid A a symmetrical fatty acid distribution (3+3) was identified, as with *Neisseria meningitidis*. The chain length of amide-linked acyl groups is constant in asymmetrically acylated lipid A whereas it varies among strains with symmetrical fatty acid distribution<sup>69</sup>.

Mutants lacking in Lipid A and both KDO show no vitality demonstrating that the minimal requirement for bacterial viability is Lipid A and at least one KDO. The O-Chain is an oligosaccharide composed of one to eight glycosyl residue units repeated a variable number of times depending on the strain. The structure of those units differs from strain to strain thus exhibiting an enormous variability<sup>70-72</sup>.

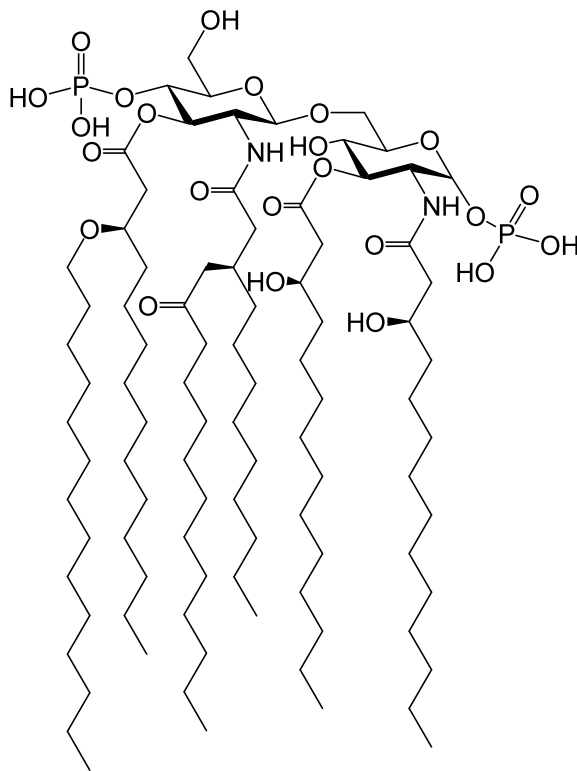


**Figure 14.** Lipid A from E.Coli

The core region is divided into an outer and an inner portion. The core is more structurally uniform than the O-chain but a little structural diversity is found primarily in the outer core region. As for lipid A portion also for the core E. Coli is a good structural model. The outer core contains the common hexose D-glucose, D-galactose and N-acetyl-D-glucosamine in the linkage shown in figure xy. Despite structural differences within the different core types, a common sequence of hexose residues possess the general structure:  $\alpha\text{HEX1} \rightarrow 2\alpha\text{Hex1} \rightarrow 2\alpha\text{Hex1} \rightarrow 3\alpha\text{Glc1} \rightarrow 3\alpha^{69}$ .

The inner core is composed of the characteristic and LPS-specific components heptose (Hep), mainly in the L-glycero-D-manno

## 1. Introduction

configuration, and 3-deoxy-D-manno-octosulonic (or 2-keto-3-deoxyoctonic) acid (Kdo). The Hep and Kdo residues are, in general, substituted by charged groups such as phosphate, pyrophosphate, 2-aminoethylphosphate and 2-aminoethylpyrophosphate, leading to an agglomeration of charged residues in this inner part of the core region. The high density of negatively charged residues is likely to be of physiological significance, as it concentrates bivalent cations such as  $\text{Ca}^{2+}$  and  $\text{Mg}^{2+}$  in the close environment of the cell surface where cations are required for the structural and functional integrity of the outer membrane<sup>69</sup>.

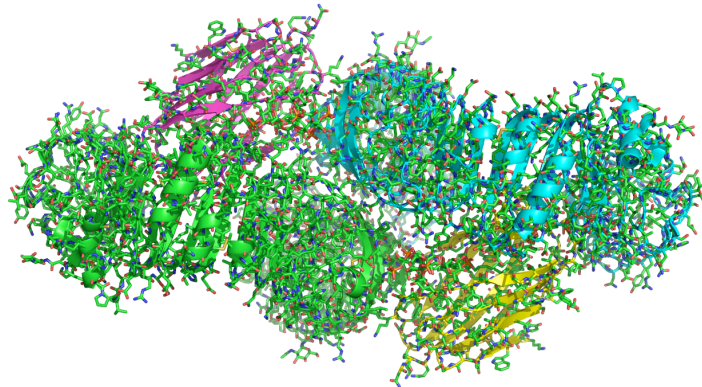
The minimal LPS required for the growth of *E. coli* consists of the lipid A and Kdo (3-deoxy-D-manno-oct-2-ulosonic acid) domains (Figs. (Figs.11 and and2)2) (1, 7, 8). In wild type strains, additional core and O-antigen sugars are present. These are generally not required for growth in the laboratory, but help bacteria resist antibiotics, the complement system, and other environmental stresses.

Subtle modifications of Lipid A structure could radically shift TLR4 response to ligand interaction. Good example is Lipid IVA that has an intrinsic antiendotoxin activity lacking only two alkyl chains in comparison to Lipid A. The difference is highlighted from comparison of crystal structure of MD2 complex with both ligands<sup>59,73,74</sup>.

In the monomeric structures of MD-2 bound to non-agonistic ligands<sup>2,3</sup>, F126 is exposed to the solvent area without interacting with any ligand or protein residues. On the contrary, in the dimerized structure of the TLR4–MD-2–LPS complex (Fig. 15), F126 together with L54, Y131 and I124 of MD-2 forms extensive hydrophobic bonds with lipid chains R2 and R3 of LPS, and F440\* of TLR4\* (Fig. 17). These interactions are important for positioning the R2 lipid chain correctly and inducing a 5 Å structural shift in the F126 loop, which moves the critical residues

## 1. Introduction

G123, I124 and K125 to positions suitable for the dimerization interaction with TLR4\*. Hence, changing F126 to alanine, with its smaller side chain, should disrupt this core interaction and prohibit receptor dimerization. Mutations of other residues in the F126 loop also interfere with LPS binding and signalling<sup>19–22</sup>. Interestingly, a mutant MD-2 with K125 changed to alanine shows normal LPS binding and receptor activation activity<sup>22</sup>. This is because the backbone atoms, but not the side chain atoms, are involved in receptor dimerization. In the crystal structures of MD2 bound to lipid IVA and to eritoran, the four lipid chains of the antagonists completely fill the available space in the pocket. *E. coli* LPS has two more lipid chains than these antagonists, so it has been proposed that global structural changes may take place in the MD-2 pocket to accommodate the extra lipid chains (Fig. 18).



## 1. Introduction

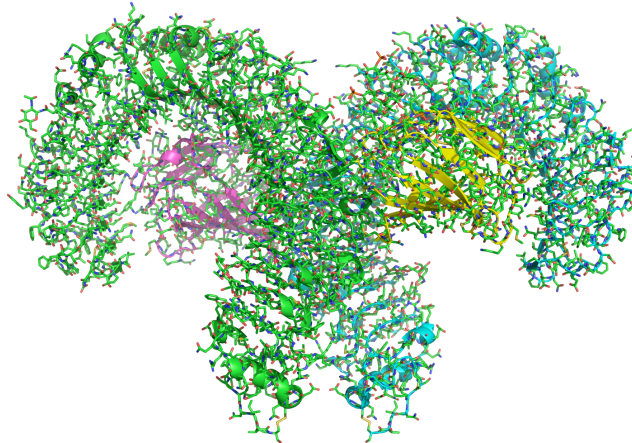


**Figure 15.** TLR4 active multimeric structure generated from the interaction of endotoxin bound MD2 (front and side view). MD2: yellow and violet TLR4: green and light blue

Unexpectedly, the crystal structure of the TLR4-MD-2- LPS complex demonstrates that the size of the MD-2 pocket is unchanged and that additional space for lipid binding is generated by displacing the glucosamine backbone upwards by ,5 Å (Fig. 16).

## 1. Introduction

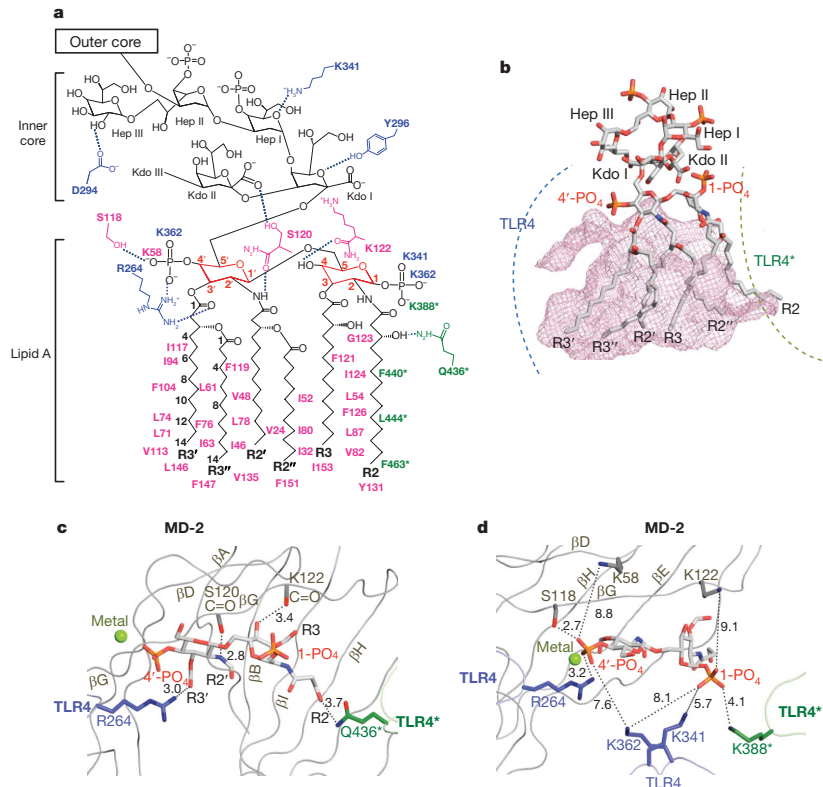


**Figure 16.** Binding of LPS to TLR4 and MD-2. (A) Chemical structure of the Ra chemotype of *E. coli* LPS. Hydrogen bonds are shown by broken blue lines. (B) The molecular surface of the MD-2 pocket is drawn in mesh. (C) Hydrogen bonds between lipid A and TLR4-MD-2. (D) Ionic and hydrogen bond interactions of the two phosphate groups of lipid A. Interaction distances in angstroms are written.

This shift of the glucosamines repositions the phosphate groups such that they can interact with positively charged residues of TLR4 and TLR4\*, thus promoting the dimerization and activation of the receptor complex. Interestingly, the glucosamine backbones of the antagonists are not only translated but also rotated by 180 degrees, so interchanging the two phosphate groups. The structure-activity relationship of the lipid A of LPS has been extensively studied and several factors governing the immunological activity of LPS have been



## 1. Introduction

identified. Of these, the total number of lipid chains is the most important factor. Lipid A with six lipid chains has optimal inflammatory activity, while lipid As with five lipid chains are ,100-fold less active, and those with four lipid chains, such as Eritoran, has anti-endotoxin (antagonist) activity.

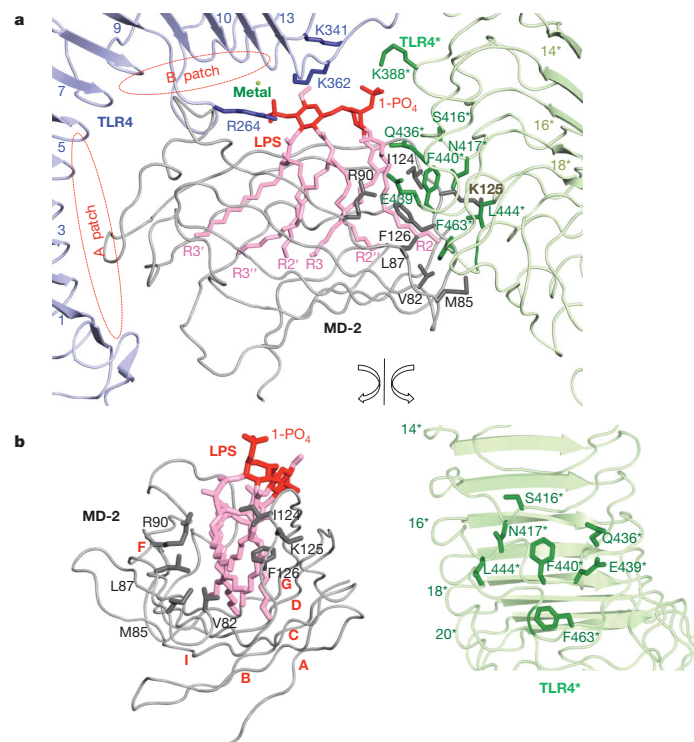


**Figure 17.** The main dimerization interface of the TLR4-MD-2-LPS complex. (A) Overall shape of the main dimerization interface. The primary interface is classified into A and B patches, which are marked in red. (B) The dimerization interface has been split and rotated to show the residues involved. The LRR module numbers of TLR4\* and the b strands of MD-2 are labelled in green and red, respectively.

## 1. Introduction

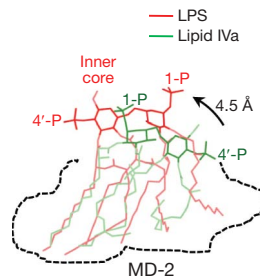


**Figure 18.** Comparison of LPS and lipid IVa. The structures of LPS and lipid IVa are shown after superimposition of MD-2. The shape of the MD-2 pocket is drawn schematically with broken lines.

The lipid chains of LPS interact hydrophobically with MD-2, and hydrophobic interactions are not sensitive to distance and angle, so if the chemical structure of the chains is changed their positions can be shifted to maximize hydrophobic contact. Therefore, in LPS with five or less lipid chains, all the lipid chains probably move further into the pocket to fill the empty space, and there should be substantial energetic penalties when they move back to the surface of MD-2 for dimerization with TLR4\*.

The two phosphate groups in the lipid A region also greatly affect the endotoxic activity of LPS. Deletion of either of these phosphate groups reduces endotoxic activity, 100-fold and the resulting mono-phosphoryl LPS (MPL) is only a weak activator of the human innate immune response<sup>75</sup>. Furthermore, an MPL based on lipid A from *Salmonella minnesota* selectively activates the TLR4-TRAM-TRIF signalling pathway but not the TLR4-Mal-MyD88 pathway<sup>76</sup>. This data suggest that deletion of the 1-phosphate not only weakens the ligand affinity but also induces structural rearrangement of the TLR4-MD-2-adaptor multimer. In the crystal structure, the 1- and 4'-phosphate groups interact with a cluster of positively charged residues from TLR4, TLR4\* and MD-2. Therefore their deletion should have a profound impact on

## 1. Introduction

the receptor–ligand interaction. In natural LPSs, chemical groups such as 2-aminoethylphosphate or L-Ara4N are occasionally attached to the phosphate groups of lipid A24. Previous studies have also shown that removal of the negative charges of the phosphate groups by chemical modification dramatically reduces the potency of LPS, whereas replacing the phosphates with other negatively charged groups such as phosphonoxyethyls, carboxyl and other isosteric groups, has only minor effects<sup>77,78</sup>. This is because the 1- and 49-phosphates in the TLR4–MD-2–LPS complex form mostly medium-range ionic bonds, and there is space for extra atoms in the binding sites. Therefore, substituting other negatively charged groups for the phosphates should not always disrupt binding, although it may modulate the activity of the resulting complexes. Domain swapping data involving horse and human TLR4–MD-2s further support the importance of the phosphate groups in LPS recognition.

## 1.4.1.2. Heme

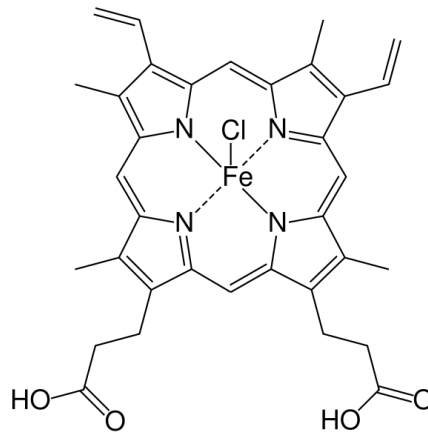


Figure 19. Iron-protoporphyrin IX (heme)

Heme (iron-protoporphyrin IX, in the two oxidation states FeII and FeIII) (Fig. 19), is a molecule that provides a multitude of crucial biological functions as prosthetic moiety in proteins involved in electron transport chains and in enzymes including catalases, peroxidases, cytochromes of P450 class<sup>79</sup>. As free heme may affect a wide spectrum of regulatory factors and can influence gene expression at almost every level by regulating transcription<sup>80,81</sup>. Several pathologic situations of increased hemolysis associated or not with the presence of an infectious agent can lead to very high levels of free heme. These syndromes encompass malaria, sickle cells disease, ischemia, reperfusion hemoglobinopathies, hematoma, hemorrhage, and muscle injury<sup>82</sup>. The presence of free heme released from hemoproteins promotes inflammation and oxidative damage to cells due to the formation oxygen radicals, that catalyze the oxidation of lipids, proteins and DNA. The role of heme in inflammation is dual; small concentration of heme act

## 1. Introduction

cytoprotective via the swift up-regulation of Heme Oxygenase-1 (HO-1), whereas large amount of heme may act as deleterious in tissues via its pro-oxidative and pro-inflammatory functions<sup>83</sup>, which cannot be neutralized anymore by heme-binding proteins or by the same HO-1. Important aspects of heme-induced inflammation have been investigated and clarified: heme promotes the expression of pro-inflammatory adhesion molecules<sup>84</sup> and increases vascular permeability promoting infiltration of leukocytes into a variety of tissues in a mouse model.

A recent paper<sup>85</sup> demonstrate that heme activation of TLR4 receptor complex is unique and rather different from the LPS triggered one. As seen before endotoxin activation is dependent from CD14 and MD2 and could be antagonized with polymyxinB and Eritoran. Heme induce TNF- $\alpha$  production by macrophages in a dose and time-dependent fashion but TNF- $\alpha$  induction is still present at a concentration of polymyxin B that fully abolish the LPS effect. Use of CD14 -/- and MyD88 -/- Knock-out mice demonstrated that those two proteins are necessary for heme-mediated production of TNF- $\alpha$  but, differently from LPS, MD2 is not required for receptor trigger. Selective antagonist of LPS do not abolish heme effect thus suggesting a different activation pattern or a different binding site for this molecule. The activation of TLR4 by heme is exquisitely strict, requiring its coordinate iron and the vinyl groups of the porphyrin ring. The vinyl groups are known to be important for the association of heme with hemeproteins. The selective inhibition of heme-induced TNF- secretion by porphyrins suggests that heme analogs and heme compete for the same binding site.

The Danger model proposes that endogenous molecules from damaged tissues activate the immune system and cause inflammation. Heme seems to act as an inflammatory molecule that could signal tissue

## 1. Introduction

damage through mechanisms dependent and independent of TLR4 without causing DC maturation. The report of apparent lack of in vivo cytokine production by heme and the blocked of heme-induced TNF- $\alpha$  by fetal calf serum in vitro indicate that the interaction of heme and TLR4/CD14 is under a strict control by serum molecules. The involvement of TLR4 in hemolytic and hemorrhagic conditions has been recently demonstrated, but the nature of the putative endogenous ligand remains elusive. In these disorders, the concentrations of heme can reach up to 50  $\mu$ M in the circulation or even higher concentrations in limited areas.

### 1.4.2. Synthetic ligands

#### 1.4.2.1. ERITORAN (E5564)

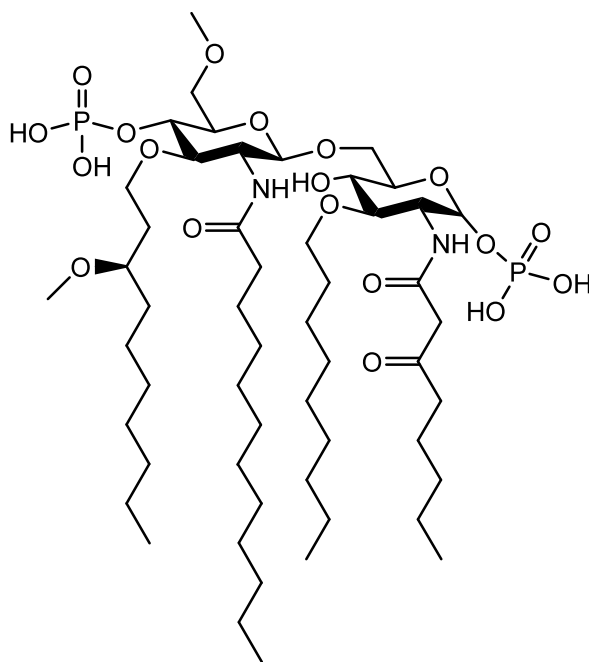


**Figure 20.** Eritoran

$\alpha$ -D-Glucopyranose,3-O-decyl-2-deoxy-6-O-[2-deoxy-3-O-[(3R)-3-methoxydecyl]-6-O-methyl-2-[[[(11Z)-1-oxo-11-octadecenyl]amino]-4-O phosphono-D-glucopyranosyl ] -2-[ ( 1, 3- dioxotetradecyl)amino]-1-(dihydrogen phosphate), tetrasodium salt (E5564) (Fig. 20) is a second-generation synthetic lipodisaccharide designed to antagonize the toxic effects of endotoxin activation<sup>86,87</sup>.

Eritoran (E5564) is one of the first mimetic of lipid A with antagonistic activity. This molecule is actually in phase II clinical trials as antiseptic agent and since its first published synthesis was extensively

## 1. Introduction

characterized both in terms of target and activity.

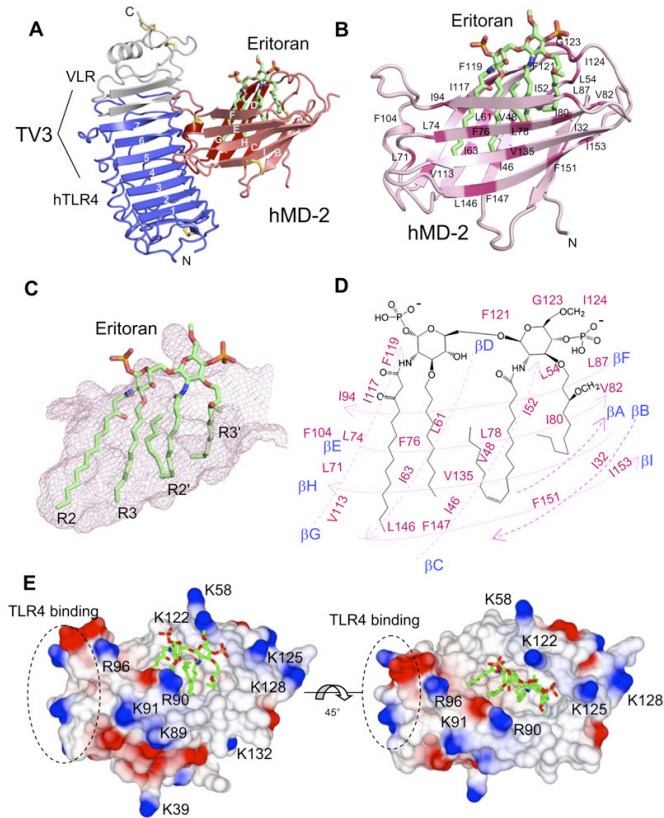


**Figure 21.** Structure of the TLR4-MD-2-Eritoran Complex (A) Overall structure of the TV3-hMD-2-Eritoran complex (TV3 is a chimeric and soluble construct of a TLR4 portion) (B) Closeup view of the human MD-2 and Eritoran complex. The carbon, oxygen, and phosphorous atoms of Eritoran are green, red, and orange, respectively. MD-2 residues interacting with the hydrophobic acyl chains of Eritoran are colored magenta and labeled. (C) Shape of the Eritoran-binding pocket. The surface of MD-2 is drawn in purple mesh. The four acyl chains of Eritoran are labeled. (D) Chemical structure of Eritoran. MD-2 residues interacting with Eritoran are labeled. The b strands are shown schematically as broken arrows. (E) Surface representation of MD-2. Positively and negatively charged surfaces are colored blue and red, respectively. Lysines and arginines interacting ionically with Eritoran are labeled.



## 1. Introduction

In vitro, E5564 inhibited at *in-vitro* nanomolar concentrations lipopolysaccharide LPS-mediated activation of primary cultures of human myeloid cells and mouse tissue culture macrophage cell lines as well as human or animal whole blood as measured by production of tumor necrosis factor- $\alpha$  and other cytokines. E5564 also blocked the ability of Gram negative bacteria to stimulate human cytokine production in whole blood. In vivo, E5564 blocked induction of LPS-induced cytokines and LPS or bacterial-induced lethality in primed mice. Notably E5564 lack agonistic activity when tested both in vitro and in vivo. E5564 blocked LPS-mediated activation of nuclear factor- $\beta$  in toll-like receptor 4/MD-2-transfected cells. Eritoran is actually the only synthetic ligand of TLR4 that has been cocrystallized with the receptor thus becoming a valuable source of information for defining antagonistic properties of TLR4 ligands<sup>73,74</sup>. Eritoran binds to the hydrophobic pocket in human MD-2, and there is no direct interaction between Eritoran and TLR4.

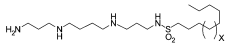
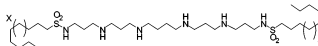
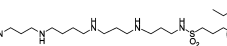
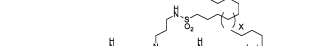
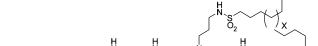
The structure formed by the four acyl chains of Eritoran (Fig. 21) complements the shape of the hydrophobic pocket and snugly occupies almost 90% of the solvent-accessible volume of the pocket, leaving only a narrow groove near its opening. R2 and R3 acyl chains adopt a fully extended conformation, the R20 and R30 acyl chains are bent in the middle. The double bond of the R20 acyl chain has a *cis* conformation, and the chain makes a 180 degree turn at the *cis* double bond to occupy the empty space in the pocket. The di-glucosamine backbone of Eritoran conserved in all LPS molecules is fully exposed to solvent. Although the di-glucosamine sugars do not interact directly with MD-2, the two phosphate groups attached to the backbone form ionic bonds with several positively charged residues located at the opening of the pocket. Those data seem to be in strict agreement with biochemical and

## 1. Introduction

molecular biology data presented in previous papers.

### 1.4.2.2. Polycationic Sulfonamides

The mechanism of action of the antagonists presented so far is based on a competition with LPS for MD2 binding thus reducing or abolishing LPS effect on TLR4. This new class of molecules acts directly on LPS, sequestering endotoxins from solution<sup>88</sup> (Fig. 23).

 <b>Series 1</b>						 <b>Series 3</b>					
MQTS	X	C-Number	ED <sub>50</sub> (μM)	NO inhibition IC <sub>50</sub> (μM)	NFκβ inhibition IC <sub>50</sub> (μM)	MQTS	X	C-Number	ED <sub>50</sub> (μM)	NO inhibition IC <sub>50</sub> (μM)	NFκβ inhibition IC <sub>50</sub> (μM)
1A	0	C8	6.64	1.44	33.3	3A	0	C8 X 2	2.6	0.577	0.607
1B	2	C10	3.7	4.42	0.50	3B	2	C10 X 2	13.5	0.692	4.2
1C	4	C12	2.69	1.34	0.41	3C	4	C12 X 2	55.2	5.00	10.3
1D	8	C16	3.87	0.45	0.28	3D	8	C16 X 2	132.6	6.3	11.7
1E	10	C18	6.01	0.48	0.36	3E	10	C18 X 2	5000	4.22	6.49
 <b>Series 2</b>						 <b>Series 4</b>					
2A	0	C8	2.84	6.47	0.816	4A	0	C8 X 2	2.17	1.82	0.669
2B	2	C10	2.89	1.09	0.278	4B	2	C10 X 2	2.40	1.10	5.17
2C	4	C12	2.92	0.39	0.190	4C	4	C12 X 2	3.98	2.27	13.2
2D	8	C16	4.71	0.12	0.200	4D	8	C16 X 2	26.4	15.1	4.85
2E	10	C18	4.45	0.23	1.06	4E	10	C18 X 2	28.3	2330	64
 <b>Series 5</b>											
5A	0	C8 X 2	2.62	0.32	0.30						
5B	2	C10 X 2	1.16	0.43	2.2						
5C	4	C12 X 2	6.82	0.51	16.4						
5D	8	C16 X 2	9.31	5.2	2.68						

**Figure 23.** Binding Affinity and Biological Activity of Monosubstituted Spermine-Sulfonamide Analogs (SPM, Series 1), Monosubstituted Homologated Spermine-Sulfonamide Analogs (HOMO-SPM, Series 2), Bis-Substituted Bis-Homologated Spermine-Sulfonamide Analogs (Bis-Sub-Bis-

## 1. Introduction

HOMO-SPM, Series 3), Disubstituted Branched Spermine-Sulfonamide Analogs (Branched-SPM, Series 4), Disubstituted Branched Homologated Spermine-Sulfonamide Analogs (Branched-HOMO-SPM, Series 5

It was synthesized a basic scaffold based on spermine and then a library of compounds was created with different direct sulfonylation of the scaffold (fig 23).

Interaction with LPS was assessed through a fluorescent dye displacement and cellular activity demonstrate a correlation between endotoxin sequestration and inhibition in  $\text{NF}\kappa\beta$  production in vitro. In vivo there is a near-millimolar concentration of albumin which bind LPS and could interfere with compounds activity but in this paper<sup>88</sup> is reported a good sequestering activity also in whole blood extracts.

From the screening of the library there was a progressive increase in cell-based LPS-sequestering activities between C8 and C16 analogs for the monosulfonamide analogs in Series 1 and 2.

### 1.4.2.3. TAK-242

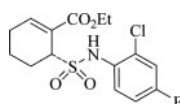


**Figure 24.** TAK-242

ethyl (6R)-6-[N-(2-chloro-4-fluorophenyl)sulfamoyl]cyclohex-1-ene-1-carboxylate (TAK-242) (Fig. 24) has a structure completely different from antagonists seen until now, the structure of this small molecule do not mimic lipid A nor resemble any known TLR4 natural ligand<sup>89</sup>. This molecule was discovered from an HTP screening of a previously synthesized library with potential anti-inflammatory activity. Although

## 1. Introduction

chemical synthesis of this small compound is not public the molecule were extensively tested for its ability to inhibit LPS mediated signaling and authors of the cited paper suggest a target protein. As for other TLR4 antagonist TAK-242 inhibit cytokines induced after LPS exposure in macrophages and dendritic cells and reduce their mRNA expression compared to LPS only exposed cells. Noteworthy the effect of TAK-242 is completely independent from CD14, and seems to rely only in MD2 interaction. Literature report other cases of aromatic ring containing molecules that selectively interact with MD2, some amongst the best studied are taxanes and the bis-ANS hydrophobic probe. For both molecules it was clearly demonstrated that CD14, even though it is an important step in LPS recognition, it is not involved in molecules activity. Their target protein is, in all the three cases, MD2 that seems to accepts hydrophobic molecules, probably in the shallow cleft where lipid A chains are usually accommodated.

### 1.4.2.4. Monomeric antagonists

In the laboratory where this project was performed was previously synthesized<sup>90,91</sup> a library of lead compounds based on a D-Glucose scaffold with two lipophylic appendages (C14) and several different substitution in position 6 of the saccharide scaffold (fig 25).

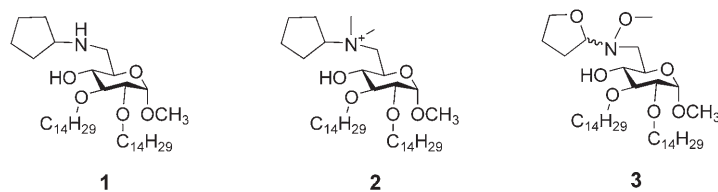


**Figure 25.** Synthetic disaccharide antagonists, Glucose derivatives 1, 2,

# 1. Introduction

and 3.

Those compounds were tested for their ability in inhibiting Lipid A-stimulated cytokine production in cells of the innate immune system such as macrophages and dendritic cells (fig 26 and 27).

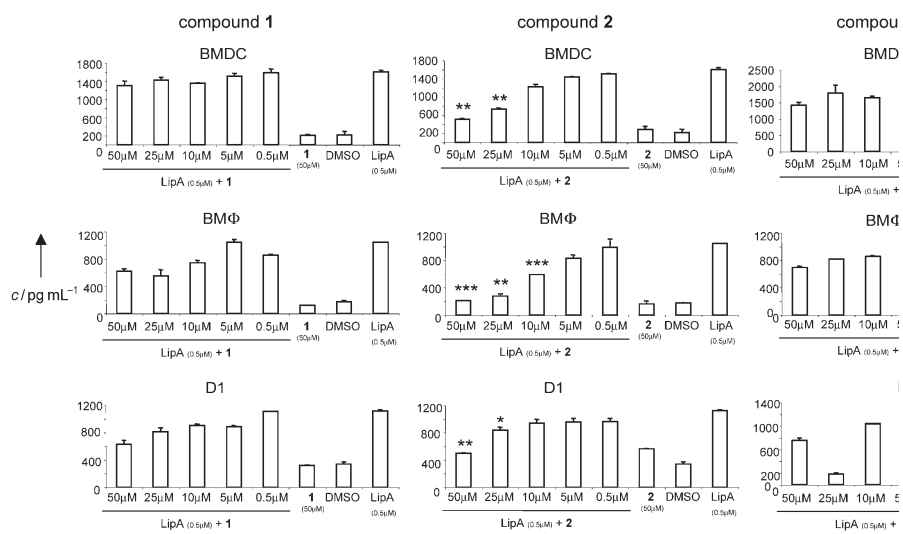


**Figure 26.** Antagonistic activity of monosaccharides 1–3 towards BMDC, BMΦ, and D1 cells. From right to left : lipid A (0.5 μM): cells treated with lipid A alone ; DMSO : cells incubated in the presence of the complete medium plus DMSO ; inhibitor (50 μM): cells treated only with monosaccharides 1–3 ; other columns : lipid A plus compounds 1–3 in increasing doses.

## 1. Introduction

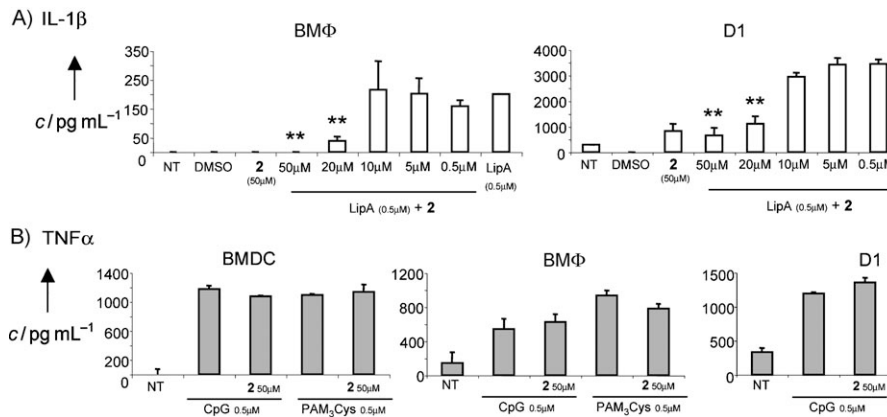


**Figure 27.** Selectivity of the monosaccharide **2** for TLR4. A) The antagonistic activity of compound **2** was investigated by testing its ability to interfere with lipid A induced IL-1 $\beta$  production B) TNF $\alpha$  production measured by ELISA 24 h after stimulation with CpG or PAM $_3$ Cys in the presence of compound **2**.

Selectivity for TLR4 receptor complex was assessed treating the same cell lines with other TLRs agonist and was observed no decrease in TNF- $\alpha$  production (fig 27 B). To further assess the specificity of those compounds NF- $\kappa$ B levels of HEK-TLR4 or HEK-TLR9 was measured after pretreatment with compounds and subsequent with, respectively, LipidA or CpG. Results shown a selective inhibition of NF- $\kappa$ B production in HEK-TLR4, but no effect on HEK-TLR9 cells. Taken together, these evidences suggest a selective action of compound **2** on the TLR4 signal pathway. Recent evidence indicates a pivotal role of TLR4 in the development and maintenance of some other pathologies such inflammation or painful neuropathies<sup>92</sup>. It was observed an interesting activity of compound **2** in inhibiting both neuropathic pain<sup>92</sup> and carrageenan-induced acute local inflammation in animal models.

## **2. MATERIALS AND METHODS**

### ***2.1. Introduction to materials and methods section***

The synthesis was guided by the lead compounds synthesized from the research group in which the PhD thesis was developed<sup>93</sup>.

The work was then focalized on the development of new screening assays to asses the activity of newly synthesized compounds. It was decided to screen these compounds on three sequential and different levels. In the first level we used a simple and reliable screening assay based on HEK-blue cells that presents the whole array of components needed for TLR4 receptor complex activation and signal trasduction but presents a reporter gene under control of NfKb promoter. HEK-BLUE assay was parallelized with the screening on HEK-TLR4 cells supplemented with purified MD2, CD14 and LBP to have a more detailed control on every LPS recognition and binding step. More promising molecules were studied for their target using biochemical assays based on the purified components of the extracellular TLR4 complex. With this kind of assay was possible to determine the target protein of active compounds leading to the possibility of a more rational design of a new generation of antagonists. Using this two screening levels we decided to discover the activity of a natural nut poorly studied TLR4 ligand. We then decided to further use those powerful biochemical techniques in combination with HEK-TLR4 cells assay to study the influence of a different LPS presentation. To provide a more stable and controlled LPS structure we coated oleic acid functionalized magnetic nanoparticles with LPS molecules.

## 2.2. Chemical section

### 2.2.1. General section

**Reagents and solvents for chemical synthesis:** reagents and solvents were purchased from Fluka or Merck and used with no further purification. Compound 3,4,11 were previously synthesized and purified from the research group of Prof. Francesco Peri<sup>92,93</sup>.

**Thin layer chromatography (TLC):** TLC were performed using as a solid phase Merck K60 (F254) silica gel.

Following solutions were used for detection:

- *Ammonium molybdate:* 21 g di  $(\text{NH}_4)\text{Mo}_7\text{O}_{24}$  + 1 g di  $\text{Ce}(\text{SO}_4)$  in 500 ml of  $\text{H}_2\text{O}$  and 31 ml of concentrate  $\text{H}_2\text{SO}_4$ ;
- *Sulfuric acid:* 45 ml EtOH + 45 ml  $\text{H}_2\text{O}$  + 10 ml  $\text{H}_2\text{SO}_4$ ;
- *Ninhydrin:* 0.2 g di ninhydrin in 100 ml EtOH.

TLC were developed heating at 100°C. UV (254 nm) detection was made when possible.

**Chromatography:** Merck 230/400 mesh silica gel were used and was performed according to the protocol described in *J. Org. Chem.*, **1978**, 93, 14.

**NMR spectroscopy:** NMR spectra were done using a Varian Mercury 400 MHz at a temperature of 300 K°. Chemical shifts were described according to TMS signal.



## 2. Materials and methods

**Mass spectrometry:** mass spectra were acquired with an ESI MS model API 2000 QTrap from Applied Biosystem.

### 2.2.2. Antagonists synthesis

#### 2.2.2.1. Synthetic pathway of compound 7

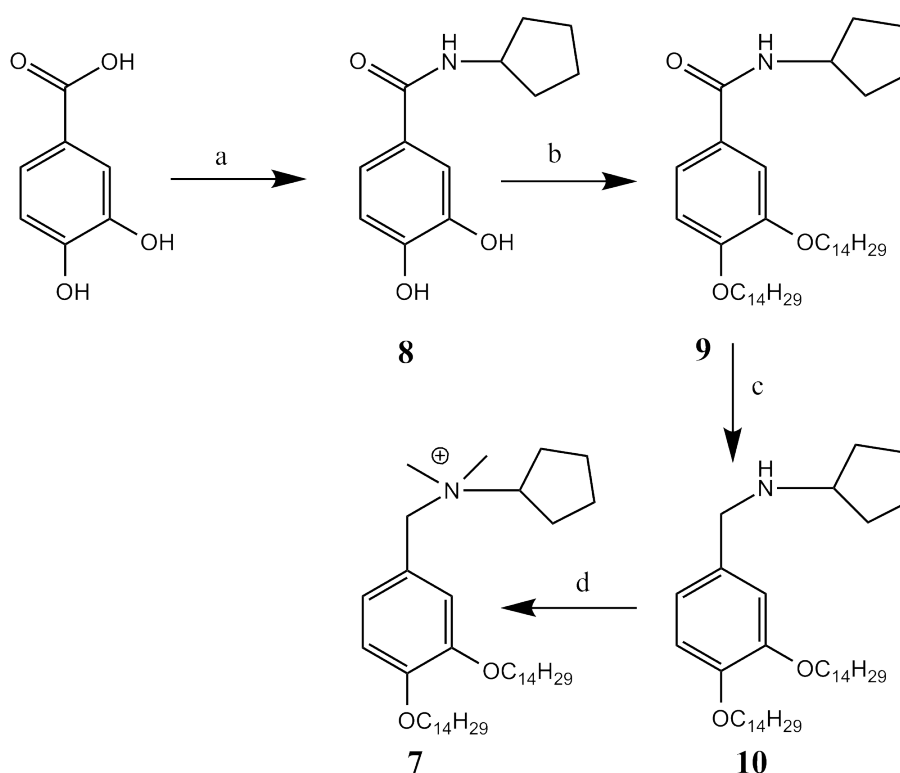
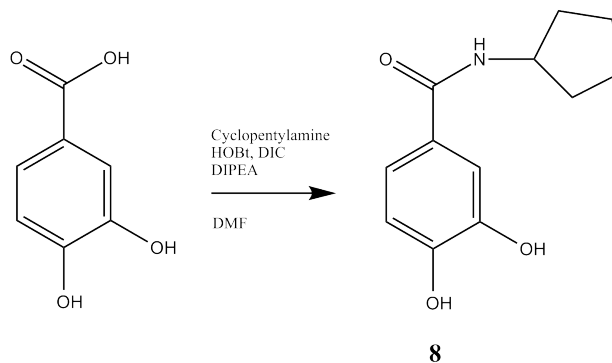


**Figure 4.** a) cyclopentylamine, HOBt, DIC, DIPEA, DMF, 84%; b)  $C_{14}H_{29}Br$ , NaH, DMF, 60%; c)  $LiAlH_4$ , THF, 30%; d)  $CH_3I$ ,  $Na_2CO_3$ , 90%.

## 2. Materials and methods

### COMPOUND 8 (N-cyclopentyl-3,4-dihydroxybenzamide)



COMPOUND	MW	MMOL	EQ.	DENSITY	QUANTITY
3,4-Dihydroxybenzoic acid	154	6,4	1,2		1 g
cyclopentylamine	85	5,32	1		524,4 $\mu$ l
HOBt	135	7,98	1,5		1078,3 mg
DIC	126	7,28	1,5	0.315	1235,6 $\mu$ l
DIPEA	129	15,98	3	0.755	2732,2 $\mu$ l
DMF				0,94	15 ml

#### Procedure:

3,4-Dihydroxybenzoic acid is solubilized in Dry DMF and cyclopentylamine, HOBt, DIC and DIPEA. Reaction was stirred under Ar for 12h and monitored with TLC ( $\text{CHCl}_3/\text{MeOH}$  7:3). When reaction was complete solvent was evaporated under reduced pressure and washed with HCl 1N,  $\text{NaHCO}_3$  and brine, using  $\text{CH}_2\text{Cl}_2$  as organic solvent. Organic

## 2. Materials and methods

phase was treated with sodium sulfate and filtered. Compound was purified with flash chromatography (CHCl<sub>3</sub>/MeOH 9,5:0,5).

Yeld= 84%

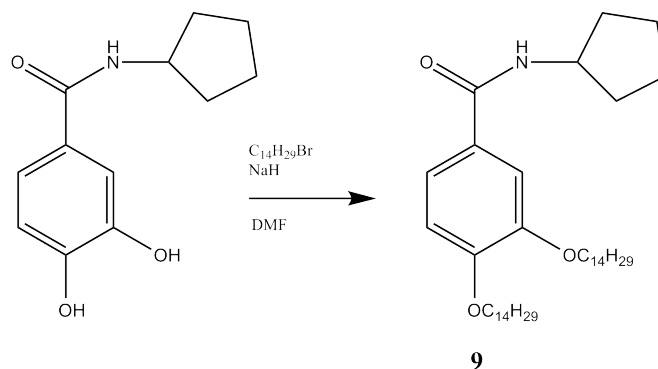
C<sub>12</sub>H<sub>15</sub>NO<sub>3</sub>, PM: 221,25

<sup>1</sup>H-NMR (CDCl<sub>3</sub>) δ(ppm): 7.25 (d, 1H, *J*=2.14 Hz, H-1), 7.18 (dd, 1H *J*=2.16, 8.26 Hz, H-3), 6.77 (d, 1H *J*=8.26 Hz, H-2), 4.26 (quint, 1H, *J*=5.17 Hz, H1'), 1.99 (m, 2H, 2xH2'), 1.76 (m, 2H, 2xH3'), 1.60 (m, 4H, 2xH3', 2xH2').

<sup>13</sup>C-NMR (CDCl<sub>3</sub>) δ (ppm)= 152.68, 130.14, 123.32, 118.55, 118.47, 55.68, 52.40, 52.18, 51.97, 51.76, 51.55, 51.33, 51.11, 45.44, 36.22, 36.19, 27.77, 26.29.

## 2. Materials and methods

### COMPOUND 9 (*N*-cyclopentyl-3,4-bis(tetradecyloxy)benzamide)



COMPOUND	MW	MMOL	EQ.	DENSITY	QUANTITY
8	221	3.25	1.2		720 mg
$C_{14}H_{29}HBr$	277	7.33	2.2	1.016	2 ml
NaH	24	9.75	3		390 mg
DMF dry				0.94	35 ml

#### Procedure:

Compound 8 was dissolved in dry DMF then NaH was added and  $C_{14}H_{29}HBr$  drop in reaction mixture. Reaction was allow to complete in 2h at 60°C (TLC clorophorm)

Then reaction was refrigerate in ice at 0°C and added MeOH. Solvents were evaporated in reduced pressure and raw material washed with HCl 1N and brine using acetone as organic solvent. Organic phase was treated with sodium sulfat and filtered. Compound was purified with a light petroleum titration.

Yeld= 60%

## 2. Materials and methods

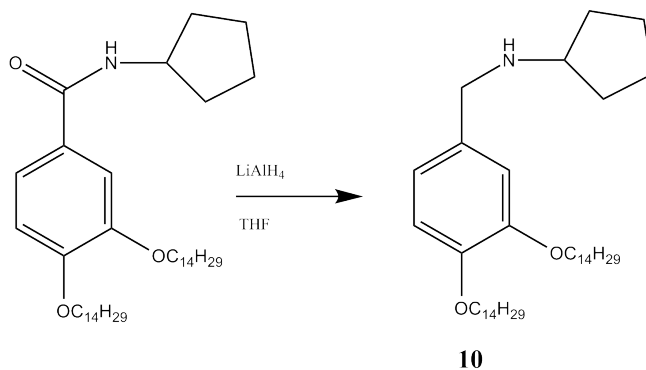
C<sub>40</sub>H<sub>71</sub>NO<sub>3</sub>, MW: 613,54

<sup>1</sup>H-NMR (CDCl<sub>3</sub>) δ(ppm) = 7.37 (d, 1H, J=2.14 Hz, H-1), 7.18 (dd, 1H J=2.16, 8.26 Hz, H-3), 6.77 (d, 1H J=8.26 Hz, H-2), 4.26 (quint, 1H, J=5.17 Hz, H1'), 1.99 (m, 2H, 2xH2'), 1.76 (m, 2H, 2xH3'), 1.60 (m, 4H, 2xH3', 2xH2').

<sup>13</sup>C-NMR (CDCl<sub>3</sub>) δ (ppm)= 167.02, 151.94, 149.14, 127.63, 119.37, 113.08, 112.39, 76.94, 69.32, 69.34, 51.88, 33.49, 32.17, 29.95, 29.86, 29.65, 29.61, 29.45, 29.35, 26.23, 24.06, 22.94, 14.37.

MS (MALDI-TOF): m/z: 614.2 [M+H]<sup>+</sup>, 637.3 [M+Na]<sup>+</sup>.

### COMPOUND 10 (N-(3,4-bis(tetradecyloxy)benzyl)cyclopentanamine)



COMPOUND	MW	MMOL	EQ.	DENSITY	QUANTITY
9	614	1,3			800 mg
LiAlH <sub>4</sub>	37,9	3,9	3		3,9 ml
THF				0.89	50 ml

## 2. Materials and methods

### Procedure:

Compound 9 was dissolved in dry THF then LiAlH<sub>4</sub> was dropped in reaction mixture. Reaction was allow to complete in 12h at 60°C (TLC clorophorm)

Then reaction was refrigerate in ice at 0°C and added MeOH. Solvents were evaporated in reduced pressure and raw material washed with brine and clorophorm. Organic phase was treated with sodium sulfate and filtered. Compound was purified with flash chromatography (CHCl<sub>3</sub>/AcOEt 9,5:0,5).

Yeld= 30%

C<sub>40</sub>H<sub>73</sub>NO<sub>2</sub>, MW: 599,56

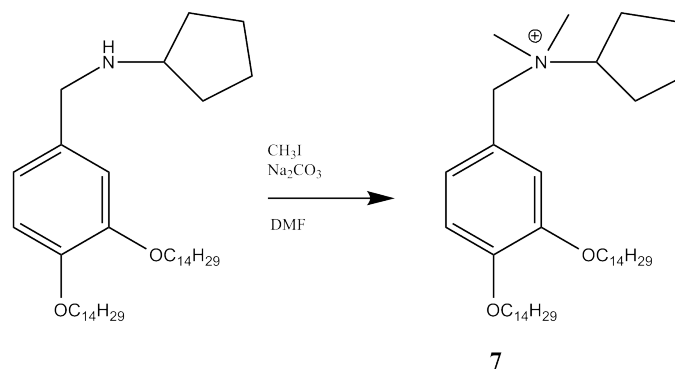
<sup>1</sup>H-NMR (CDCl<sub>3</sub>) δ(ppm) = 0.81 (t, 6H, *J*=6.86, 6.86 Hz, 2xCH<sub>3</sub> aliph), 1.21 (m, 44H, 2xC<sub>11</sub>H<sub>22</sub>), 1.38 (m, 2H, 2xH<sub>3</sub>'), 1.48 (m, 2H, 2xH<sub>3</sub>'), 1.61 (m, 2H, CH<sub>2β</sub>), 1.75 (m, 6H, 4xH<sub>2</sub>', CH<sub>2β</sub>), 3.03 (quint, 1H, *J*=6.8, Hz, H-1'), 3.62 (s, 2H, CH<sub>2</sub> benz), 3.89 (t, 2H, *J*=6.58, 6.58 Hz, 2xH<sub>α</sub>), 3.92 (t, 2H *J*=6.57, 6.57 Hz, 2xH<sub>α</sub>), 6.74 (m, 2 H, H<sub>arom</sub>), 6.80 (m, 1H, H<sub>arom</sub>).

<sup>13</sup>C-NMR (CDCl<sub>3</sub>) δ (ppm)= 149.41, 148.32, 148.02, 143.89, 143.05, 130.74, 125.76, 120.73, 114.33, 144.15, 94.76, 77.25, 76.93, 76.47, 69.67, 69.47, 64.31, 59.28, 57.74, 52.71, 51.61, 33.5, 33.28, 32.17, 30.54, 30.07, 29.95; 29.91, 29.89, 29.69, 29.61, 28.82, 26.28, 24.34, 22.93, 17.31 (CH<sub>2</sub> of C<sub>14</sub> chains); 14.37 (CH<sub>3</sub>alif).

MS (MALDI-TOF): *m/z*: 601.15 [M+H]<sup>+</sup>, 624.01 [M+Na]<sup>+</sup>.

## 2. Materials and methods

### COMPOUND 7 (N-(3,4-bis(tetradecyloxy)benzyl) N'-N''-dimethylcyclopentylamonium)



COMPOUND	MW	MMOL	EQ.	DENSITY	QUANTITY
10	600	0,05			30 mg
CH3I	142	0,1	2	2,280	6,2 $\mu$ l
Na <sub>2</sub> CO <sub>3</sub>	105	0,15	3		15,89 mg
DMF dry				0.94	2 ml

#### Procedure:

Compound 10 was dissolved in dry DMF then Na<sub>2</sub>CO<sub>3</sub> e CH<sub>3</sub>I were added. Reaction was allow to complete in 3h at 60°C (TLC CHCl<sub>3</sub>/MeOH 9:1)

Solvents were evaporated in reduced pressure and raw material extracted from water with clorophorm. Organic phase was treated with sodium sulfate and filtered. Compound was purified with a light petroleum titration.

Yeld= 90%

## 2. Materials and methods

$C_{42}H_{78}NO_2^+$ , MW: 628,6

$^1H$ -NMR ( $CDCl_3$ )  $\delta$ (ppm) = 7.30 (d, 1H,  $J=2.1$  Hz, H-1), 7.12 (dd, 1H,  $J=2.1$ , 8.2 Hz, H-3), 6.86 (d, 1H,  $J=8.2$  Hz, H-2), 4.82 (s, 2H,  $CH_2$  -N), 4.26 (quint, 1H,  $J=8.3$  Hz, H1'), 4.05 (t, 2H  $J=6.4$  Hz,  $2xH\alpha$ ), 3.98 (t, 2H,  $J=6.5$ , Hz,  $2xH\alpha$ ), 3.13, 3.13 (s 3H  $CH_3N$ , s 3H,  $CH_3N$ ), 2.15 (m, 2H,  $2xH2'$ ), 1.98 (m, 2H,  $2xH2'$ ), 1.82 (m, 6H,  $2xCH_2\beta$ ,  $2xH3'$ ), 1.59 (m, 44H,  $2xC_{11}H_{22}$ ), 0.87 (bt, 6H  $J=6.85$ , 6.85 Hz,  $2xCH_3$  aliph).

$^{13}C$ -NMR ( $CDCl_3$ )  $\delta$  (ppm)= 151.29, 149.411, 126.4, 119, 118.39, 113.19, 77.3, 76.98, 74.3, 70.15, 69.28, 67.48, 47.397 ( $CH_3$  legati all'N); 32.157, 29.95, 29.91, 29.78, 29.693, 29.61, 29.53, 29.37, 27.17, 26.27, 24.4, 22.9 ( $CH_2$  delle catene  $C_{14}$  lineari) ; 14.36 ( $CH_3$ ).

MS (MALDI-TOF): m/z: 629.1  $[M+H]^+$ , 752.07  $[M+Na]^+$ .



## 2. Materials and methods

### 2.2.2.2. Synthesis pathway of compounds 1, 2, 5, 6

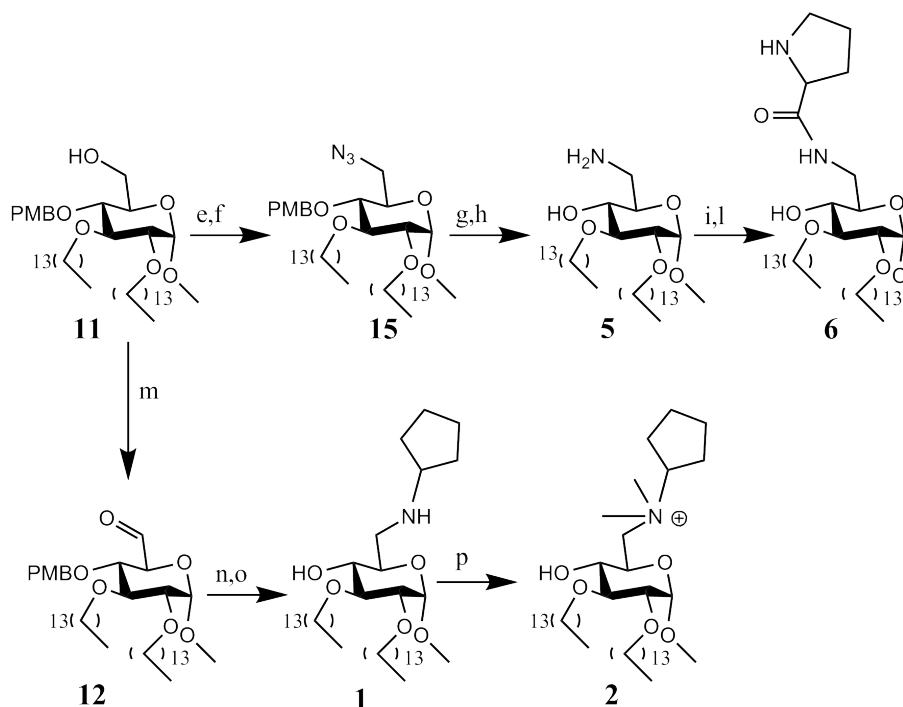
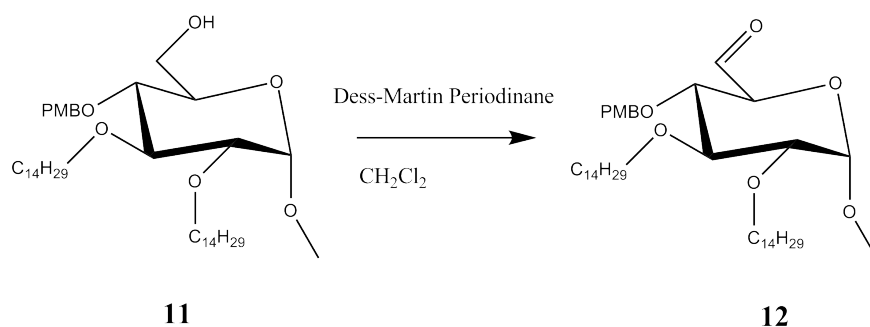


**Figure 5.** Reagents and conditions: (m) Dess-Martin periodinane,  $\text{CH}_2\text{Cl}_2$ , rt, 1h; (n) cyclopentylamine,  $\text{NaBH}_3\text{CN}$ , AcOH,  $\text{CH}_2\text{Cl}_2$ , MeOH, 24 °C, 12 h; (o) trifluoroacetic acid,  $\text{CH}_2\text{Cl}_2$ , 24 °C, 1h; (p)  $\text{CH}_3\text{I}$ ,  $\text{Na}_2\text{CO}_3$ , DMF, 24 °C, 12 h; (e)  $\text{MsCl}$ , pyridine, 24 °C, 5h; (e)  $\text{TsCl}$ , DMAP, pyridine, 24 °C, 12 h; (f)  $\text{NaN}_3$ , TBAI, DMF, 75 °C, 4 h; (g)  $\text{PPh}_3$ ,  $\text{H}_2\text{O}$ , THF, 70 °C; (h) *N*-Fmoc-Pro, HOBT, DIC, DIPEA, DMF, 24 °C, 4h; (l) piperidine/DMF 2:8, 24 °C, 1h.

## 2. Materials and methods

### COMPOUND 12 (Methyl 4-*O*-(4-methoxybenzylidene)-2,3-di-*O*-tetradecil- $\alpha$ -D-glucosodialdo-1,5-pyranose



COMPOUND	MW	MMOL	EQ.	DENSITY	QUANTITY
11	706	2.12	1		1.5 g
Dess-Martin Periodinano	424	3.18	1.5		2.34 g
CH <sub>2</sub> Cl <sub>2</sub> dry				1,33	10 ml

#### Procedure:

Compound 11 was prepared as previously described. The compound was dissolved in dry CH<sub>2</sub>Cl<sub>2</sub> then Dess-Martin periodinane was. Reaction was stirred to completion for 3h at rt (TLC EDP:AcOEt 8:2)

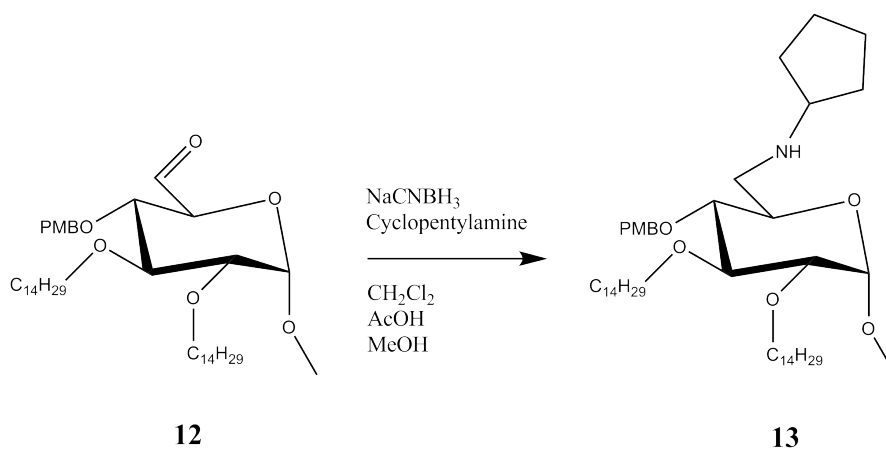
Then saturated aqueous solution of NaHCO<sub>3</sub>/Na<sub>2</sub>S<sub>2</sub>O<sub>3</sub> was added and compound extracted with CH<sub>2</sub>Cl<sub>2</sub> and the same extraction repeated with brine. Organic phase was treated with sodium sulfate and filtered.

## 2. Materials and methods

Compound require no further purification and being instable is used directly for the next reaction without characterization.

$C_{43}H_{76}O_7$ , MW: 705,0

### COMPOUND 13 (Methyl 6-deoxy-6-ciclopentylamino-4-O-(4'-methoxy benzyl)-2,3-di-O-tetradecil- $\alpha$ -D-glucopyranoside)



COMPOUND	MW	MMOL	EQ.	DENSITY	QUANTITY
12	674	2,427	1		1,69 g
Cyclopentilamine	85	9,708	4	0,862	970 $\mu$ l
NaCNBH <sub>3</sub>	62	9,708	4		641 mg
MeOH dry				0,79	8ml
AcOH				1,05	500 $\mu$ l
CH <sub>2</sub> Cl <sub>2</sub> dry				1,33	20 ml

## 2. Materials and methods

### Procedure:

Compound 12 is dissolved in dry AcOH, CH<sub>2</sub>Cl<sub>2</sub> and MeOH . After addition of NaCNBH<sub>3</sub> reaction was stirred for 2h at 60°C (TLC Tol/AcOEt 7:3).

Then solvents are evaporated under reduced pressure and added saturated aqueous solution of NaHCO<sub>3</sub> with a following extraction in CH<sub>2</sub>Cl<sub>2</sub> and the same extraction repeated with brine. Organic phase was treated with sodium sulfate and filtered. Compound was purified with flash chromatography (MeOH/AcOEt 0,5:9,5).

Yield=75%

C<sub>48</sub>H<sub>88</sub>NO<sub>6</sub>, MW: 774,6604

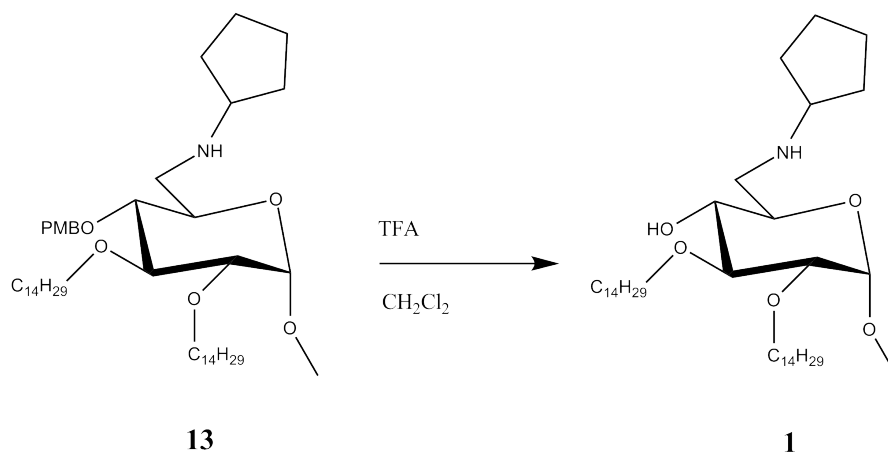
<sup>1</sup>H-NMR (CDCl<sub>3</sub>) δ = 0.95 (m, 6H), 1.21 (m, 44H), 1.40-1.60 (m, 12 H), 2.62 (dd, 1H, J =12.1, 6.8 Hz), 2.84 (dd, 1H, J =12.1, 2.8 Hz), 3.00 (quintet, 1H, J =6.8 Hz), 3.26 (dd, 1H, J =9.6, 3.4 Hz), 3.31 (t, 1H, J= 9.3 Hz), 3.37 (s, 3H), 3.50-4.0 (m, 6H), 3.79 (s, 3H), 4.55-4.80 (ABq, 2H), 4.71 (d, 1H, J=3.5 Hz), 6.80-7.20 (A<sub>2</sub>X<sub>2</sub>, 4H).

<sup>13</sup>C NMR (400 MHz, CDCl<sub>3</sub>): δ=14.6, 23.1, 26.4, 26.7, 29,8, 29,9-30.1 (CH<sub>2</sub> of C<sub>14</sub> chains), 31.0, 32.4, 49.5, 55.59, 55.64, 59.9, 69.6, 72.0, 74.0, 74.8, 79.4, 81.1, 81.9, 98.1, 114.0, 129.9, 130.8, 159.4.

MS (MALDI-TOF): m/z: 775 [M+H]<sup>+</sup>, 797.6 [M+Na]<sup>+</sup>

## 2. Materials and methods

### COMPOUND 1 (Methyl 6-deoxy-6-ciclopentylamino-2,3-di-O-tetradecil- $\alpha$ -D-glucopyranoside)



COMPOUND	MW	MMOL	EQ.	DENSITY	QUANTITY
13	774	1,29			1 g
TFA				1,48	4 ml
CH <sub>2</sub> Cl <sub>2</sub> dry				1,33	4 ml

#### Procedure:

Compound 13 is dissolved in dry CH<sub>2</sub>Cl<sub>2</sub>. After addition of TFA at 0°C reaction was stirred for 1h at rt (TLC AcOEt /MeOH 9:1).

Then solvents are evaporated under reduced pressure and added saturated aqueous solution of NaHCO<sub>3</sub> with a following extraction in CH<sub>2</sub>Cl<sub>2</sub> and the same extraction repeated with brine. Organic phase was treated with sodium sulfate and filtered. Compound was purified with flash chromatography (AcOEt/MeOH 9.5/0.5).

## 2. Materials and methods

Yield=80%

$C_{40}H_{80}NO_5$ , MW: 653,60

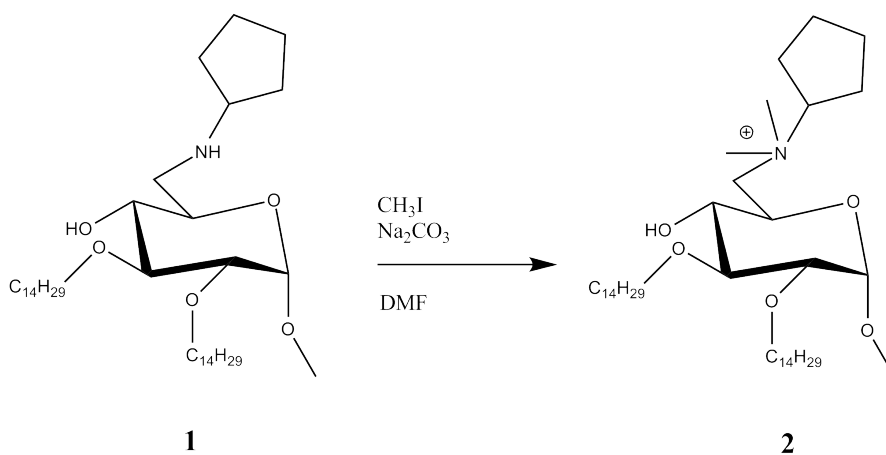
$[\alpha]^{20}_D$ : +18,4 (c 0,5 in  $CHCl_3$ )

$^1H$ -NMR ( $CDCl_3$ )  $\delta$ = 0.95 (m, 6H), 1.21 (m, 44H), 1.40-1.60 (m, 12 H), 2.59 (bs, 1H), 2.81 (dd, 1H,  $J$ =11.9, 7.6 Hz), 2.97 (dd, 1H,  $J$ =11.9, 4.9 Hz), 3.09 (quint., 1H,  $J$ =6.6 Hz), 3.26 (dd, 1H,  $J$ =9.3, 3.5 Hz), 3.40 (s, 3H), 3.40-3.60 (m, 5H), 3.71 (m, 1H), 3.81 (m, 1H), 4.72 (d, 1H,  $J$ =3.6 Hz).  $^{13}C$ -NMR ( $CDCl_3$ )  $\delta$ = 14.6, 23.1, 24.33, 24.37, 26.4, 26.5, 29.8, 29.9-30.1 ( $CH_2$  of  $C_{14}$  chains), 30.8, 32.3, 33.1, 33.4, 51.7, 55.6, 60.3, 68.6, 71.9, 74.0, 75.6, 80.5, 81.2, 98.5.

MS (MALDI-TOF): m/z:  $[M+H]^+$ : 654.6031,  $[M+Na]^+$ : 676.5850.

## 2. Materials and methods

### COMPOUND 2 (Methyl 6-deoxy-6-*N,N',N''*-dimethylcyclopentyl-amonium-2,3-di-*O*-tetradecyl- $\alpha$ -D-glucopyranoside)



COMPOUND	MW	MMOL	EQ.	DENSITY	QUANTITY
1	654	0,115	1		75,7 mg
CH <sub>3</sub> I	141,94	0,347	3	2,280	21,6 $\mu$ l
Na <sub>2</sub> CO <sub>3</sub>	105,99	0,463	4		49 mg
DMF dry				0,94	1,5 ml

#### Procedure:

Compound 1 is dissolved in dry DMF. After addition of Na<sub>2</sub>CO<sub>3</sub> and CH<sub>3</sub>I reaction was stirred for 1h at rt (TLC AcOEt/MeOH 7:3).

Then solvents are evaporated under reduced pressure and added water with a following extraction in CH<sub>2</sub>Cl<sub>2</sub>. Organic phase was treated with sodium sulfate and filtered. Compound require no further purification.

Yield=94%

## 2. Materials and methods

$C_{42}H_{85}NO_5$ , MW: 682,63

$[\alpha]^{20}_D$ : 21,6 (c 0,5 in  $CHCl_3$ )

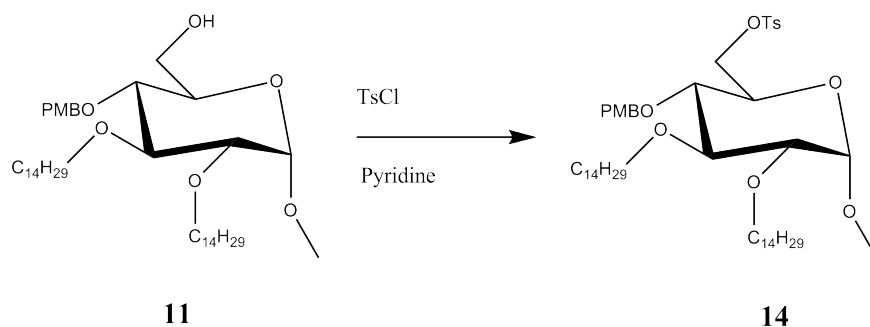
$^1H$ -NMR ( $CDCl_3$ )  $\delta$ = 0.80 (bt, 6H,  $J$ = 6.8 Hz), 1.21 (m, 44H), 1.51 (m, 4H), 1.66 (m, 1 H), 1.80 (m, 2H), 2.15 (m, 1H), 3.13 (dd, 1H,  $J$  =9.8, 3.5 Hz), 3.21 (s, 3H), 3.23 (s, 3H), 3.32 (bt, 1H,  $J$ =9.2 Hz), 3.42 (s, 3H), 3.40-3.55 (m, 4H), 3.68 (bt, 1H,  $J$ =6.9 Hz), 3.91 (bs, 1H), 4.05 (bt, 1H,  $J$ =9.0 Hz), 4.13 (bt, 1H,  $J$ =8.5 Hz), 4.19 (d, 1H,  $J$ =14.1 Hz), 4.66 (d, 1H,  $J$ =3.5 Hz).  $^{13}C$ -NMR ( $CDCl_3$ )  $\delta$ = 14.6, 23.1, 24.33, 24.37, 26.4, 26.5, 29.8, 29.9-30.1 ( $CH_2$  of  $C_{14}$  chains), 30.8, 32.3, 50.5, 57.8, 66.1, 67.3, 71.7, 72.3, 74.0, 76.7, 79.7, 80.2, 99.6.

MS (MALDI-TOF): m/z:  $[M+H]^+$ : 682.634.



## 2. Materials and methods

### COMPOUND 14 (Methyl 6-tosyl-4-O-(4-methoxybenzyl)-2,3-di-O-tetradecyl- $\alpha$ -D-glucoopyranoside)



COMPOUND	MW	MMOL	EQ.	DENSITY	QUANTITY
11	707	4.24			3 g
TsCl	190	6.36	1.5		1.21 g
DMAP					Cat
Py dry					36.4 ml

#### Procedure:

Compound 11 is dissolved in dry Py. After addition of TsCl and DMAP (at 0°C) reaction was stirred for 21h at rt (TLC EDP/AcOEt 8:2).

Then solvents are evaporated under reduced pressure and purified with flash chromatography (AcOEt/EDP 9:1).

Yield=100%

C<sub>50</sub>H<sub>84</sub>O<sub>9</sub>S, MW: 861.6

## 2. Materials and methods

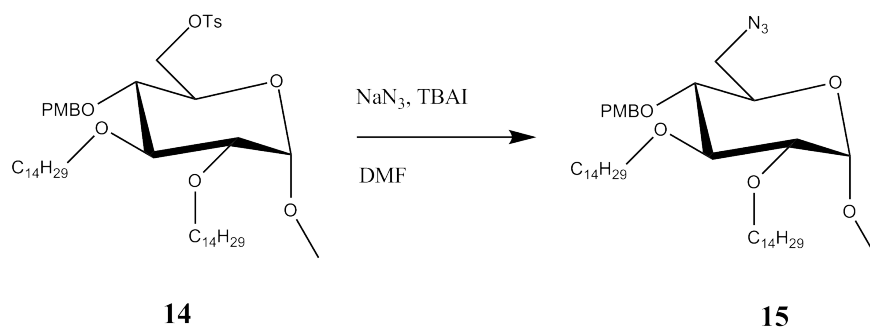
$^1\text{H}$  NMR (400 MHz,  $\text{CDCl}_3$ ),  $\delta(\text{ppm}) = 7.78$  e  $7.31$  (AA'XX' system, 4H,  $J = 8.8$  Hz,  $\text{H}_{\text{TOSYL}}$ );  $7.14$  e  $6.84$  (AA'XX' system, 4H,  $J = 8.5$  Hz,  $\text{H}_{\text{PMB}}$ );  $4.76$  e  $4.38$  (AB system, 2H,  $J = 3.5$  Hz,  $\text{CH}_2$  del PMB);  $4.69$  (d, 1H,  $J = 3.5$  Hz, H-1);  $4.20$  (dd, 1H,  $J = 10.4, 4.2$  Hz, H-6a);  $4.15$  (dd, 1H,  $J = 10.4, 4.2$  Hz, H-6b);  $3.80$  (s, 3H,  $\text{OCH}_3$ );  $3.72$ – $3.90$  (m, 7H, H-3, H-5, H-4, H- $\alpha$ );  $3.35$  (s, 3H,  $\text{OCH}_3$ );  $3.20$  (dd, 1H,  $J = 3.5, 9.7$  Hz, H-2);  $2.42$  (s, 3H,  $\text{CH}_3$  tosyl);  $1.57$  (m, 4H,  $\text{H}\beta$  del  $\text{C}_{14}$ );  $1.24$  (s, 44H,  $\text{CH}_2$  of  $\text{C}_{14}$ );  $0.89$  (t, 6H,  $J = 5.8$  Hz,  $\text{CH}_3$  del  $\text{C}_{14}$ ).

$^{13}\text{C}$ -NMR ( $\text{CDCl}_3$ ),  $\delta$  (ppm) =  $159.5$  ( $\text{C}_{\text{PMB}}$ );  $145.0$  ( $\text{C}_{\text{Ts}}$ );  $133.0$  ( $\text{C}_{\text{Ts}}$ );  $130.3$  ( $\text{C}_{\text{Ts}}$ );  $130.0$  ( $\text{C}_{\text{PMB}}$ );  $129.9$  ( $\text{C}_{\text{PMB}}$ );  $128.2$  ( $\text{C}_{\text{Ts}}$ );  $114.0$  ( $\text{C}_{\text{PMB}}$ );  $98.1$  (C-1);  $55.5$  e  $55.4$  ( $\text{OCH}_3$ );  $32.1, 29.9, 29.8, 29.6, 29.6, 26.5, 26.2, 22.9$  ( $\text{CH}_2$  of  $\text{C}_{14}$  chains);  $14.3$  ( $\text{CH}_3$  alif).

MS (ESI):  $m/z = 861.6$  (M);  $884.6$  (M+Na);  $900.6$  (M+K).

## 2. Materials and methods

### COMPOUND 15 (Methyl 6-azide-4-O-(4-methoxybenzyl)-2,3-di-O-tetradecil- $\alpha$ -D-glucopyranoside)



COMPOUND	MW	MMOL	EQ.	DENSITY	QUANTITY
14	861	4.06			3.5 g
NaN <sub>3</sub>	65	12.18	3		0.791 g
TBAI					Cat
DMF dry				0.94	40 ml

#### Procedure:

Compound 14 is dissolved in dry DMF. After addition of NaN<sub>3</sub> and TBAI reaction was stirred O.N. at 80° C (TLC EDP/AcOEt 9.5:0.5).

Then solvents are evaporated under reduced pressure and purified with flash chromatography (AcOEt/EDP 9.5:0.5).

Yield=79%

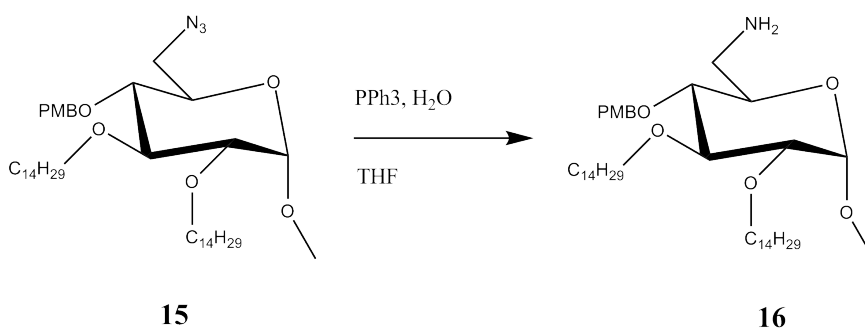
C<sub>43</sub>H<sub>77</sub>N<sub>3</sub>O<sub>6</sub>, MW: 732

## 2. Materials and methods

$^1\text{H}$  NMR (400 MHz,  $\text{CDCl}_3$ ),  $\delta$  (ppm) = 7.23 e 6.87 (AA'XX' system, 4H,  $J$  = 8.4 Hz,  $H_{\text{PMB}}$ ); 4.83 e 4.50 (AB system, 2H,  $J$  = 10.6 Hz,  $\text{CH}_2$  del PMB); 4.76 (d, 1H,  $J$  = 3.2 Hz, H-1); 2.86 (m, 1H, H-5); 3.79 (s, 3H,  $\text{OCH}_3$  del PMB); 3.90-3.20 (m, 9H); 3.40 (s, 3H,  $\text{OCH}_3$ ); 1.61-1.55 (m, 4H,  $H\beta$  del  $\text{C}_{14}$ ); 1.24 (s, 44H,  $\text{CH}_2$  del  $\text{C}_{14}$ ); 0.53 (t, 6H,  $J$  = 5.8 Hz,  $\text{CH}_3$  del  $\text{C}_{14}$ ).

$^{13}\text{C}$ -NMR ( $\text{CDCl}_3$ ),  $\delta$  (ppm) = 160.0 ( $\text{C}_{\text{PMB}}$ ); 130.3 ( $\text{C}_{\text{PMB}}$ ); 129.8 ( $\text{C}_{\text{PMB}}$ ); 114.1 ( $\text{C}_{\text{PMB}}$ ); 98.2 (C-1); 81.7; 81.0; 78.2; 73.9 e 71.9 ( $\text{OCH}_2$ ); 70.2; 55.48 e 55.44 ( $\text{OCH}_3$ ); 51.7 (C-6); 32.13, 30.8, 30.3, 29.9, 29.8, 29.6, 29.5, 26.4, 26.2, 22.9 ( $\text{CH}_2$  delle catene lineari  $\text{C}_{14}$ ); 14.8 ( $\text{CH}_3$  alif).

### COMPOUND 16 (Methyl 6-amino-4-*O*-(4-methoxybenzyl)-2,3-di-*O*-tetradecil- $\alpha$ -D-glucopyranoside)



COMPOUND	MW	MMOL	EQ.	DENSITY	QUANTITY
15	732	0.068			50 mg
PPh3	262	0.136	2		35.67 mg
THF					5 ml
H2O					0.5 ml

## 2. Materials and methods

### Procedure:

Compound 15 was dissolved in dry THF/H<sub>2</sub>O (10:1). After addition of PPh<sub>3</sub> reaction was stirred 1,5h at 70° C (TLC EDP/AcOEt 9:1 e AcOEt/MeOH/trimetilamine 9:1:0.05).

Then solvents are evaporated under reduced pressure and purified with flash chromatography (AcOEt/MeOH/EtN<sub>3</sub> 9:1:0.05).

Yield=93%

C<sub>43</sub>H<sub>79</sub>NO<sub>6</sub>, MW: 706.6

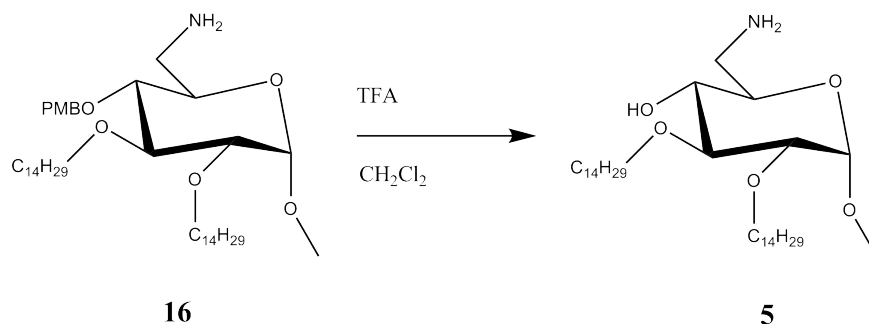
<sup>1</sup>H NMR (400 MHz, CDCl<sub>3</sub>), δ (ppm) = 7.20 e 6.80 (AA'XX', 4H, J= 8.8Hz, H<sub>PMB</sub>); 4.80 e 4.45 (AB system, 2H, J=11.0 Hz, CH<sub>2</sub> del PMB); 4.65 (d, 1H, J= 3.2Hz, H-1); 3.80 (s, 3H, OCH<sub>3</sub> del PMB); 3.80-3.20 (m, 7H); 3.40 (s, 3H, OCH<sub>3</sub>); 3.40 (m, 1H, H-5); 2.98 (dd, 1H, J= 13.5, 2.6 Hz, H-6a); 2.90 (m, 1H, H-6a); 2.60 (dd, 1H, J= 13.5, 4.5 Hz, H-6b); 1.26 (m, 4H, Hβ del C<sub>14</sub>); 1.01-0.91 (m, 44H, CH<sub>2</sub> del C<sub>14</sub>); 0.53 (t, 6H, J= 6.5 Hz, CH<sub>3</sub> del C<sub>14</sub>).

<sup>13</sup>C-NMR (CDCl<sub>3</sub>), δ (ppm)= 160.0 (C<sub>PMB</sub>); 130.0 (C<sub>PMB</sub>); 130.0 (C<sub>PMB</sub>); 114,1 (C<sub>PMB</sub>); 98.04 (C-1); 82.06; 81.18; 78.32; 74.69 e 73.97 (OCH<sub>2</sub>); 71.97; 55.53 e 55.21 (OCH<sub>3</sub>); 43.01 (C-6); 32.17, 30.88, 30.32, 29.96, 29.92, 29.75, 29.62, 26.54, 26.28, 22.95 (CH<sub>2</sub> delle catene lineari C<sub>14</sub>); 14.39 (CH<sub>3</sub> alif).

MS (ESI): m/z= 706.6 (M).

## 2. Materials and methods

### COMPOUND 5 (Methyl 6-amino-2,3-di-O-tetradecyl- $\alpha$ -D-glucopyranoside)



COMPOUND	MW	MMOL	EQ.	DENSITY	QUANTITY
16	706	0.354			250 mg
TFA				1.48	3.3 ml
CH <sub>2</sub> Cl <sub>2</sub>				1.33	5 ml

#### Procedure:

Compound 16 is dissolved in dry CH<sub>2</sub>Cl<sub>2</sub>. After addition of TFA at 0°C reaction was stirred for 1h at rt (TLC AcOEt /MeOH 9:1).

Then solvents are evaporated under reduced pressure and added saturated aqueous solution of NaHCO<sub>3</sub> with a following extraction in CH<sub>2</sub>Cl<sub>2</sub> and the same extraction repeated with brine. Organic phase was treated with sodium sulfate and filtered. Compound was purified with flash chromatography (AcOEt/MeOH/H<sub>2</sub>O 8:2:0.1 then AcOEt/MeOH/H<sub>2</sub>O 7:3:0.1).

Yield=77%

C<sub>35</sub>H<sub>71</sub>NO<sub>5</sub>, MW: 586.6

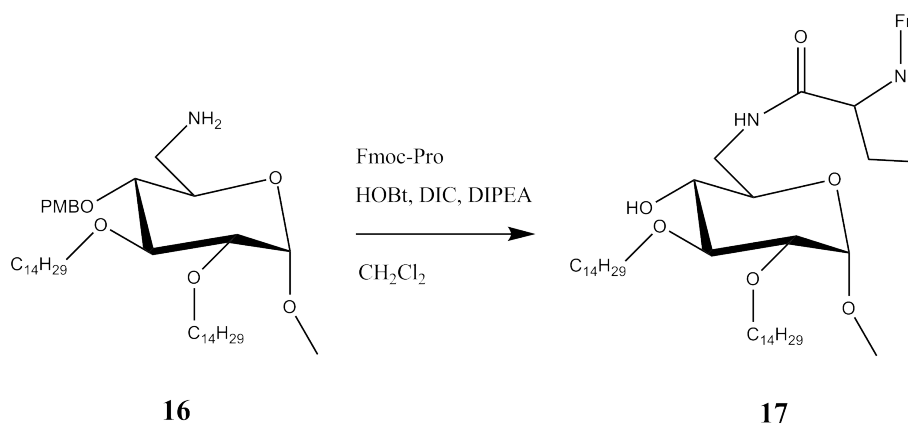
## 2. Materials and methods

$^1\text{H}$  NMR (400 MHz,  $\text{CDCl}_3$ ),  $\delta$  (ppm) = 4.75 (d, 1H,  $J$ = 3.5 Hz, H-1); 3.87 (m, 1H, H $\alpha$ ); 3.70-3.75 (m, 7H); 3.40 (s, 3H,  $\text{OCH}_3$ ); 3.27 (dd, 1H,  $J$ = 9.5, 3.5 Hz, H-2); 3.00 (dd, 1H,  $J$ = 11.0, 4.7 Hz, H6a); 2.20 (bs, 2H,  $\text{NH}_2$ ); 1.57 (m, 4H, H $\beta$  del  $\text{C}_{14}$ ); 1.24 (m, 44H,  $\text{CH}_2$  del  $\text{C}_{14}$ ); 0.86 (t, 6H,  $J$ = 6.5 Hz,  $\text{CH}_3$  del  $\text{C}_{14}$ ).

$^{13}\text{C}$ -NMR ( $\text{CDCl}_3$ ),  $\delta$  (ppm)= 98.7 (C-1); 81.2; 80.7; 73.8; 72.6; 71.6; 71.0; 55.4 ( $\text{OCH}_3$ ); 43.7 (C-6); 32.1, 30.6, 30.2, 30.0, 29.9, 26.3, 26.2, 22.9 ( $\text{CH}_2$  delle catene lineari  $\text{C}_{14}$ ); 14.3 ( $\text{CH}_3$  alif).

Massa (ESI):  $m/z$ = 586.6 (M).

### COMPOUND 17 (Methyl 6-dehoxy-6-Fmoc-proline-2,3-di-*O*-tetradecil- $\alpha$ -D-gluco-pyranoside)



## 2. Materials and methods

COMPOUND	MW	MMOL	EQ.	DENSITY	QUANTITY
5	586	0.153			90 mg
Fmoc-Pro	337	0.168	1.1		56.7 mg
HOBt	135	0.305	2		41.34 mg
DIC	126	0.305	2	0.815	47.34 $\mu$ l
DIPEA	129	0.460	3	0.755	78.57 $\mu$ l
DMF				0.94	4 ml

### Procedure:

Compound 5 is dissolved in dry DMF. After addition of Fmoc-Pro, HOBt, DIC, DIPEA reaction was stirred for 4h at rt (TLC AcOEt).

Then solvents are evaporated under reduced pressure and added saturated aqueous solution of HCl 1N with a following extraction in  $\text{CH}_2\text{Cl}_2$  and the same extraction repeated with  $\text{NaHCO}_3$  and brine. Organic phase was treated with sodium sulfate and filtered. Compound was purified with flash chromatography (AcOEt/EDP 6:4).

Yield=80%

$\text{C}_{55}\text{H}_{88}\text{N}_2\text{O}_8$ , MW: 905

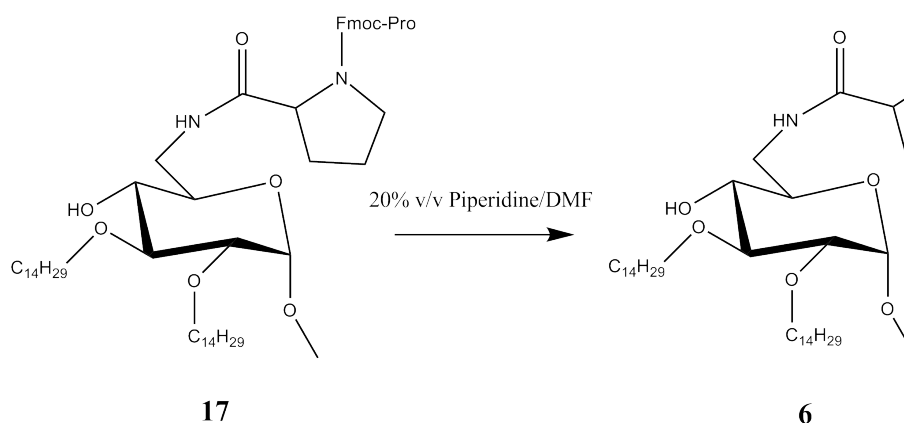
$^1\text{H}$  NMR (400 MHz,  $\text{CDCl}_3$ ),  $\delta$  (ppm) = 7.71 (m, 2H,  $\text{H}_{\text{Fmoc}}$ ); 7.53 (m, 2H,  $\text{H}_{\text{Fmoc}}$ ); 7.34 (m, 2H,  $\text{H}_{\text{Fmoc}}$ ); 7.25 (m, 2H,  $\text{H}_{\text{Fmoc}}$ ); 7.08 (bs, 1H, NH); 6.20 (bs, 1H, NH); 4.60 (bd, 1H, H-1); 4.20 (m, 2H); 4.10 (m, 1H); 4.00-3.00 (m, 13H); 3.26 (s, 3H,  $\text{OCH}_3$ ); 2.30 (m, 1H,  $\text{H}_{\beta\text{Pro}}$ ); 1.87 (m, 2H,  $\text{H}_{\gamma\text{Pro}}$ ).



## 2. Materials and methods

$^{13}\text{C}$ -NMR ( $\text{CDCl}_3$ ),  $\delta$  (ppm)= 128.0; 127.3; 127.0; 126.0; 125.2; 124.8; 120.2; 118.6; 98.5 (C-1); 94.0 (C $\alpha$ Pro); 55.3; 47.4; 32.1, 30.2, 30.0, 29.9, 29.8, 29.7, 29.6, 26.2, 22.9 (CH $_2$  delle catene lineari C $_{14}$ ); 14.3 (CH $_3$  alif).

### COMPOUND 6 (Methyl 6-dehoxy-6-proline-2,3-di-*O*-tetradecil- $\alpha$ -D-glucopyranoside



COMPOUND	MW	MMOL	EQ.	DENSITY	QUANTITY
17	905	0.099			90 mg
Piperidine	85.15			0.862	720 $\mu\text{l}$
DMF				0.94	2.8 ml

#### Procedure:

Compound 17 is dissolved in dry Piperidine:DMF 2:8. Reaction was stirred for 4h at rt (TLC AcOEt).

Then solvents are evaporated under reduced pressure and purified with flash chromatography (AcOEt/MeOH 8:2).

## 2. Materials and methods

Yield=90,6%

$C_{40}H_{78}N_2O_6$ , MW: 684

$^1H$  NMR (400 MHz,  $CDCl_3$ ),  $\delta$  (ppm) = 7.92 (dd,  $J$ = 7.0, 4.7 Hz, NHCO); 4.66 (d, 1H,  $J$ =3.5 Hz, H-1); 3.84 (m, 1H, H-5); 3.78-3.68 (m, 3H); 3.54-3.50 (m, 3H); 3.46 (t, 1H,  $J$ = 9.1Hz); 3.32 (s, 3H,  $OCH_3$ ); 3.19-3.09 (m, 3H); 3.17 (dd, 1H,  $J$ = 3.6, 9.3 Hz, H-2); 2.95 (m, 1H,  $H\delta_a$ ); 2.80 (m, 1H,  $H\delta_b$ ); 2.10 (m, 1H, H- $\beta\alpha$  prolina); 1.82 (m, 1H,  $H\beta$  prolina); 1.65 (m, 2H,  $H\gamma$  prolina); 1.50 (m, 4H,  $H\beta$  del  $C_{14}$ ); 1.30-1.10 (m, 44H,  $CH_2$  del  $C_{14}$ ), 0.81 (t, 6H,  $J$ = 6.6 Hz,  $CH_3$  del  $C_{14}$ ).

$^{13}C$ -NMR ( $CDCl_3$ ),  $\delta$  (ppm)= 177.8 (C=O); 98.9 (C-1); 80.6; 80.4; 74.0 e 72.0 ( $OCH_2$ ); 71.0; 70.7; 55.3 ( $OCH_3$ ); 47.5 (C-6); 39.7; 32.1, 30.6, 30.3, 29.9, 29.5, 26.4, 26.2, 22.9 ( $CH_2$  delle catene lineari  $C_{14}$ ); 14.3 ( $CH_3$  alif).

Massa (ESI):  $m/z$ = 683.6 (M); 722.8 (M+K).

## 2. Materials and methods

### 2.2.3. Agonist synthesis

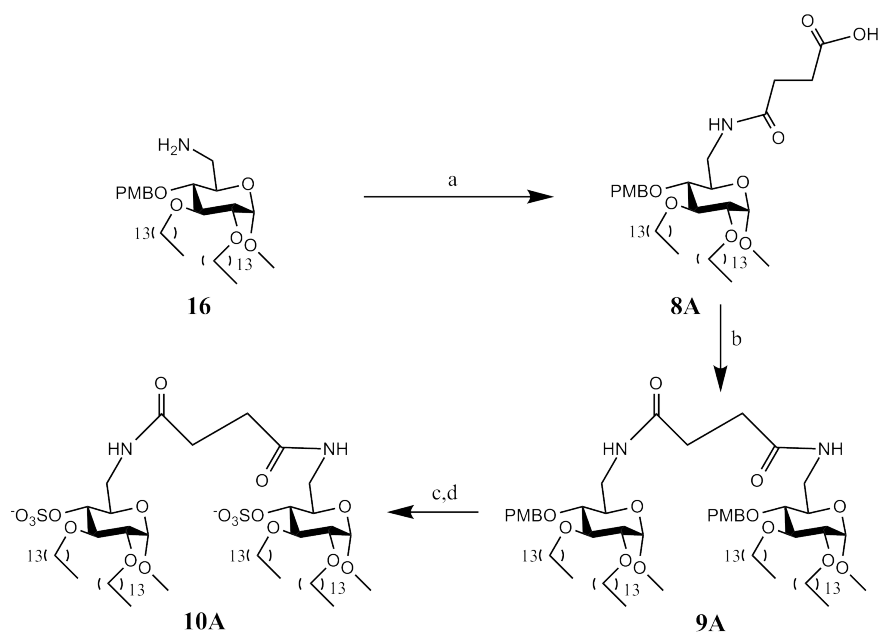
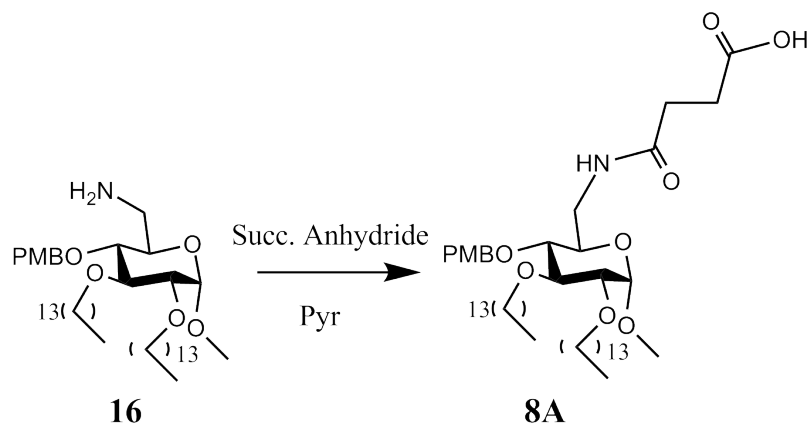


Figure 6

## 2. Materials and methods

### COMPOUND 8A (Methyl 6-anhydrous-6-succinylamino-4-(4-methoxy benzyl)-2,3-di-O-tetradecil- $\alpha$ -D-glucopyranoside



COMPOUND	MW	MMOL	EQ.	DENSITY	QUANTITY
16	706	0.155	1		0.110 g
Succinic anhydride	100	0.31	2		0.031 g
Dry Pyridine					3 ml

#### Procedure:

Compound 16 is dissolved in dry Py. After addition of Succinic anhydride, reaction was stirred for 1h at rt (TLC AcOEt/MeOH 6:4).

Then solvents are evaporated under reduced pressure and purified with flash chromatography (AcOEt/MeOH 9.5:0.5).

Yield=80%

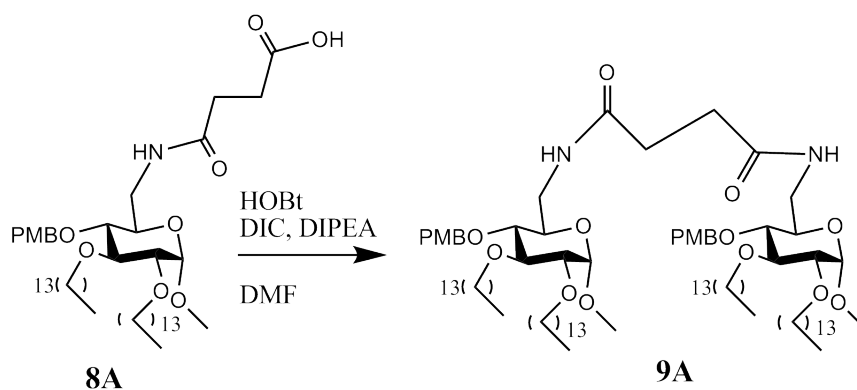
## 2. Materials and methods

C<sub>47</sub>H<sub>83</sub>NO<sub>9</sub>, MW: 806.16

<sup>1</sup>H NMR (400 MHz, CDCl<sub>3</sub>), δ (ppm) = 7.20 e 6.80 (AA'XX', 4H, J= 8.8Hz, H<sub>PMB</sub>); 5.75 (bs, 1H, NH) 4.70 e 4.45 (AB system, 2H, J=10.2 Hz, CH<sub>2</sub> del PMB); 4.65 (d, 1H, J= 3.2Hz, H-1); 3.80 (s, 3H, OCH<sub>3</sub> del PMB); 3.50-3.20 (m, 7H); 3.30 (s, 3H, OCH<sub>3</sub>); 3.20 (dd, 1H, J=9.7, 3.4 Hz); 3.10 (t, 1H, J=9 Hz); 2.60 (m, 2H, CH<sub>2</sub> ammido), 2.35 (m, 2H, CH<sub>2</sub> ammido) 1.26 (m, 4H, Hβ del C<sub>14</sub>); 1.01-0.91 (m, 44H, CH<sub>2</sub> del C<sub>14</sub>); 0.53 (t, 6H, J= 6.5 Hz, CH<sub>3</sub> del C<sub>14</sub>).

<sup>13</sup>C-NMR (CDCl<sub>3</sub>), δ (ppm)= 175.19 (COOH); 172.15 (C ammido); 159.47, 130.38, 130, 114.15 (C Benzene); 97.75 (C-1); 81.62, 80.63, 77.23 (C-2, C-3, C-4); 74.62 (OCH<sub>2</sub> PMB); 73.56, 72 (Cα catene lipofilo); 68 (C-5); 55.24 (2C, OCH<sub>3</sub>); 40.20 (C-6); 29-22 (CH<sub>2</sub>); 14.35 (CH<sub>3</sub>).

### COMPOUND 9A (*N-N'* bis (methyl 6-anhydrous-6-amino-4-*O*-(4-methoxy benzyl)-2,3-di-*O*-tetradecil-α-*D*-glucopiranosil) succinimide)



## 2. Materials and methods

COMPOUND	MW	MMOL	EQ.	DENSITY	QUANTITY
8A	806	0.11	1		0.095 g
16	706	0.14	1.2		0.031 g
HOBt	135.13	0.16	1.5		0.022 g
DIPEA	129.25	0.33	3	0.755	0.056 ml
DIC	126.26	0.16	1.5	0.85	0.110 g
DMF dry					12 ml

### Procedure:

Compound 8A is dissolved in dry DMF. After addition of Compound 16, HOBt, DIPEA and DIC (at 0°C) reaction was stirred for 16h at rt (TLC AcOEt/EDP 9:1). To stop reaction EtOH was added then solvents are evaporated under reduced pressure and purified with flash chromatography (CHCl<sub>3</sub>/AcOEt 7:3).

Yield=70%

C<sub>90</sub>H<sub>160</sub>N<sub>2</sub>O<sub>14</sub>, MW:1494.24

<sup>1</sup>H NMR (400 MHz, CDCl<sub>3</sub>), δ (ppm) = 7.20 e 6.80 (AA'XX', 8H, J= 8.8Hz, H<sub>PMB</sub>); 5.90 (bs, 2H, NH) 4.70 e 4.45 (AB system, 4H, J=11 Hz, CH<sub>2</sub> del PMB); 4.65 (d, 2H, J= 3.4Hz, H-1); 3.80 (dd, 2H); 3.75 (s, 6H, OCH<sub>3</sub> del PMB); 3.50-3.20 (m, 11H); 3.40 (m, 2H) 3.30 (s, 6H, OCH<sub>3</sub>); 3.20 (dd, 2H, J=9, 3.4 Hz); 3.10 (t, 2H, J=9 Hz); 2.40 (m, 4H, CH<sub>2</sub> linker), 1.26 (m, 10H,

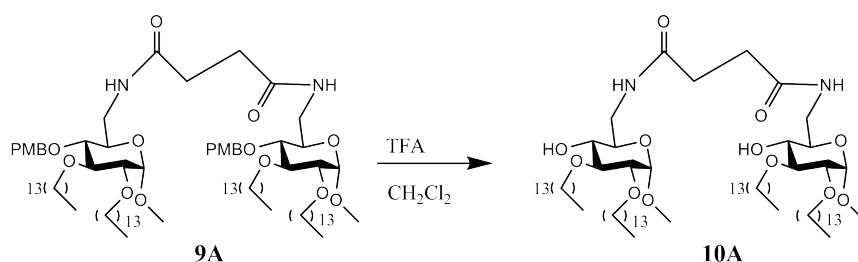
## 2. Materials and methods

H $\beta$  del C<sub>14</sub>); 1.01-0.91 (m, 90H, CH<sub>2</sub> del C<sub>14</sub>); 0.53 (t, 14H, J= 7 Hz, CH<sub>3</sub> del C<sub>14</sub>).

<sup>13</sup>C-NMR (CDCl<sub>3</sub>),  $\delta$  (ppm)= 159.41, 130.30, 130.14, 113.94 (C Benzene); 97,85 (C-1); 81.55, 80.77, 78.31 (C-2, C-3, C-4); 74.70 (OCH<sub>2</sub> PMB); 73.83, 71.86 (C $\alpha$  alkyl chains); 55.31 (2C, OCH<sub>3</sub>); 31-22 (CH<sub>2</sub>); 14.21 (CH<sub>3</sub>).

## 2. Materials and methods

### COMPOUND 10A (*N-N* di (3-*O*-Methyl -4,5-di-*O*-tetradecyl- $\alpha$ -D-glucopyranoside) succinamide)



COMPOUND	MW	MMOL	EQ.	DENSITY	QUANTITY
9A	1494	0.036	1		0.055 g
TFA					4 ml
$\text{CH}_2\text{Cl}_2$					4 ml

#### Procedure:

Compound 9A is dissolved in dry  $\text{CH}_2\text{Cl}_2$ . After addition of TFA at  $0^\circ\text{C}$  reaction was stirred for 1h at rt (TLC AcOEt).

Then solvents are evaporated under reduced pressure and added saturated aqueous solution of  $\text{NaHCO}_3$  with a following extraction in  $\text{CH}_2\text{Cl}_2$  and the same extraction repeated with brine. Organic phase was treated with sodium sulfate and filtered. Compound was purified with titration in AcOEt and solid compound is recovered filtering.

Yield=80%

$\text{C}_{74}\text{H}_{144}\text{N}_2\text{O}_{12}$ , MW:1253.94



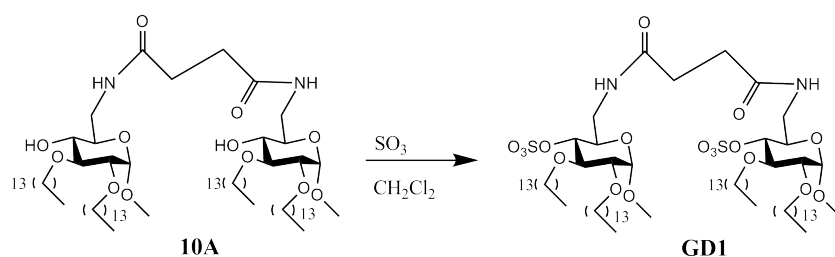
## 2. Materials and methods

$^1\text{H}$  NMR (400 MHz,  $\text{CDCl}_3$ ),  $\delta$  (ppm) = 6.20 (bs, 2H, NH); 4.65 (bs, 2H, H-1); 3.90 (bs, 2H); 3.70 (m, 4H); 3.50-3.30 (m, 11H); 3.40 (s, 6H,  $\text{OCH}_3$ ); 3.20 (bs, 7H); 2.40 (bs, 4H,  $\text{CH}_2$  linker), 1.50 (m, 10H,  $\text{H}\beta$  del  $\text{C}_{14}$ ); 1.10-1.30 (m, 100H,  $\text{CH}_2$  del  $\text{C}_{14}$ ); 0.80 (t, 14H,  $J = 7$  Hz,  $\text{CH}_3$  del  $\text{C}_{14}$ ).

$^{13}\text{C}$ -NMR ( $\text{CDCl}_3$ ),  $\delta$  (ppm) = 173.41 (C amide); 98.50 (C-1); 80.65, 70.76, 70.27 (C-2, C-3, C-4); 74.07, 71.91 ( $\text{C}\alpha$  catene lipofile); 55.28 ( $\text{OCH}_3$ ); 39.94 (C-6); 32-22 ( $\text{CH}_2$ ); 14.36 ( $\text{CH}_3$ ).

## 2. Materials and methods

### COMPOUND GD1 (*N-N'* bis (methyl 6-anhydrous-6-amino-4-*O*-sulfate-2,3-di-*O*-tetradecil- $\alpha$ -D-glucopyranosil) succinimide)



COMPOUND	MW	MMOL	EQ.	DENSITY	QUANTITY
10	1254	0.047	1		0.060 g
SO <sub>3</sub> complex py	159.16	0.28	6		0.046 g
CH <sub>2</sub> Cl <sub>2</sub> dry					4 ml

#### Procedure:

Compound 10A is dissolved in dry CH<sub>2</sub>Cl<sub>2</sub>. After addition of SO<sub>3</sub> complex py reaction was stirred for 46h at rt (TLC AcOEt/MeOH 6:4).

Then solvents are evaporated under reduced pressure and crude compound crystallized in chloroform. Precipitate is then washed with TOL to eliminate residues of compound 10A. Filtered material is then extracted in a biphasic solution of chloroform and aqueous solution of

## 2. Materials and methods

0,1N HCl and organic phase anydrified with sodium sulfate and dried under reduced pressure.

Yield=50%

$C_{74}H_{144}N_2O_{18}S_2$ , MW:1414.07

$^1H$  NMR (400 MHz,  $CDCl_3$ ),  $\delta$  (ppm) = 4.70 (bs, 2H, H-1); 4.20 (bs, 2H); 3.80-3.50 (m, 16H); 3.40 (s, 6H,  $OCH_3$ ); 3.20 (bs, 2H); 3-2.60 (bs, 4H,  $CH_2$  linker), 1.50 (m, 10H,  $H\beta$  del  $C_{14}$ ); 1.10-1.30 (m, 100H,  $CH_2$  del  $C_{14}$ ); 0.80 (t, 14H,  $J = 7$  Hz,  $CH_3$  del  $C_{14}$ ).

$^{13}C$ -NMR ( $CDCl_3$ ),  $\delta$  (ppm)= 98,22 (C-1); 94.59, 80.91, 79.93 (C-2, C-3, C-4); 73.61, 71.98 ( $C\alpha$  catene lipofile); 55.68 ( $OCH_3$ ); 35.36 (C-6); 32-22 ( $CH_2$ ); 14.38 ( $CH_3$ ).

## 2. Materials and methods

### 2.2.4. *Hydrophobic nanoparticles coating*

Iron oxide nanoparticles functionalized with oleic acid were provided from Prof. Davide Prosperi. 40 ng of [<sup>3</sup>H]LPS were solubilized in 50  $\mu$ L Tris 20 mM pH 7, EDTA 5 mM then oleic acid coated nanoparticles (240 ng in 40  $\mu$ L hexane) was added and the mixture sonicated for 15' in a sealed silicon coated container. After this treatment the container was opened and placed in a 37 C waterbath for hexane evaporation (45'). Mixture was then purified with a neodimium dioxide magnet O.N. at 40C. 40  $\mu$ L of supernatant was removed and analyzed for [<sup>3</sup>H]LOS with a scintillation counter, while precipitate was resuspended in 40  $\mu$ L PBS 20 mM W/O Ca<sup>2+</sup> and Mg<sup>2+</sup> and [<sup>3</sup>H]LOS presence analyzed as previous. The same purification was repeated four times at 1 day distance each.

### 2.3. *Biology section*

**Synthetic compounds stock solutions:** stocks of purified coproheme and heme (ca. 15 mM) were freshly prepared in 0.1 M NaOH and then further diluted with PBS/0.1% HSA to the desired concentration. Stocks of molecules 1-7 were prepared prior to use in 1/1 DMSO/EtOH solution and then diluted with PBS/0.1% HSA to the desired concentration. In all situations no changes in buffer pH were detected.

**Materials:** TNF- $\alpha$ , LPS and Lipid A from *E.Coli* were purchased from Sigma. [<sup>3</sup>H]LOS or [<sup>14</sup>C]LOS (25,000cpm/pmol; 3000 cpm/pmol, respectively) was isolated from an acetate auxotroph of *Neisseria meningitidis* serogroup B metabolically labeled and isolated as described.<sup>11</sup> LBP and sCD14 were gifts from Xoma (Berkley, CA) and Amgen Corp. (Thousand Oaks, CA), respectively. Human serum albumin

## 2. Materials and methods

(HSA) was obtained as an endotoxin-free, 25% stock solution (Baxter Health Care, Glendale, CA). Chromatography matrices (Sephacryl HR S200 and S300) were purchased from GE Healthcare. Express Five™ medium was purchased from Invitrogen and supplemented with 2 mM glutamine per the manufacturer's instructions. sMD-2, sCD14, tCD14 and the sMD-2:TLR4 dimer were produced as previously described and stored at 4 °C. Preparative amounts of sMD-2 and a truncated form of CD14 were generated from infections of High Five (Invitrogen) insect cells with baculovirus containing the cDNA for human MD-2 inserted into pBAC3 (His<sub>6</sub>-MD-2) or for human tCD14 (amino acids 1-156, tCD14-His<sub>6</sub>) inserted into pBAC11 as described previously (15). Conditioned medium containing MD-2 was stored at -80°C until needed. tCD14-His<sub>6</sub> was purified using Ni FF Sepharose resin (GE Healthcare) on an Explorer100 FPLC (GEHealthcare) with an imidazole gradient. Purified tCD14-His<sub>6</sub> was stored at 4°C (15). Conditioned medium containing MD-2 associated with TLR4 ectodomain (TLR4<sub>ECD</sub>), MD-2/TLR4<sub>ECD</sub>, was produced by transient transfection in HEK293T cells as described previously (15). Expression vectors containing cDNA of interest for production of FLAG-TLR4<sub>ECD</sub>, amino acids 24-631, (pFLAG-CMV-TLR4) and MD-2-FLAG-His (pEF-BOS) have been previously described and characterized (15). Media containing secreted proteins were concentrated 10-20-fold using Millipore Centricon-10 before use. Conditioned medium containing secreted MD-2/TLR4<sub>ECD</sub> proteins maintained activity to react with [<sup>3</sup>H]LOS·sCD14 for at least 6 months when stored at 4°C. [<sup>3</sup>H]LOS<sub>agg</sub> and [<sup>3</sup>H]LOS·sCD14 complex were prepared as previously described (8). Briefly, [<sup>3</sup>H]LOS<sub>agg</sub> (M<sub>r</sub> > 20 x 10<sup>6</sup>) were obtained after hot phenol extraction of [<sup>3</sup>H]LOS from metabolically labeled bacteria, followed by ethanol precipitation of [<sup>3</sup>H]LOS<sub>agg</sub>, and ultracentrifugation. Monomeric [<sup>3</sup>H]LOS·CD14 complexes (M<sub>r</sub> ~ 60,000)

## 2. Materials and methods

were prepared by treatment of [<sup>3</sup>H]LOS<sub>agg</sub> for 30 min at 37°C with substoichiometric LBP (molar ratio 200:1 LOS:LBP) and 1-1.5 x molar excess sCD14 followed by gel exclusion chromatography (Sephacryl S200, 1.6 x 70 cm column) in PBS, pH 7.4, 0.1 % HSA to isolate monomeric [<sup>3</sup>H]LOS·sCD14 complex. [<sup>3</sup>H]LOS·MD-2 (M<sub>r</sub> ~25,000) was generated by treatment of [<sup>3</sup>H]LOS·sCD14 (30 min at 37°C) with High Five insect cell medium containing His<sub>6</sub>-MD-2 followed by isolation of [<sup>3</sup>H]LOS·MD-2 by S200 chromatography. Radiochemical purity of [<sup>3</sup>H]LOS·sCD14 and [<sup>3</sup>H]LOS·MD-2 was confirmed by S200 chromatography (12).

**HEK-Blue™ cell culture:** HEK-Blue™-4 cells (HEK-Blue™ LPS Detection Kit, InvivoGen) were cultured according to manufacturer's instructions. Briefly, cells were cultured in DMEM high glucose medium supplemented with 10% fetal bovine serum (FBS), 2mM glutamine, 100 U/mL penicillin, 100 µg/ml streptomycin, 1X Normocin™ (InvivoGen). HEK-Blue™-4 cells were maintained with the addition of 1X HEK-Blue™ Selection (InvivoGen).

**HEK-Blue™ cells assay:** The activity of compounds 1-7 as inhibitors of the TLR4 signal pathway was tested in vitro using HEK-Blue™ LPS Detection Kit (InvivoGen). HEK-Blue™-4 cells are HEK293 cells stably transfected with TLR4, MD2, and CD14 genes. In addition, these cells stably express an optimized alkaline phosphatase gene engineered to be secreted (sAP), placed under the control of a promoter inducible by several transcription factors such as NF-κB and AP-1. This reporter gene allows to monitor the activation of TLR4 signal pathway by endotoxin (LPS or lipid A). Moreover, using HEK-Blue™ detection medium, phosphatase activity can be quantified spectrophotometrically.

## 2. Materials and methods

All compounds were dissolved in DMSO/ ethanol 1:1 and then diluted in PBS and added 20  $\mu$ L per well of a flat-bottom 96-well plate at three different concentrations (1, 5, 10  $\mu$ M). The final organic solvent (DMSO/ethanol) concentration per well is less than 0.5%. HEK-Blue-4 cells were detached by the use of diluted trypsin-EDTA solution (1/3 in PBS), and the cell concentration was estimated by using a counting cell. The cells were diluted in HEK- Blue detection medium (InvivoGen), and 200  $\mu$ L of cell suspension (20000 cells) were added to each well. One hour after incubation with compounds at 37  $^{\circ}$ C in a CO<sub>2</sub> incubator, cells were stimulated with 20  $\mu$ L of lipid A (0.01  $\mu$ M) or with TNFR (1 ng/mL) per well. The plate was incubated at 37  $^{\circ}$ C in a CO<sub>2</sub> incubator for 24 h. Lipid A and TNFR induce TLR4 pathway activation, leading to alkaline phosphatase secretion. The phosphatase activity is detected by the use of HEK-Blue detection medium, and it can be quantified spectrophotometrically: the plate reading was assessed by using a spectrophotometer set on 630 nm. As positive control, we treated the cells with lipid A (0.01  $\mu$ M) or TNFR (1 ng/mL) alone.

**Alkaline phosphatase inhibition:** Active molecules (2, 5, 6 and 7) were incubated at maximum concentration (10 mM) with recombinant calf intestinal alkaline phosphatase (CIP) (Biolabs) at different concentrations (0.4, 0.2, 0.02 mU/mL) in the presence of HEK-Blue™ Detection medium. The plate reading was assessed by using a spectrophotometer set on 630 nm. HEK-Blue™-4 cells were diluted in DMEM without FBS and 100  $\mu$ L of cell suspension (20000 cells) were added to each well. Cells were stimulated with 20  $\mu$ L of lipid A (0.01  $\mu$ M) per well. The plate was incubated at 37 $^{\circ}$ C in a CO<sub>2</sub> incubator for 24h. 100  $\mu$ L of supernatant for each well was incubated for 5h with 100  $\mu$ L of HEK-Blue™ Detection medium in the presence or not (C) of

## 2. Materials and methods

molecules **2**, **5** and **7** at 10 mM. sAP activity was assessed measuring absorbance at 630 nm as previously described

**Animal assay for endotoxin shock protection:** C57BL/6J male mice were intraperitoneally (i.p.) injected with 20 mg/kg LPS (from *E. coli* 055:B5, Sigma, Italy), and survival of mice was observed over 4 days. Compounds were administered i.p. 30 min before the LPS.

**CellTiter Blue® cell viability assay (Promega):** Cells were seeded at a density of  $2 \times 10^4$  cells/mL in 50 ml medium per well in 96-well-plate. Compounds **2**, **5**, **6** and **7** were diluted with PBS and were added to the cells to yield a final concentration of 10 mM. 24h after incubation at 37°C, the medium was removed and CellTiter-Blue® medium (fresh medium and CellTiter-Blue® Reagent) were added to the cells of each well. After 2h of incubation the absorbance at 600 nm and 570 nm was read. As controls, we set up triplicate wells with cells and 0.5% DMSO/EtOH; triplicate wells without cells (No-cell Control); triplicate wells without cells containing test compounds to test for possible interference with CellTiter-Blue® Reagent chemistry. As positive control for cytotoxicity (C+), we set up triplicate wells containing cells treated with a compound known to be toxic to the cells.

**Preparation of [<sup>3</sup>H]LOS-Protein(s) Complexes in the presence of synthetic molecules:** [<sup>3</sup>H]LOSMD-2·TLR4 complex was generated by a three-step process. sCD14 (0,8 nM) was pre-incubated with LBP (4 pM) ( $\pm$  synthetic molecules at different concentrations) for 30 min at 37 °C in PBS, pH 7.4, 0.1% HSA. After this time [<sup>3</sup>H]LOSagg (0,8 nM) was added and the mixture was incubated for 30 min at 37°C, then supplemented with preformed MD-2·TLR4 dimer (0.125 ml, ca. 0.2 nM, final



## 2. Materials and methods

concentration, of reactive MD-2·TLR4<sub>ECD</sub> heterodimer) and incubated again for 15 min at 37 °C. [<sup>3</sup>H]LOS-MD-2 complex was prepared with a similar three step process by adding MD-2 (1.2 nM) instead of MD-2·TLR4 in the last incubation step. [<sup>3</sup>H]LOS-CD14 was generated by a first incubation of sCD14 (0,8 nM) ( ± synthetic compounds) in PBS, 1% HSA, 30 min at 37 °C followed by treatment with [<sup>3</sup>H]LOSagg (0,8 nM) for 30 min at 37 °C.

**Effect of the synthetic molecules on LOS transfer from [<sup>3</sup>H]LOS-sCD14 to either His-tagged tCD14 or sMD-2:** Conditioned medium containing either His-tagged protein (corresponding to a final concentration in the incubation mixture of ca. 1.2 nM) was pre-incubated with sCD14 (0.8 nM) ± the synthetic molecules in PBS, 1% HSA, 30 min at 37 °C. sCD14 was added to the preincubation to facilitate interaction of the synthetic compound with either His-tagged protein. LBP was not needed. This pre-incubation was followed by incubation for 30 min at 37 °C with [<sup>3</sup>H]LOS-sCD14 (0.8 nM) to allow transfer of [<sup>3</sup>H]LOS to available His-tagged tCD14 or MD-2. Products of the reactions were analyzed by size exclusion chromatography (see above) and/or by co-capture to HISLINK resin (see below).

**Determination of Apparent Size:** Sephacryl S300 used for determination of apparent Mr was calibrated with the following proteins: blue dextran (2 x 10<sup>6</sup>, V0), thyroglobulin (650,000), ferritin (440,000), catalase (232,000), IgG (158,000), HSA (66,000), ovalbumin (44,500), myoglobin (17,500), vitamin B12 (1200, Vi). For size determination, the complex containing [<sup>3</sup>H]LOS was resolved in the presence of at least three protein standards. For the analysis of [<sup>3</sup>H]LOS.MD-2.TLR4 complex, a volume of 0.9 ml of reaction mixture

## 2. Materials and methods

prepared as described was loaded on a Sephacryl HR S300 column (height 65 cm) pre-equilibrated in PBS, pH 7.4, 0,03% HSA and eluted in the same buffer at a flow-rate of 0,5 ml/min at room temperature using AKTA Purifier or Explorer 100 fast protein liquid chromatography (GE Healthcare), with the collection of 1 ml fractions after 0,3 CV. Radioactivity in collected fractions was analyzed by liquid scintillation spectroscopy (Beckman LS liquid scintillation counter). Total recovery of [<sup>3</sup>H]LOS was 70% in all experiments. In the case of [<sup>3</sup>H]LOS.MD-2 and [<sup>3</sup>H]LOS.CD14 complexes, the chromatographic analysis was carried out in the same experimental conditions, by loading 0.9 ml samples on Sephacryl HR S200 column (height 30 cm).

**Capture Assays with Ni<sup>++</sup>-Chelating Resin:** tCD14-His6 was preincubated in 0,3 ml PBS, 0,1% HSA in presence of LBP (4 pM) for 30' at 37C ± different concentrations of synthetic compounds. [<sup>3</sup>H]LOSagg (0,8 nM) was added followed by another incubation for 30 min at 37 °C. Mixture was then incubated with Ni<sup>++</sup>HISLINK (20 uL) resin for 15 min at 25 °C, allowing His-tagged tCD14 to adsorb onto beads. The resin was spun down, supernatant was removed, and the resin was washed with PBS, 1% HSA. The [<sup>3</sup>H]LOS absorbed on beads or dissolved in supernatant was quantified by liquid scintillation spectroscopy.

**Monomeric endotoxin transfer and capture test:** tCD14-His6 (1,2 nM) was incubated in 0,3 ml PBS, 0,1% HSA for 30 min at 37 °C ± synthetic compounds. Preformed [<sup>3</sup>H]LOS.sCD14 (0,8 nM) was then added and incubated for 1h at 37 °C. [<sup>3</sup>H]LOS.tCD14-His6 formed by LOS transfer from sCD14, was then absorbed on Ni<sup>++</sup> HISLINK resin (20 uL) by incubating for 15 min at 25 °C and radioactivity was analyzed as previously described. A control experiment was run by incubating

## 2. Materials and methods

sMD2-His6 (1,2 nM) synthetic compounds for 30 min at 37 °C, then supplementing preformed [<sup>3</sup>H]LOS sCD14 (0,8 nM) and incubating for 1h at 37 °C. The [<sup>3</sup>H]LOS MD-2-His6 .complex formed by LOS transfer from sCD14 was then captured on Ni<sup>++</sup> HISLINK resin (20 µL).

**Endotoxin displacement assay:** tCD14-His6 or His-tagged MD2 (1,2 nM) were preincubated in 0,3 ml PBS, pH=7,4, 0.1% HSA in presence of LBP (4 pM) with [<sup>3</sup>H]LOSagg (0,8 nM) or [<sup>3</sup>H]LOS·sCD14 (0,8 nM) for 30' at 37C different concentrations of synthetic compounds was added followed by another incubation for 30 min at 37 °C. His-tagged containing complexes were then captured with Ni<sup>++</sup> HISLINK (20 µL) resin by incubating for 15 min at 25 °C. Resin was washed two times with PBS, pH=7,4, 1% HSA and radioactivity was analyzed.

**Evaluation of transfer of [<sup>3</sup>H]LOS to His6-tagged proteins by co-capture to metal chelating resin:** His6-sMD-2 (1.2 nM, final concentration or no His6-sMD-2 as negative control) was pre-incubated in 0.3 ml PBS, 1% for 30' at 37°C ± different concentrations of synthetic compounds. [<sup>3</sup>H]LOS·sCD14 (0.8 nM) was added followed by another incubation for 30 min at 37 °C. The reaction mixture was then incubated with HISLINK resin (20 µL) for 15 min at 25 °C, allowing His-tagged sMD-2 to be adsorbed onto the beads. The resin was spun down for 2 min at 2000x g, the supernatant was removed and the resin washed 2x with PBS, 1% HSA using the same procedure. The [<sup>3</sup>H]LOS absorbed onto the beads or recovered in the supernatant was quantified by liquid scintillation spectroscopy.

**HEK Cell Activation Assay:** HEK-TLR4 cells have been previously characterized and were cultured as described. For cell activation assays,

## 2. Materials and methods

HEK-TLR4 or parental HEK cells were grown to confluency in 96-well plates. Cell monolayers were washed two times with warm PBS w/o Ca<sup>2+</sup> and Mg<sup>2+</sup> and incubated overnight at 37°C, 5% CO<sub>2</sub>, and 95% humidity in 200 µl DMEM 0.1% HSA. The O.N. incubation was performed in presence of synthetic compounds at different concentrations (0-50 µM), and [<sup>3</sup>H]LOS (1 ng), [<sup>3</sup>H]LOS.sCD14 (0,1 ng) or [<sup>3</sup>H]LOS.MD2 (0,03 ng) as stimuli. sCD14 (0,8 nM), sMD2 HEK containing media (ca. 1,2 nM) and LBP (0,8 pM) were supplemented when [<sup>3</sup>H]LOS alone is used as endotoxin donor or sMD2 (ca. 1,2 nM) when [<sup>3</sup>H]LOS.sCD14 is provided. After O.N. incubation plates were centrifugated at 1000 rpm for 5' and supernatant was collected. Activation of HEK cells was assessed by measuring the accumulation of extracellular IL-8 by ELISA according to supplier protocol (BD Clontech, Inc., Palo Alto, CA).

**Assay of glycolipid molecule 1-sCD14 interaction by saturation transfer difference (STD) nuclear magnetic resonance (NMR) spectroscopy:** A freshly prepared stock (1.5 mM) of molecule 2 (in 1:1 DMSO-d<sub>6</sub>:methanol-d<sub>4</sub>, v/v) was diluted to 19 µM in a buffer containing 10 mM sodium phosphate (pH 6.8) in 100% <sup>2</sup>H<sub>2</sub>O (sample A). An aliquot of sample A (0.5 ml) was mixed with 2 µl of a 120 µM stock solution of sCD14 (in the same sodium phosphate buffer) to give a final concentration of sCD14 of 0.5 µM (sample B). This sample was used to collect the STD NMR data. The control sample (sample C) contained 0.5 µM sCD14 alone in the same buffer (10 mM sodium phosphate (pH 6.8) in 100% <sup>2</sup>H<sub>2</sub>O).

STD NMR data were collected at 25 °C on a Bruker Avance II 800 MHz NMR spectrometer equipped with a sensitive cryoprobe. STD data were collected as previously described (33-36). Since no aromatic resonances

## 2. Materials and methods

are present for molecule **2**, the sCD14 protein can be selectively saturated by irradiating (on-resonance) at 7.6 and 8.0 ppm on the protein resonances with a train of Gauss-shaped pulses with a total length of saturation time of 1.0 s. The off-resonance radiation was performed at a chemical shift of 13.0 ppm where no resonances were observed. The on-resonance and off-resonance spectra were collected in an interleaved fashion. The total number of scan collected was 10K. The spectra were processed with the topspin v2.1 software on the Bruker spectrometer.

1. Peri F, *et al.* (2007) Inhibition of lipid a stimulated activation of human dendritic cells and macrophages by amino and hydroxylamino monosaccharides. (Translated from eng) *Angew Chem Int Ed Engl* 46(18):3308-3312 (in eng).
2. Bettoni I, *et al.* (2008) Glial TLR4 receptor as new target to treat neuropathic pain: efficacy of a new receptor antagonist in a model of peripheral nerve injury in mice. (Translated from eng) *Glia* 56(12):1312-1319 (in eng).

## 3. RESULTS AND DISCUSSIONS

### 3.1. Library development

Based on informations gained from this previous library a new set of compounds was synthesized (Fig. 1) as described in materials and methods section (section 2.3).

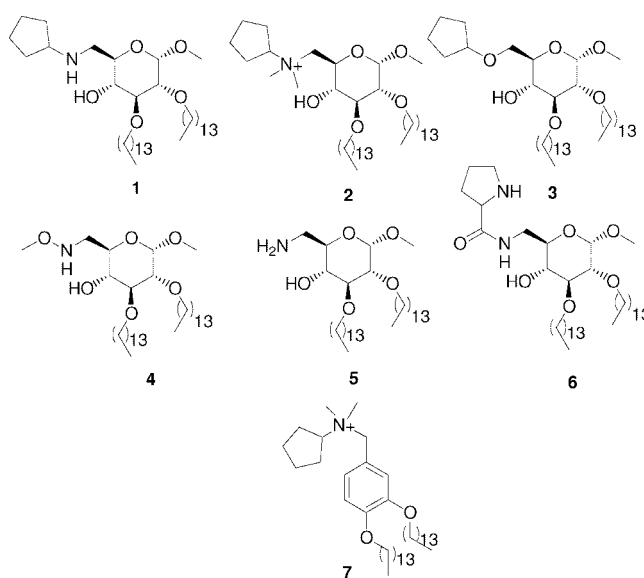


**Figure 1.** Structure of Glycolipids 1-6 and of benzylammonium lipid 7

### 3. Results and discussions

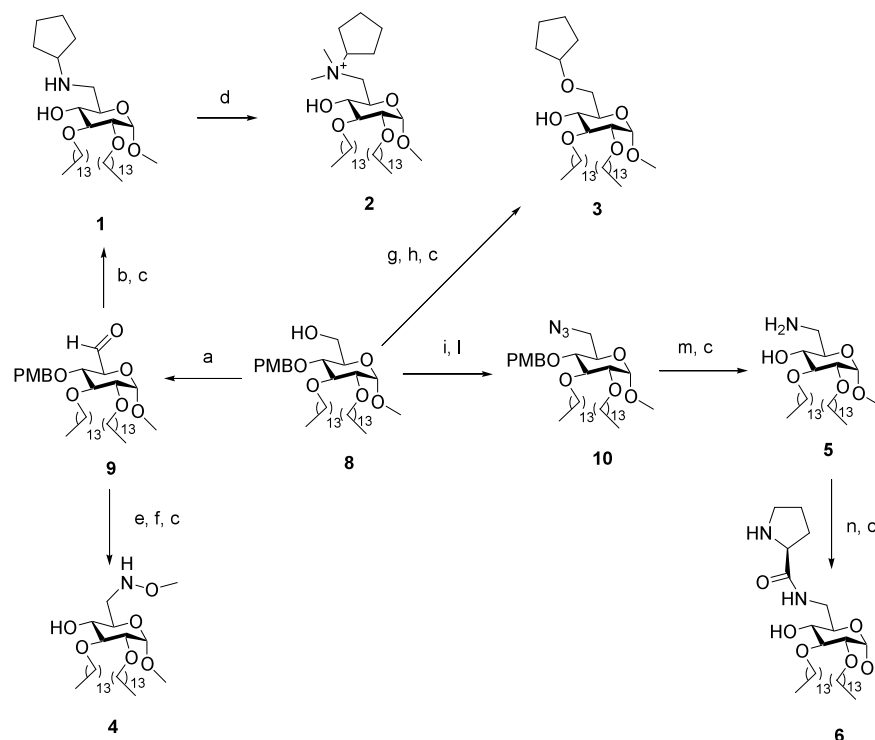


**Figure 2.** Synthetic route to glycolipids **1-6**. <sup>a</sup>Reagents and conditions: (a) Dess-Martin periodinane, CH<sub>2</sub>Cl<sub>2</sub>, rt, 1h; (b) cyclopentylamine, NaBH<sub>3</sub>CN, AcOH, CH<sub>2</sub>Cl<sub>2</sub>, MeOH, 24 °C, 12 h; (c) trifluoroacetic acid, CH<sub>2</sub>Cl<sub>2</sub>, 24 °C, 1h; (d) CH<sub>3</sub>I, Na<sub>2</sub>CO<sub>3</sub>, DMF, 24 °C, 12 h; (e) CH<sub>3</sub>ONH<sub>2</sub>.HCl, pyridine, 24 °C, 12 h; (f) NaBH<sub>3</sub>CN, AcOH, CH<sub>2</sub>Cl<sub>2</sub>, 24 °C, 2 h; (g) MsCl, pyridine, 24 °C, 5h; (h) cyclopentanol, NaH, DMF, 24 °C, 12 h; (i) TsCl, DMAP, pyridine, 24 °C, 12 h; (l) NaN<sub>3</sub>, TBAI, DMF, 75 °C, 4 h; (m) PPh<sub>3</sub>, H<sub>2</sub>O, THF, 70 °C; (n) *N*-Fmoc-Pro, HOBT, DIC, DIPEA, DMF, 24 °C, 4h; (o) piperidine/DMF 2:8, 24 °C, 1h.

### 3. Results and discussions

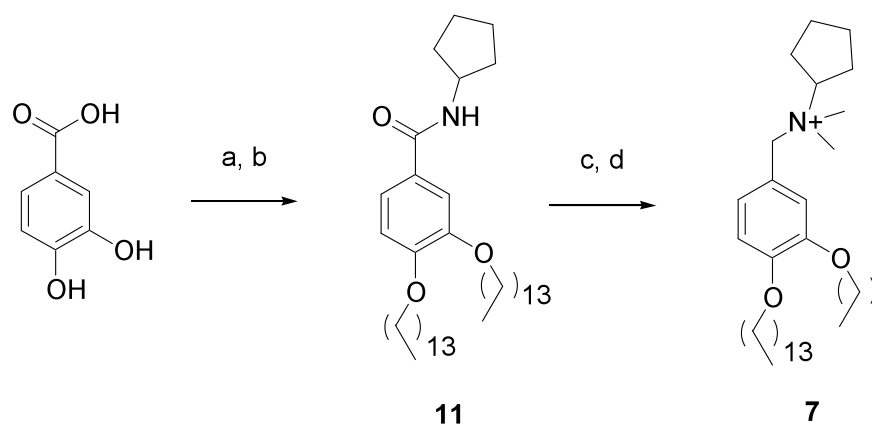


**Figure 3.** Four-step synthesis of compound 7. Reagents and conditions: (a) cyclopentylamine, HOBt, DIC, DIPEA, DMF, 24 °C, 12 h; (b) tetradecyl bromide, NaH, DMF, 60 °C, 2h; (c) LiAlH<sub>4</sub>, THF, 60 °C, 12 h; (d) CH<sub>3</sub>I, Na<sub>2</sub>CO<sub>3</sub>, DMF, 24 °C, 3 h.

The library was designed taking into account important structural features highlighted in the previous study. Chemical modifications of the lead 2 were focused on the amino group on C-6 of glucose and on its substituents (Fig. 2). It was designed compound 3, in which the nitrogen atom on glucose C-6 has been replaced by the oxygen of a cyclopentyl ether, and compound 5 conserving a primary amino group and lacking the cyclopentyl ring. In compound 4 it was inserted an O-methyl hydroxylamine function in C-6 while in compound 6 the C-6 amine was condensed with a proline residue. The unique cyclic structure of this amino acid provides a secondary amine inserted into a five-membered cycle. In compound 7 the cyclic core of the glucopyranose scaffold of 2 has been replaced by an aromatic ring (Fig. 3). The mutual disposition of the C-6 nitrogen (or oxygen, in the case of 3) and of the two tetradecyl ethers was conserved in all derivatives. The C-6, C-2 and C-3 positions of glucose of compounds 1-6 correspond to C-1, C-3 and C-4 positions of the benzene ring in 7. The protonation state of the nitrogen could greatly influence the biological activity and the pharmacokinetic of



### 3. Results and discussions

these molecules, so all compounds but 3 are fully protonated and therefore positively charged at neutral pH. Compounds 1-7 were prepared starting from commercially available and inexpensive compounds: the methyl- $\beta$ -D-glucopyranoside was transformed into glycolipids 1-6 according to the synthetic way described in section 2.3.2, whereas 3,4-dihydroxy benzoic acid was transformed in compound 7 through the four-step synthesis depicted in the same section.

#### 3.1.1. Inhibition of LPS-dependent TLR4 activation<sup>94</sup>

The activity of the library was assayed using a newly available screening kit based on HEK-blue cells (invivogen). Those cells are stable transfected with the components of TLR4 receptor complex (namely TLR4, MD2 and CD14, whilst LBP is supplemented with the culture medium) and receptor activation is coupled to a reporter gene (an optimized secreted alkaline phosphatase) under control of an NF- $\kappa$ B inducible promoter. Cleavage of a pro-chromogenic substrate in the media, allow a colorimetric endpoint measurement for the detection and quantification of receptor activation.

Therefore, we exploited this system to screen our compounds for their TLR4 antagonistic activity. As previously described (section 2.4 ), HEK-Blue<sup>TM</sup>-4 cells Lipid A dependent activation was screened after pretreatment with three different concentrations of all compounds, and phosphatase activity, measured after 24h, is summarized in Fig 4. As shown compounds 3 and 4 did not interfere with lipid A activity at least at the maximum concentration employed and compound 1 showed a weak inhibition (23%) only at the highest concentration (10 mM). On the other hand, compounds 2, 5, 6 and 7 exhibited a significant inhibition of the lipid A activity decreasing the phosphatase activity in a

### 3. Results and discussions

concentration-dependent manner. It was possible to calculate a linear regression relating the inhibitory activity and the compound concentration (for compound **2**  $r^2=0.5624$   $p<0.05$ ; for compound **5**  $r^2=0.6810$ ,  $p<0.01$ ; for compound **6**  $r^2=0.6389$ ,  $p<0.05$ ; for compound **7**  $r^2=0.8553$ ,  $p<0.001$ ). The  $IC_{50}$  comparison (Table 1) demonstrates that in this experiment **7** is the most active compound in suppressing lipid A activity: its potency is more than 3-fold greater than that of compounds **2**, **5** and **6**.

### 3. Results and discussions

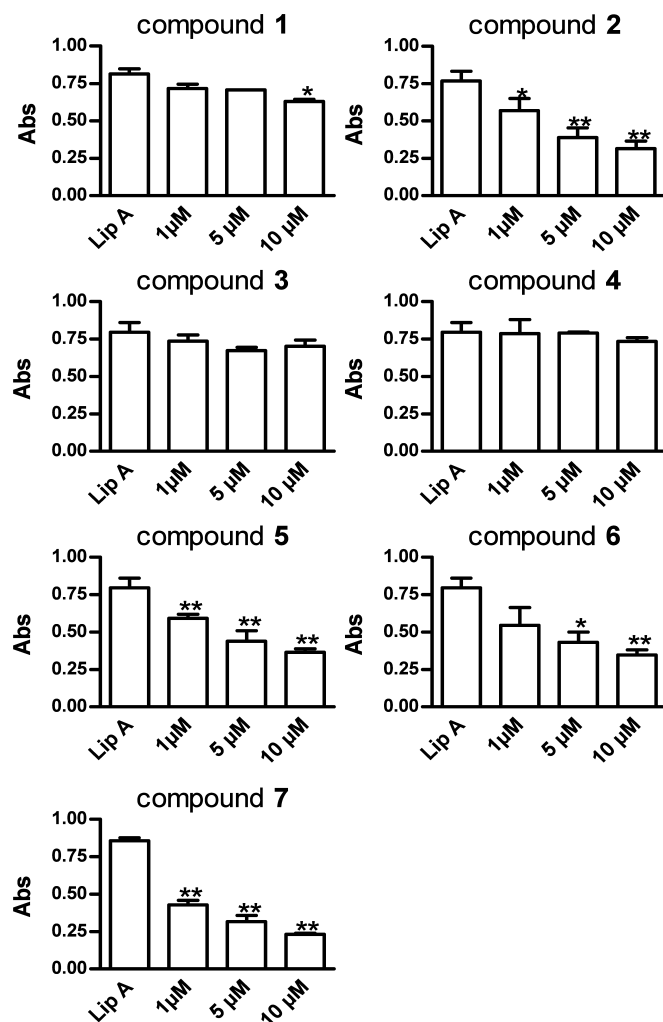


**Figure 4.** In vitro TLR4 antagonistic activity of compounds 1-7. HEK-Blue-4 cells stably transfected with TLR4 and an optimized alkaline phosphatase gene engineered to be secreted (sAP) were treated with

### 3. Results and discussions

lipid A (10 nM) alone or lipid A in the presence of one among compounds **1-7** at three different concentrations (1, 5, 10  $\mu\text{M}$ ). NF- $\kappa\text{B}$  activation was evaluated by measuring phosphatase activity, expressed as absorbance (Abs) at 630 nm. The results are representative for three independent experiments and data are expressed as mean ( SEM \* $p < 0.05$ ; \*\* $p < 0.01$  (ANOVA; Dunnett's test).

**Table 1.** IC<sub>50</sub> on lipidA-induced TLR4 activation

CMPD	IC <sub>50</sub> ( $\mu\text{M}$ )	CONFIDENCE INTERVALS
1	>10	-
2	5.013	3.430-7.327
3	>10	-
4	>10	-
5	5.487	3.102-9.705
6	5.871	3.531-9.726
7	1.675	0.910-3.084

The activity of those compounds could be attributed to a selective inhibition of Lipid A stimulation or to a generic cytotoxic effect on HEK-BLUE cells. To discriminate between those two possibilities cells were grown for 24 h in presence of the highest concentration of compounds and viability was evaluated using CellTiter Blue assay (Promega) (see section 2.4 for detailed information).

Figure 5 clearly demonstrate that there is no inhibitory effect of compounds **2**, **5** and **6** on HEK-Blue™ cell viability was detected. Compound **7** showed a diminution of the cell viability of about 17%; however there is no statistical difference between the percentage of

### 3. Results and discussions

vitality cell in presence and absence of compound 7, as demonstrated by Kruskal-Wallis ANOVA for non parametric data.

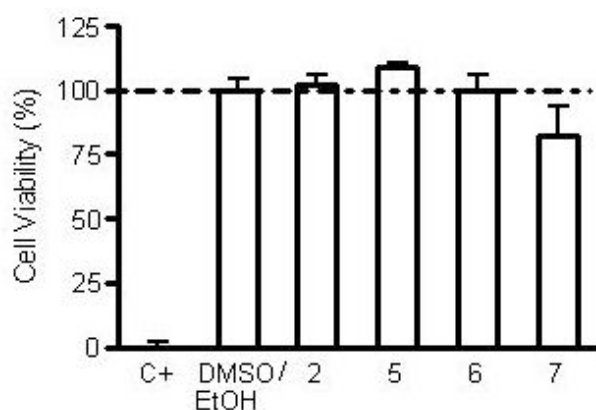


**Figure 5.** Viability of HEK-Blue-4 cells in the presence of active compounds 2, 5, 6, and 7. Cells were seeded and grown for 24 h in the presence of the most effective molecules at maximum concentration (10  $\mu$ M). The cell viability was determined using CellTiter Blue cell viability assay (Promega). As controls, we set up triplicate wells with cells and 0.5% DMSO/EtOH and triplicate wells containing cells treated with a compound known to be toxic to the cells (C+). Kruskal-Wallis ANOVA for nonparametric data has been applied to analyze the differences among groups.

Reduced production of sAP could also be due to a generic partial inhibition of metabolic activity in compounds treated cells, thus reducing the quantity of protein produced by the cells but not their overall viability. A direct stimulation with TNF- $\alpha$  allow a NF- $\kappa$ B production independent from TLR4 activation hence it should not be affected from compounds pretreatment. As described in section 2.4

### 3. Results and discussions

HEK-Blue™ cells were preincubated with molecules 2, 5 and 7 (10  $\mu$ M) then TNF- $\alpha$  was added and 24 h later 630 nm absorbance was measured for each well (Fig 6).

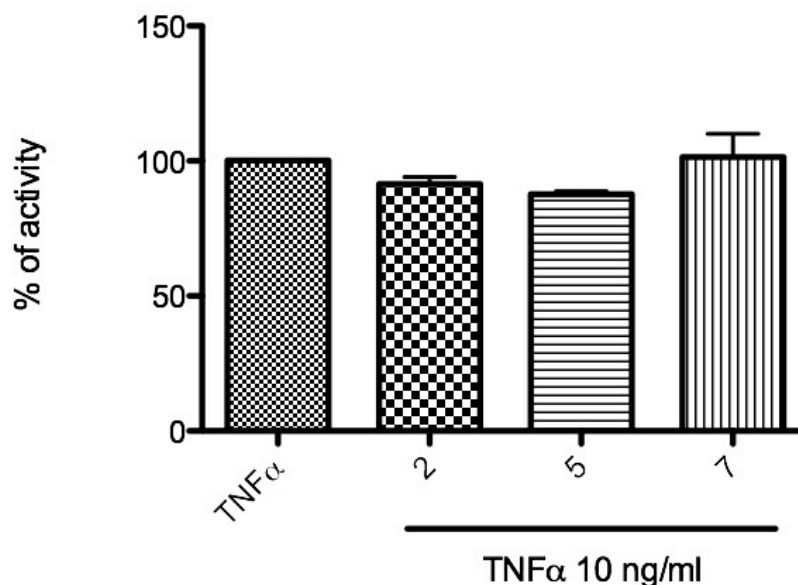


**Figure 6.** In vitro TNF- $\alpha$  activation of HEK-Blue-4 cells. HEK-Blue-4 cells were treated with TNF- $\alpha$  (1 ng/mL) alone or in the presence of compounds 2, 5, and 7 (10  $\mu$ M). sAP production was evaluated by measuring absorbance (Abs) at 630 nm.

Data shows no influence of compounds on TNF- $\alpha$  dependent activation of HEK-Blue™, strongly suggesting that compounds elicit a TLR4 related antagonism of NF- $\kappa$ B production.

Detection of endotoxin activation of HEK-Blue™ cells is based on sAP activity in the culture medium. It was hence necessary to test the possibility that molecules could interfere with sAP efficiency in cleaving the chromogenic substrate. A commercial sAP (0.4  $\mu$ g/ml), with or without 10  $\mu$ M of compounds 2, 5 and 7, were added to invivogen

### 3. Results and discussions

detection medium in absence of HEK-Blue™ cells (sections 2.4). After 1h at 37oC 630 nm absorbance was measured (Fig 7). The experiment show no influence of compounds 2 5 and 7 with sAP activity.

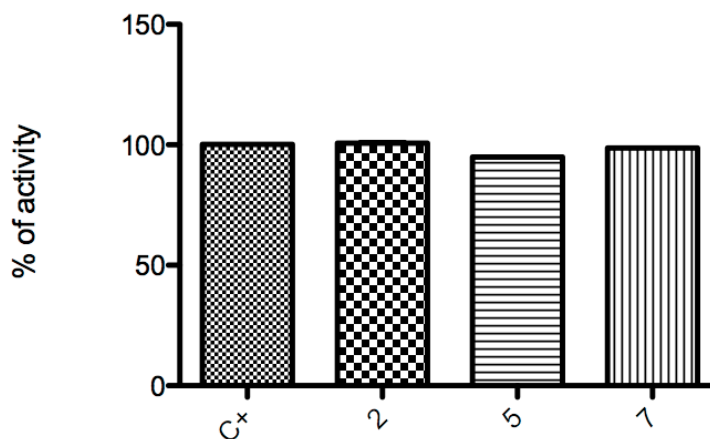


**Figure 7.** Viability of HEK-Blue-4 cells in the presence of active compounds **2**, **5**, **6**, and **7**. Cells were seeded and grown for 24 h in the presence of the most effective molecules at maximum concentration (10  $\mu$ M). The cell viability was determined using CellTiter Blue cell viability assay (Promega). As controls, we set up triplicate wells with cells and 0.5% DMSO/EtOH and triplicate wells containing cells treated with a compound known to be toxic to the cells (C+). Kruskal-Wallis ANOVA for nonparametric data has been applied to analyze the differences among groups.

Considering those preliminary results on TLR4 selectivity and according to IC50 values obtained in previous experiments, active compounds **1**, **2**, **5** and **7** were tested for their capacity to protect animal against LPS-induced lethality. For the lethal endotoxin shock model (section 2.4) 20 mg/kg of LPS (*E. coli* 055:B5, Sigma, Italy) was intraperitoneally (i.p.)

### 3. Results and discussions

injected to C57BL/6J male mice, and survival of mice was observed over 4 days.

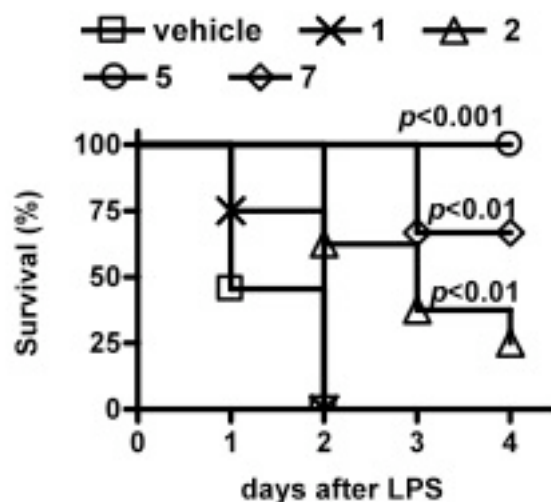


**Figure 8.** Effect of the different compounds on LPS-induced lethality in mice. Compounds were administered ip at 10 mg/kg, 30 min before LPS challenge. Statistical analysis was performed using the log rank test for nonparametric data. Each group consisted of eight mice.

Compounds were administered i.p. 30 min before the LPS. As shown in Figure 8, i.p. injection of 20 mg/kg LPS was lethal to mice and all mice died within two days.

The administration of 10 mg/kg of the three molecules significantly increased survival of mice. Particularly, the compound 2 increased the survival rate from 0% to 25%, compound 7 from 0% to 67% and all mice that received compound 5 survived. We further studied the protection from LPS induced lethality exerted by compound 5 and we



### 3. Results and discussions

found that also a smaller dose (3 mg/kg) evoked a 100% survival of mice treated with LPS (data not shown). Further work is in progress in order to establish the smallest effective dose of compound **5** and to test whether the compound rescues mice even when administered after the LPS challenge. Compound **1**, that has the weakest TLR4 antagonistic activity in vitro, was not effective either in the lethal endotoxin shock model. All mice treated with this compound died within the 2<sup>nd</sup> day, exactly as mice treated with LPS alone.

#### 3.1.2. Discussion

By comparing the in vitro and in vivo activity of compounds **1-7** it is possible to elucidate some aspects of structure-activity relationship in this series. Compounds **3** and **4** lacking a protonatable amino group, were inactive in antagonizing the lipid A effect on HEK cells. Compound **6** is relatively unstable when dissolved in solution at r.t.: its half-life of about 48h is compatible with the in vitro tests duration but significant degradation is observed after the time required for in vivo tests (5 days). We are investigating the mechanism of degradation of this compound and, once clarified it, we will be able to design chemically stable structural variants. Glycolipids **2**, **5** and **6** are active lipid A antagonists on HEK cells and protect mice from LPS-induced lethality in a statistically significant way. Notably, compound **5** is the most active in vivo and the 100% survival observed at 3 mg/Kg dose suggests a possible use of this compound at lower concentrations. The potency of **5** is comparable to that of the best anti-sepsis agents so far developed (compound TAK-242, in clinical phase III, showed comparable activity in this test with an ED<sub>50</sub> of 0.3 mg/Kg).<sup>13</sup> The second most potent

### 3. Results and discussions

compound in vivo and the most potent in vitro is molecule **7**, with an aromatic ring instead of the pyranose ring of glucose.

#### 3.2. Specific interaction between synthetic ligands and CD14

Endotoxin recognition, as outlined in the introductory section, is a complex process involving an array mainly composed of four proteins: TLR4, CD14, MD2 and LBP. Interaction with each of those proteins could lead to inhibition of endotoxin-derived stimulus. Rational modifications of the most promising compounds in the library require the knowledge of their target protein. The aim of this section is to clarify the mode of action of these molecules with particular focus on the lead compound “molecule 2”, by analyzing possible interactions with the extracellular components that bind and shuttle endotoxin to TLR4 (LBP, CD14, and MD-2, free or TLR4-bound).

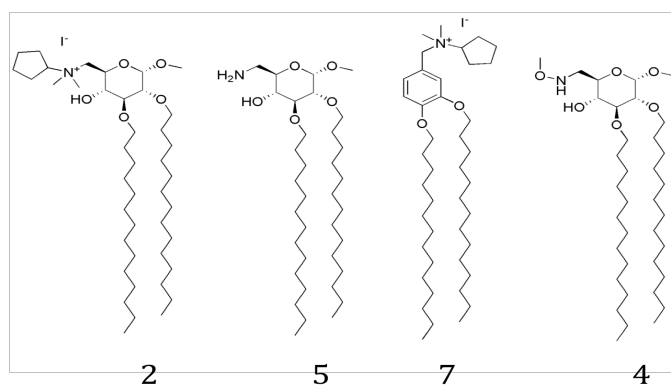


**Figure 9.** Structure of methyl 6-deoxy- 6-*N*-dimethyl-*N*-cyclopentylammonium-2,3-di-*O*-tetradecyl- $\alpha$ -D-glucopyranoside (2), methyl 6-deoxy- 6-amino-2,3-di-*O*-tetradecyl- $\alpha$ -D-glucopyranoside (5), *N*-(3,4-bis-tetradecyloxy-benzyl)-*N*-cyclopentyl-*N,N*-dimethylammonium (7), and methyl 6-deoxy- 6-methoxyamino-2,3-di-*O*-tetradecyl- $\alpha$ -D-glucopyranoside (4).

### 3. Results and discussions

#### ***3.2.1. Biochemical characterization of synthetic ligands with CD14***

Molecule 2 (Fig 9) was selected as a lead compound for biochemical characterization. To better define the mechanism of the inhibitory action of molecule 2 on LPS (lipid A)-triggered TLR4 activation, we tested the ability of this compound to inhibit LBP/CD14-dependent transfer of endotoxin ( $[^3\text{H}]\text{LOS}$ ) monomers from  $[^3\text{H}]\text{LOS}$  aggregates to MD-2/TLR4, resulting in reduced formation of a  $[[^3\text{H}]\text{LOS}\cdot\text{MD-2}\cdot\text{TLR4ECD}]_2$  ( $M_r \sim 190,000$ ) complex. For this purpose, sCD14 was pre-incubated with LBP in the presence or absence of molecule 2 (10 mM), and then incubated with  $[^3\text{H}]\text{LOSagg}$  followed by conditioned medium containing preformed MD-2·TLR4ECD heterodimer. Size-exclusion chromatography of the reaction mixture (Fig 10) showed that, in the absence of molecule 2, virtually all  $[^3\text{H}]\text{LOS}$  aggregates ( $\text{LOSagg}$ ) were converted to later eluting species (i.e., smaller  $[^3\text{H}]\text{LOS}$ -containing complexes) corresponding to  $[^3\text{H}]\text{LOS}\cdot\text{sCD14}$  ( $M_r \sim 60,000$ ) and  $[[^3\text{H}]\text{LOS}\cdot\text{MD-2}\cdot\text{TLR4ECD}]_2$  ( $M_r \sim 190,000$ ). The generation of  $[^3\text{H}]\text{LOS}\cdot\text{sCD14}$  reflects extraction and transfer of  $[^3\text{H}]\text{LOS}$  monomers from  $[^3\text{H}]\text{LOSagg}$  to sCD14 by the combined action of LBP and sCD14. Formation of  $[[^3\text{H}]\text{LOS}\cdot\text{MD-2}\cdot\text{TLR4ECD}]_2$  reflects transfer of  $[^3\text{H}]\text{LOS}$  monomers from  $[^3\text{H}]\text{LOS}\cdot\text{sCD14}$  to MD-2·TLR4ECD. Thus, the chromatographic profile of  $[^3\text{H}]\text{LOSagg}$  incubated first with LBP and sCD14 and then with conditioned medium containing sMD-2·TLR4ECD suggests that, under these experimental conditions, there is nearly complete extraction and transfer of  $[^3\text{H}]\text{LOS}$  monomers from  $[^3\text{H}]\text{LOSagg}$  to  $[^3\text{H}]\text{LOS}\cdot\text{sCD14}$  followed by transfer of  $[^3\text{H}]\text{LOS}$  monomers from about half of the  $[^3\text{H}]\text{LOS}\cdot\text{sCD14}$  formed to MD-

### 3. Results and discussions

2·TLR4ECD. In contrast, in the presence of 10  $\mu$ M molecule 2, accumulation of both  $[^3\text{H}]\text{LOS}\cdot\text{sCD14}$  and  $[[^3\text{H}]\text{LOS}\cdot\text{MD}\cdot 2\cdot\text{TLR4ECD}]_2$  was markedly reduced and most  $[^3\text{H}]\text{LOS}$  was recovered in the void volume presumably as large  $[^3\text{H}]\text{LOS}$  aggregates (Fig. 10). The inhibition of accumulation of  $[^3\text{H}]\text{LOS}\cdot\text{sCD14}$  suggested a primary effect of molecule 2 on LBP/sCD14-dependent extraction and transfer of  $[^3\text{H}]\text{LOS}$  monomers from  $[^3\text{H}]\text{LOS}_{\text{agg}}$  to  $[^3\text{H}]\text{LOS}\cdot\text{sCD14}$ .

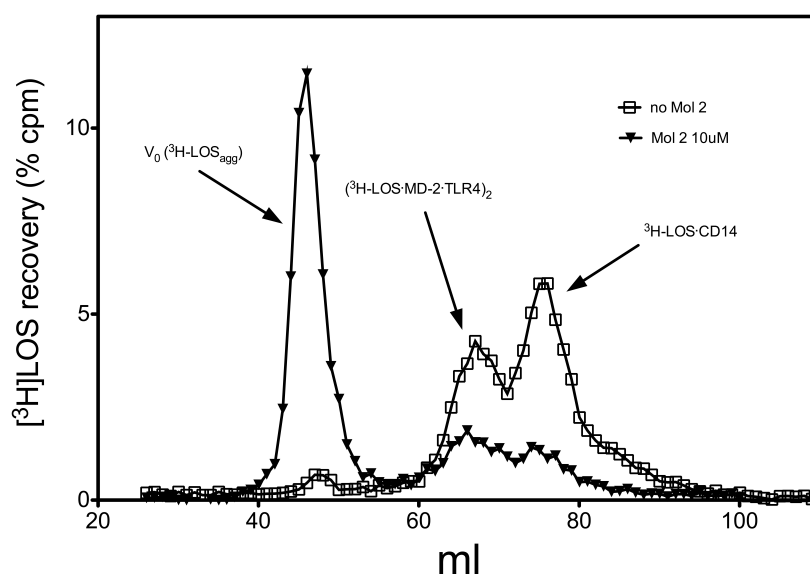
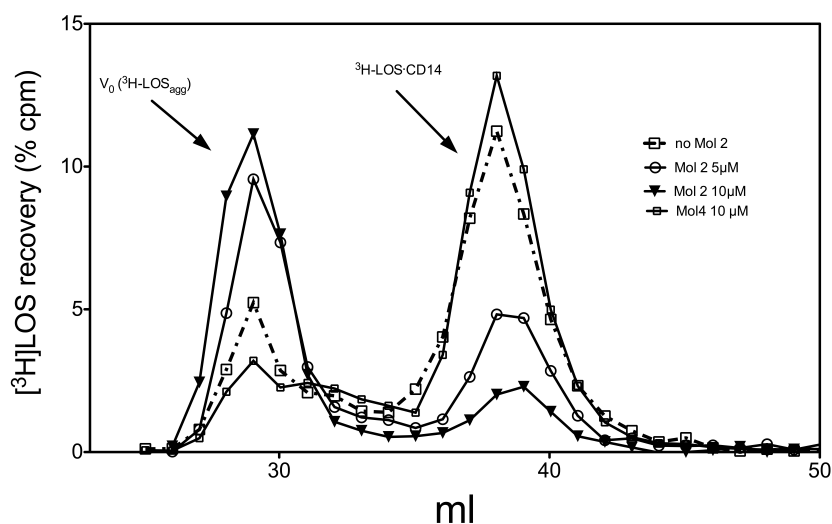


**Figure 10.** Molecule 2 inhibits conversion of  $[^3\text{H}]\text{LOS}_{\text{agg}}$  to  $[^3\text{H}]\text{LOS}\cdot\text{sCD14}$  and  $[[^3\text{H}]\text{LOS}\cdot\text{MD}\cdot 2\cdot\text{TLR4}]_2$ . sCD14 (0.8 nM) was pre-incubated  $\pm$  molecule 1 (10  $\mu$ M) for 30 min at 37  $^{\circ}\text{C}$  in the presence of LBP (4 pM). Subsequently,  $[^3\text{H}]\text{LOS}_{\text{agg}}$  (0.8 nM) was added and this mixture was incubated for 30 min at 37 $^{\circ}$  C. After the second incubation, conditioned HEK293T cell medium containing preformed reactive MD-2·TLR4<sub>ECD</sub> heterodimer (ca. 0.2 nM, final concentration) was added and incubated again for 15 min at 37  $^{\circ}\text{C}$ . This reaction mixture was applied to Sephacryl S300 as described under Experimental Procedures to measure conversion of  $[^3\text{H}]\text{LOS}_{\text{agg}}$  (void volume) to  $[^3\text{H}]\text{LOS}\cdot\text{sCD14}$  ( $M_r \sim 60,000$ ) and  $[[^3\text{H}]\text{LOS}\cdot\text{MD}\cdot 2\cdot\text{TLR4}]_2$  ( $M_r \sim 190,000$ ). The chromatographic profiles shown are representative of  $\geq 4$  experiments. Overall recoveries of  $[^3\text{H}]\text{LOS}$  were  $\geq 70\%$ .

### 3. Results and discussions

To test this hypothesis more directly, we examined the effect of increasing concentration of molecule 2 on LBP/sCD14-dependent conversion of [<sup>3</sup>H]LOSagg to [<sup>3</sup>H]LOS·sCD14. As shown in Fig. 11, molecule 2 caused a dose-dependent reduction in conversion of [<sup>3</sup>H]LOSagg to [<sup>3</sup>H]LOS·sCD14, with decreased accumulation of [<sup>3</sup>H]LOS·sCD14 accompanied by increased recovery of [<sup>3</sup>H]LOS as high Mr LOS aggregates (Fig. 11). In contrast, molecule 4, a compound with a chemical structure similar to molecule 2 (Fig. 9) but not active as an inhibitor of LPS-triggered TLR4 activation in vitro and in vivo, had little or no effect on LBP/sCD14-dependent conversion of [<sup>3</sup>H]LOSagg to [<sup>3</sup>H]LOS·sCD14 (Fig. 11). Thus, the ability of molecule 2, but not molecule 4, to inhibit LPS-triggered TLR4 signaling was paralleled by its ability to inhibit LBP/sCD14-dependent formation of monomeric E.CD14 complex.



### 3. Results and discussions

**Figure 11.** Dose-dependent inhibition by molecule 2 but not by molecule 4 of LBP/sCD14-dependent extraction and transfer of [<sup>3</sup>H]LOS monomers from [<sup>3</sup>H]LOS aggregates to sCD14. sCD14 (0.8 nM) was pre-incubated with LBP (4 pM) and varying concentrations of the indicated synthetic molecules (0, 5, 10 μM) for 30 min at 37 °C in PBS, pH 7.4, 0.1% HSA. [<sup>3</sup>H]LOS<sub>agg</sub> (0.8 nM) was then added to the reaction mixture followed by an incubation for 30 min at 37° C and reaction products were analyzed using Sephacryl S200 chromatography. The chromatographic profiles shown are representative of ≥3 experiments. Overall recoveries of [<sup>3</sup>H]LOS were ≥ 70%.

One possible mechanism by which molecule 2 inhibits formation of E·CD14 could be by competing with E (e.g., [<sup>3</sup>H]LOS) for binding to CD14. In that case, increasing CD14 concentration should reduce the inhibitory effect of molecule 2. To test this hypothesis, we examined the effect of increasing the sCD14 concentration five-fold on the ability of molecule 2 to inhibit conversion of [<sup>3</sup>H]LOS<sub>agg</sub> to [<sup>3</sup>H]LOS·sCD14. A less inhibitory effect of molecule 2 was observed under these conditions (Fig. 12), consistent with a direct competition between molecule 2 and LOS for CD14.

### 3. Results and discussions

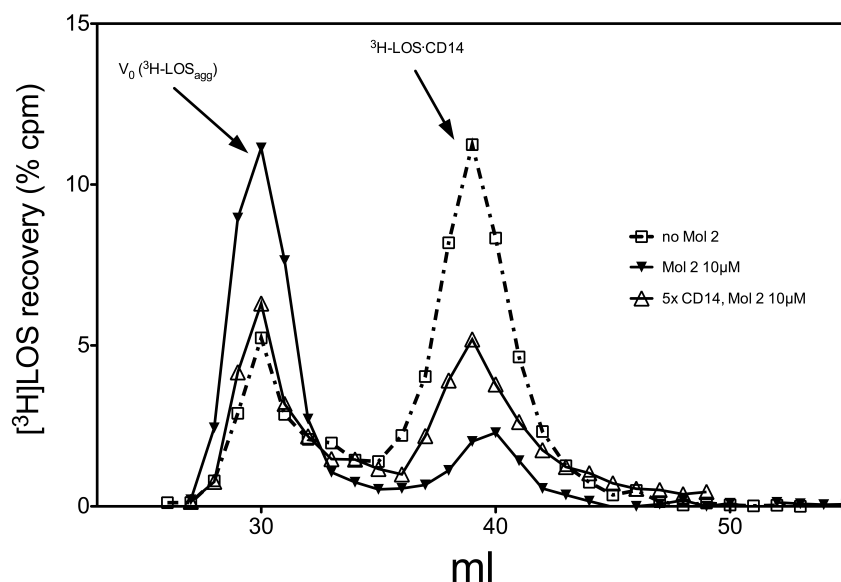


**Figure 12.** Inhibition by molecule 1 of transfer of [<sup>3</sup>H]LOS from LOS aggregates to sCD14 is reduced by increasing sCD14 concentration. Incubations and analysis were as described in (A) except for the addition of 5x higher sCD14 concentration (4 nM). The chromatographic profiles shown are representative of  $\geq 3$  experiments. Overall recoveries of [<sup>3</sup>H]LOS were  $\geq 70\%$ .

As reported in<sup>95,96</sup> , CD14 and MD2 binding site presents strong similarity and a propension to bind ligands with a amphiphilic properties like molecule 2. Crystallographic and NMR studies of endotoxin in complex with CD14 and MD2 clearly shown that both co-receptors binds the lipid A moiety accommodating the lipid component deep in the binding cavity and interacting with the polar one trough a positively charged cluster at the top of the binding site. Chromatographic analysis gave strong preliminary data in favor of a CD14 based mechanism of action for molecule 2 but do not completely exclude the possibility that this compound could also interact with MD2 hence, so far, interaction with MD2 could not be excluded. To test this

### 3. Results and discussions

hypothesis we examined the effect of molecule 2 on transfer of [ $^3\text{H}$ ]LOS monomers from CD14 to MD-2. For this purpose, conditioned medium containing sMD-2 was pre-incubated +/- molecule 2 ( $10\mu\text{M}$ ) in the presence of LBP. This pre-incubated mixture was then incubated with [ $^3\text{H}$ ]LOS-sCD14 to measure the degree of transfer of LOS from sCD14 to MD-2 that had been pre-incubated  $\pm$  molecule 2 to assess the extent to which MD-2 is occupied by molecule 2, inhibiting transfer of [ $^3\text{H}$ ]LOS from CD14 to MD-2. Fig. 13 shows that, in contrast to its effects on conversion of [ $^3\text{H}$ ]LOSagg to [ $^3\text{H}$ ]LOS-sCD14, molecule 2 had little or no effect on transfer of [ $^3\text{H}$ ]LOS monomers from [ $^3\text{H}$ ]LOS-sCD14 to MD-2, indicating that little or no MD-2 is occupied by molecule 2.

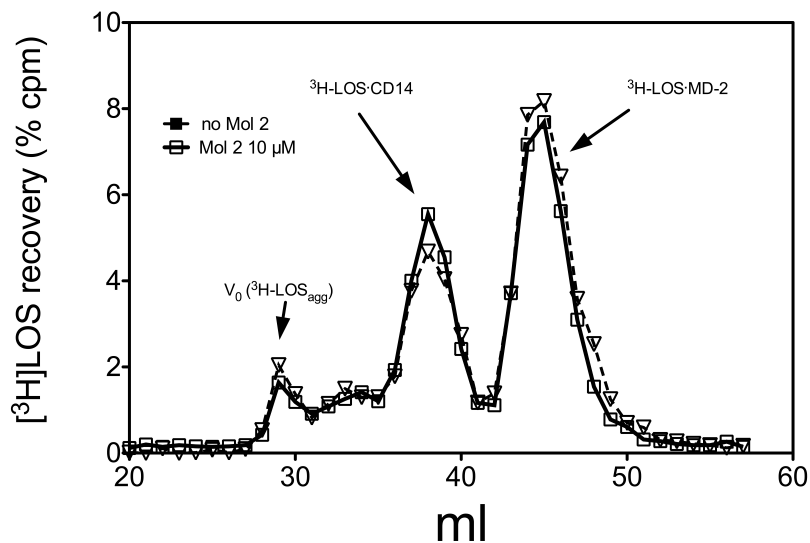


**Figure 13.** Molecule 2 does not inhibit transfer of [ $^3\text{H}$ ]LOS monomers from CD14 to MD-2. sMD-2 ( $1.2\text{ nM}$ ) containing medium was pre-incubated with  $\pm$  molecule 1 for 30 min at  $37^\circ\text{C}$  to give molecule 1 an opportunity to interact with MD-2. This pre-incubation mixture was then incubated for an additional 30 min at  $37^\circ\text{C}$  with [ $^3\text{H}$ ]LOS-sCD14 ( $0.8\text{ nM}$ ) to allow for transfer of [ $^3\text{H}$ ]LOS to unoccupied MD-2. The reaction mixture products were analyzed by Sephacryl S200



### 3. Results and discussions

chromatography. Chromatograms shown are representative of  $\geq 3$  independent experiments. Overall recoveries [ $^3\text{H}$ ]LOS were  $> 70\%$ .

sCD14 is necessary for monomer endotoxin shuffling from aggregates to MD2 and could be possible that also molecule 2, under micellar form at  $10\ \mu\text{M}$ , requires sCD14 to be loaded on MD2. For this reason the next experiment was done adding sCD14 in the first preincubation step (Fig 14).

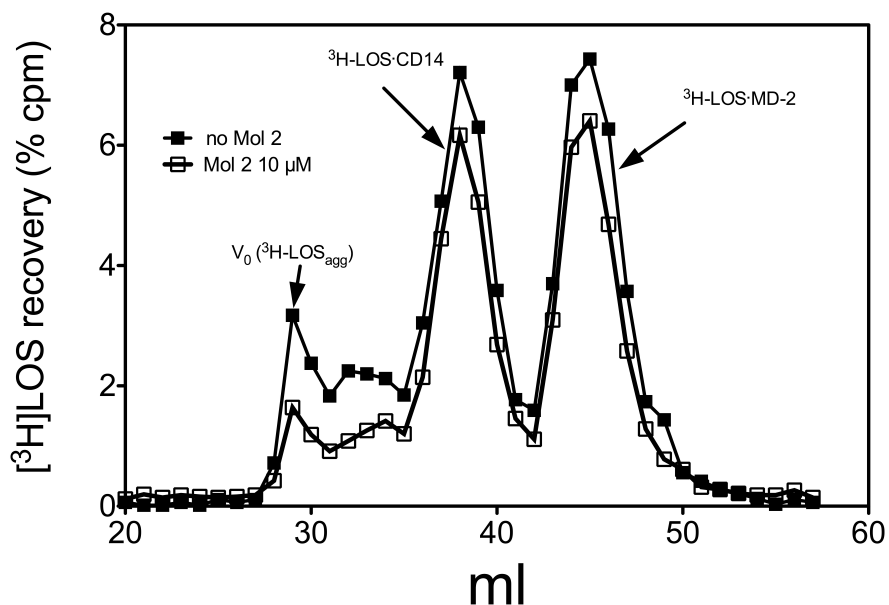


**Figure 14.** Molecule 2 does not inhibit transfer of [ $^3\text{H}$ ]LOS monomers from CD14 to MD-2. sMD-2 ( $1.2\ \text{nM}$ ) containing medium was pre-incubated with sCD14 ( $0.8\ \text{nM}$ )  $\pm$  molecule 1 for 30 min at  $37\ ^\circ\text{C}$  to give molecule 1 an opportunity to interact with MD-2. This pre-incubation mixture was then incubated for an additional 30 min at  $37\ ^\circ\text{C}$  with [ $^3\text{H}$ ]LOS-sCD14 ( $0.8\ \text{nM}$ ) to allow for transfer of [ $^3\text{H}$ ]LOS to unoccupied MD-2. The reaction mixture products were analyzed by Sephacryl S200 chromatography. Chromatograms shown are representative of  $\geq 3$  independent experiments. Overall recoveries [ $^3\text{H}$ ]LOS were  $> 70\%$ .

### 3. Results and discussions

The above experiments demonstrate an ability of molecule 2 to inhibit extraction and transfer of [<sup>3</sup>H]LOS monomers from [<sup>3</sup>H]LOS aggregates to CD14 without affecting subsequent transfer of E monomers from [<sup>3</sup>H]LOS·sCD14 to MD-2. This targeted inhibitory effect could be explained by a selective effect on extraction of E monomers from [<sup>3</sup>H]LOS aggregates that is needed for generation of [<sup>3</sup>H]LOS·sCD14 or a selective effect on net transfer of [<sup>3</sup>H]LOS monomers to sCD14 vs. sMD-2. To test the latter possibility more directly, we took advantage of the ability of monomeric E·sCD14 complexes to serve as a donor of E monomers to either CD14 or MD-2. For this purpose, we used [<sup>3</sup>H]LOS·sCD14 (full-length sCD14, no His tag) as [<sup>3</sup>H]LOS donor and either His6-tagged truncated sCD14 (tCD14; residues 1-156) or His6-tagged sMD-2 as [<sup>3</sup>H]LOS acceptors. Thus, [<sup>3</sup>H]LOS transfer from [<sup>3</sup>H]LOS·sCD14 to tCD14-His6 or to His6-sMD-2 could be readily measured by assay of co-capture of [<sup>3</sup>H]LOS to HISLINK resin as described in Methods.

### 3. Results and discussions

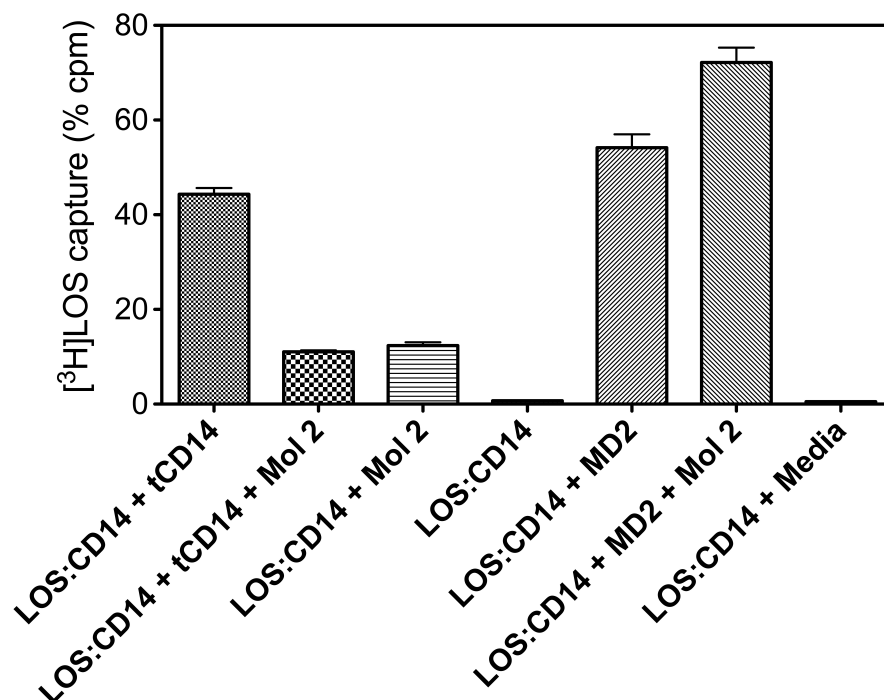


**Figure 15.** Molecule 2 selectively inhibits transfer of [<sup>3</sup>H]LOS monomer to tCD14 but not to MD-2. His-tagged tCD14 or sMD2 (1.6 nM) was pre-incubated for 30' at 37°C with 10 uM molecule 2, followed by addition of [<sup>3</sup>H]LOS·sCD14 (0.8 nM) and further incubation for 30 min at 37 °C. Transfer of [<sup>3</sup>H]LOS to His-tagged tCD14 and MD-2 was assayed by co-capture of [<sup>3</sup>H]LOS to the HISLINK resin as described under Experimental Procedures. Capture of [<sup>3</sup>H]LOS·sCD14 (no His-tag) before and after incubation in medium without His-tagged protein was < 4% and subtracted from each of the experimental samples shown. Data shown are representative of 3 experiments, each in duplicate, and are expressed as mean ± SEM.

As expected, transfer of [<sup>3</sup>H]LOS from [<sup>3</sup>H]LOS·sCD14 to tCD14-His<sub>6</sub> and to His<sub>6</sub>-sMD-2 was similar (Fig. 15). Molecule 2 markedly inhibited transfer of [<sup>3</sup>H]LOS from full-length sCD14 (no His tag) to tCD14-His<sub>6</sub> but did not inhibit transfer of [<sup>3</sup>H]LOS to His<sub>6</sub>-sMD-2 (Fig. 13). Note that the presence of molecule 2 increased by about 10% the nonspecific capture of [<sup>3</sup>H]LOS after incubation of LOS·sCD14 ± MD-2 (Fig. 15). This

### 3. Results and discussions

may be explained by the ability of molecule **2** to promote displacement of [<sup>3</sup>H]LOS from LOS-sCD14 (see below), followed by non-specific adsorption of some of the displaced monomeric [<sup>3</sup>H]LOS to the HISLINK resin. These results demonstrate that molecule **2** inhibits transfer (binding) of [<sup>3</sup>H]LOS monomer to CD14 but not to sMD-2.

Molecule **2** could inhibit net binding of [<sup>3</sup>H]LOS to CD14 by inhibiting transfer of [<sup>3</sup>H]LOS to CD14 and/or by promoting displacement of bound [<sup>3</sup>H]LOS from CD14. To test the latter possibility more directly, we incubated [<sup>3</sup>H]LOS<sub>agg</sub> with tCD14 in the presence of LBP at 37 °C for 30 min in PBS/0.1% albumin, thus generating [<sup>3</sup>H]LOS·tCD14-His<sub>6</sub>. This mixture containing [<sup>3</sup>H]LOS·tCD14-His<sub>6</sub> complex was then incubated ± 10 μM molecule **2** at 37 °C for 30 min. Loss of [<sup>3</sup>H]LOS from tCD14-His<sub>6</sub> was observed by co-capture on the HISLINK resin (Fig. 16).

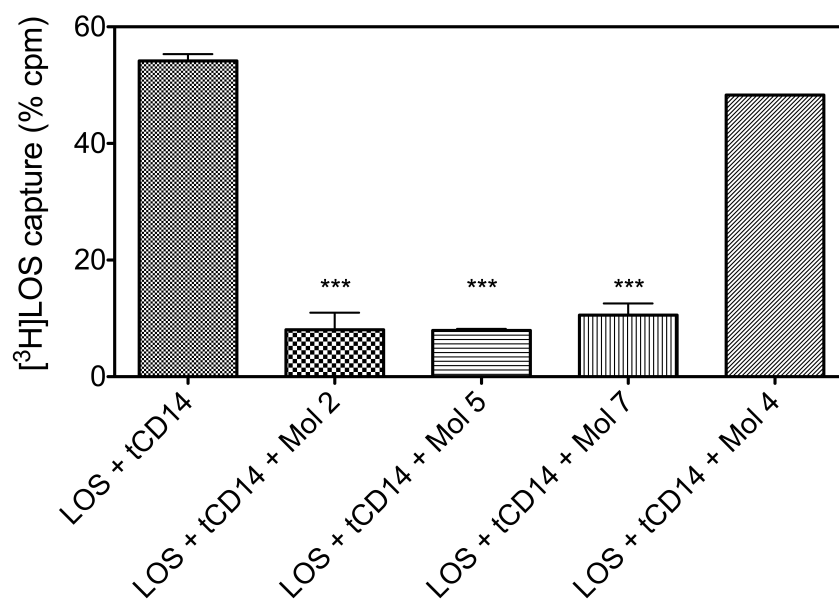


**Figure 16.** Molecules 2, 5, 7, but not molecule 4, promote displacement of [<sup>3</sup>H]LOS from [<sup>3</sup>H]LOS·tCD14-His<sub>6</sub>. [<sup>3</sup>H]LOS·tCD14-His<sub>6</sub> was formed by pre-incubation of tCD14-His<sub>6</sub> with [<sup>3</sup>H]LOS<sub>agg</sub> (0.8 nM) + LBP (4 pM),

### 3. Results and discussions

and then incubated an additional 30 min at  $37^{\circ}\text{C} \pm 10\ \mu\text{M}$  molecule 2-7, as indicated. The amount of remaining  $[^3\text{H}]\text{LOS}\cdot\text{tCD14}\cdot\text{His}_6$  was assayed by co-capture of  $[^3\text{H}]\text{LOS}$  To HISLINK resin as described under Experimental Procedures. Non-specific binding of  $[^3\text{H}]\text{LOS}_{\text{agg}}$  incubated in the absence of  $\text{tCD14}\cdot\text{His}_6$  was  $< 9\%$  and subtracted from each of the experimental samples shown. Results shown represent the mean of 3 experiments each in duplicates and data are expressed as mean  $\pm$  SEM. \*\*\*indicates conditions in which incubation with the indicated synthetic molecule resulted in a statistically significant ( $p < 0.01$  (ANOVA; Dunnett's test)) reduction in co-capture of  $[^3\text{H}]\text{LOS}$  (i.e., retention of  $[^3\text{H}]\text{LOS}\cdot\text{tCD14}\cdot\text{His}_6$ ).

To exclude the possibility of an assay related artifact the same reaction mixture with molecule 2 was analyzed by gel sieving chromatography (fig 17).

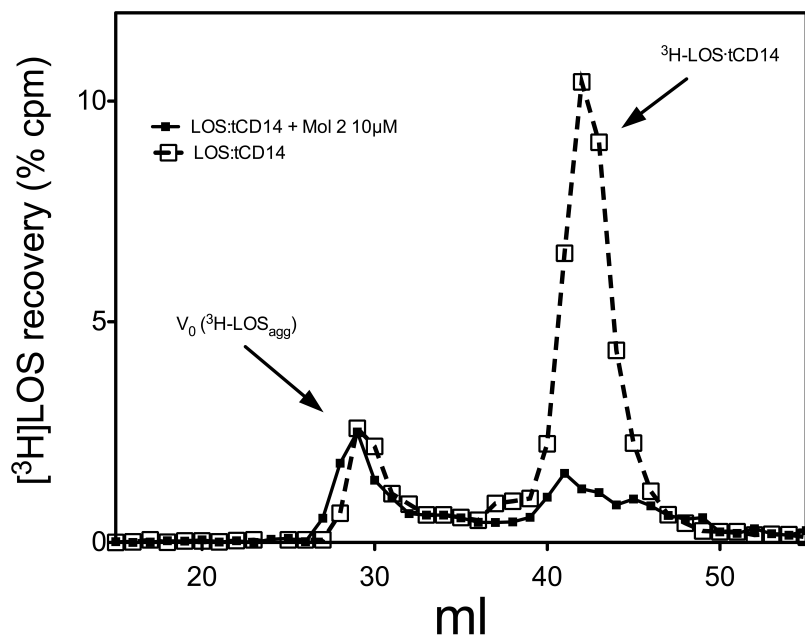


**Figure 17.** Molecules 2, promote displacement of  $[^3\text{H}]\text{LOS}$  from  $[^3\text{H}]\text{LOS}\cdot\text{tCD14}\cdot\text{His}_6$ .  $[^3\text{H}]\text{LOS}\cdot\text{tCD14}\cdot\text{His}_6$  was formed by pre-incubation of  $\text{tCD14}\cdot\text{His}_6$  with  $[^3\text{H}]\text{LOS}_{\text{agg}}$  (0.8 nM) + LBP (4 pM), and then

### 3. Results and discussions

incubated an additional 30 min at 37° C ± 10 µM molecule 2, as indicated. The reaction mixture products were analyzed by Sephacryl S200 chromatography. Chromatograms shown are representative of  $\geq 3$  independent experiments. Overall recoveries [<sup>3</sup>H]LOS were > 70%.

Those two assays showed a marked diminution of [<sup>3</sup>H]LOS bound to tCD14-His<sub>6</sub> induced by incubation with molecule 2. Closely similar effects were seen with molecules 1 and 4, but not with molecule 7 (Fig. 15), paralleling the ability of molecules 1-4, but not 7, at 1-10 µM concentrations, to inhibit LPS-triggered TLR4 signaling *in vitro* and *in vivo*.

Previous experiments were done with tCD14, which, as stated previously, is a truncated but fully active form of sCD14. To prevent differential behaviors among [<sup>3</sup>H]LOS·tCD14-His<sub>6</sub> and [<sup>3</sup>H]LOS·CD14 complexes in response to molecule 1, the same experiment was done with full length sCD14 and results analyzed with gel sieving chromatography (Fig. 18).

### 3. Results and discussions

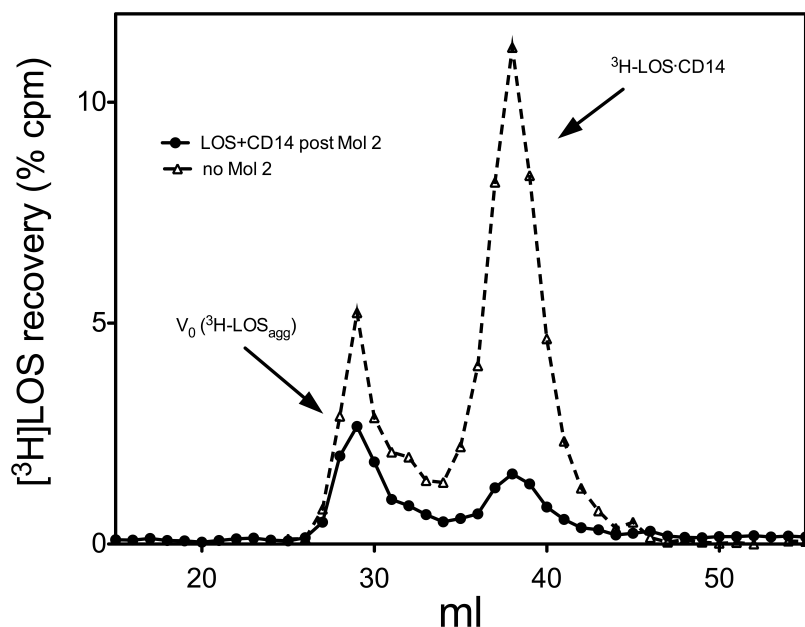


**Figure 18.** Molecules 2, promote displacement of  $^3\text{H}$ LOS from  $^3\text{H}$ LOS-sCD14.  $^3\text{H}$ LOS-sCD14 was formed by pre-incubation of sCD14 with  $^3\text{H}$ LOS<sub>agg</sub> (0.8 nM) + LBP (4 pM), and then incubated an additional 30 min at  $37^\circ\text{C} \pm 10$   $\mu\text{M}$  molecule 2, as indicated. The reaction mixture products were analyzed by Sephacryl S200 chromatography. Chromatograms shown are representative of  $\geq 3$  independent experiments. Overall recoveries  $^3\text{H}$ LOS were  $> 70\%$ .

Samples treated with molecule 2 present a loss in recovery and, albeit CD14 containing peaks markedly reduce their area, LOSagg peaks show no increase (for comparison see Fig. 17-18) (Fig. 19).

### 3. Results and discussions

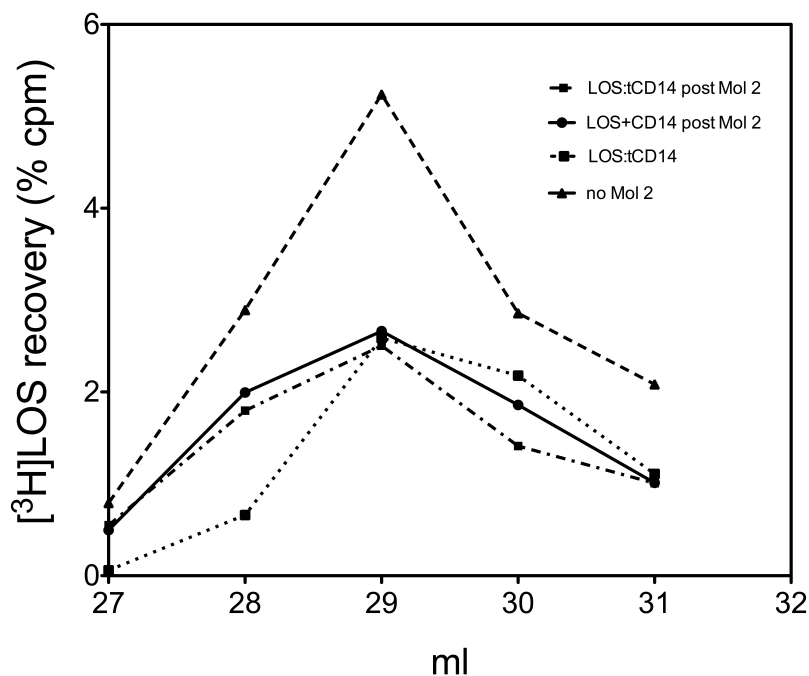


**Figure 19.** [<sup>3</sup>H]LOS<sub>agg</sub> peaks after endotoxin displacement with molecule 2 from [<sup>3</sup>H]LOS:sCD14 and [<sup>3</sup>H]LOS:tCD14-His<sub>6</sub> preformed complexes. Graph is derived from figure 18 and 17 with no further data analysis or handling.

One possible explanation relies on LOS monomer behavior in aqueous solutions. At low-level concentrations used for those assays, once endotoxin monomer is displaced from CD14 it could not reassemble into micelles and thus is prone to stick on plastic-wares and chromatography devices used for the experiments. Treatment with 2% SDS solution of eppendorf tubes used for incubation, recover 19,8% of radioactivity lost in the analysis.

We decided to modify the binding assay previously described to develop a fast and reliable screening system for CD14 interacting compounds.



### 3. Results and discussions

We used LOS<sub>agg</sub> as endotoxin donor and His tagged tCD14 as acceptor. As described in section 2.4 we preincubated tCD14 with increasing concentrations of molecules in presence of LBP. LOS<sub>agg</sub> was then added and mixture incubated again for 30' at 37C, analysis of LOS:tCD14 complex formation was done, as previous, with a co-capture of tCD14 containing complexes. Prior to use this assay for IC50 calculation of compounds we calculated the correct amount of tCD14 to use. Increasing amount of tCD14 undergone the same experimental protocol as previous and results were once more analyzed with co-capture (Fig. 20).

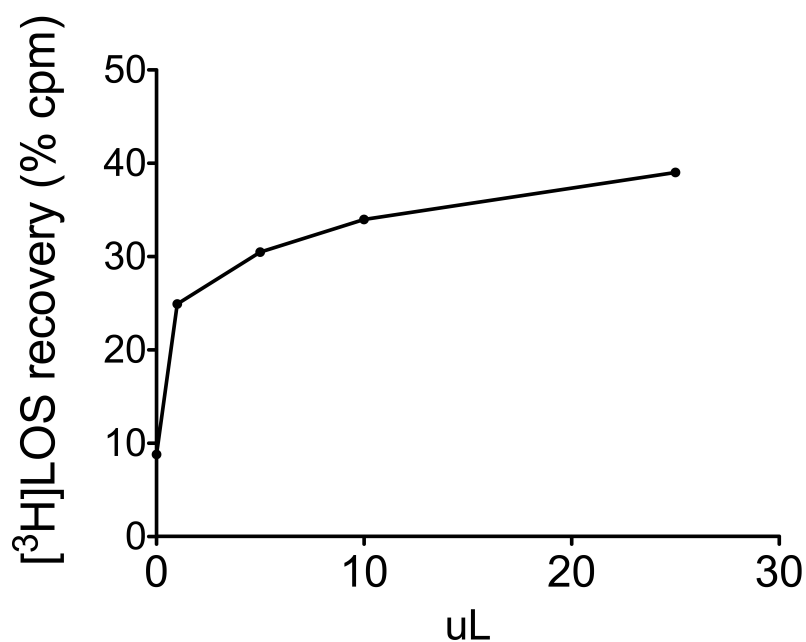


**Figure 20.** Calibration of tCD14-His<sub>6</sub> amount for optimal transfer of [<sup>3</sup>H]LOS monomers from [<sup>3</sup>H]LOS<sub>agg</sub> to tCD14-His<sub>6</sub>. tCD14-His<sub>6</sub> (0, 1, 5, 10, 25  $\mu$ L, corresponding to 0,064, 0,32, 0,64, 1,6 nM) was pre-incubated + LBP (4 pM) for 30' at 37°C. [<sup>3</sup>H]LOS<sub>agg</sub> (0.8 nM) was then added and samples were incubated for an additional 30 min at 37 °C. Results shown are representative of  $\geq 3$  independent experiments, each in

### 3. Results and discussions

duplicate. Non-specific binding, measured as [ $^3\text{H}$ ]LOS binding in absence of tCD14-His<sub>6</sub>, was subtracted from each sample.

Capture material is analyzed for his radioactive content ([ $^3\text{H}$ ]LOS), assuming that only tCD14 containing complexes binds to the Ni-chelating resin but to confirm this hypothesis we examined the reaction mixture before and after incubation with HISLINK beads (section 2.4) (Fig. 21).

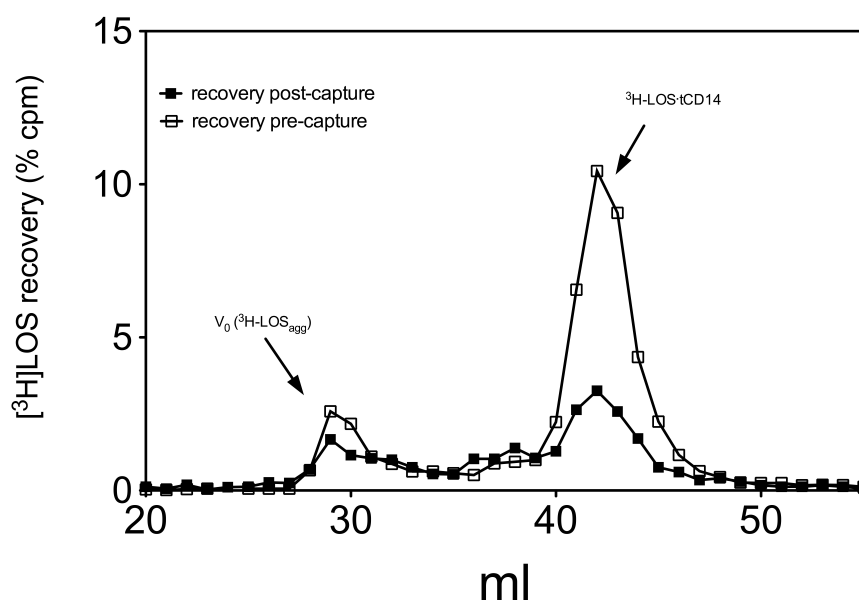


**Figure 21.** tCD14-His<sub>6</sub> containing complexes reduction after co-capture assay. tCD14-His<sub>6</sub> (1,6 nM) was pre-incubated + LBP (4 pM) for 30' at 37°C. [ $^3\text{H}$ ]LOS<sub>agg</sub> (0.8 nM) was then added and samples were incubated for an additional 30 min at 37 °C. HISLINK beads were added (20  $\mu\text{L}$ ) and supernatant analyzed by Sephacryl S200 chromatography. Chromatograms shown are representative of  $\geq 3$  independent experiments. Overall recoveries [ $^3\text{H}$ ]LOS were > 70%.

### 3. Results and discussions

To have another comparison between formation of tCD14 containing complexes and radioactivity capture with affinity beads we split in two the same reaction mixture and analyzed it with both methods (Fig. 22).

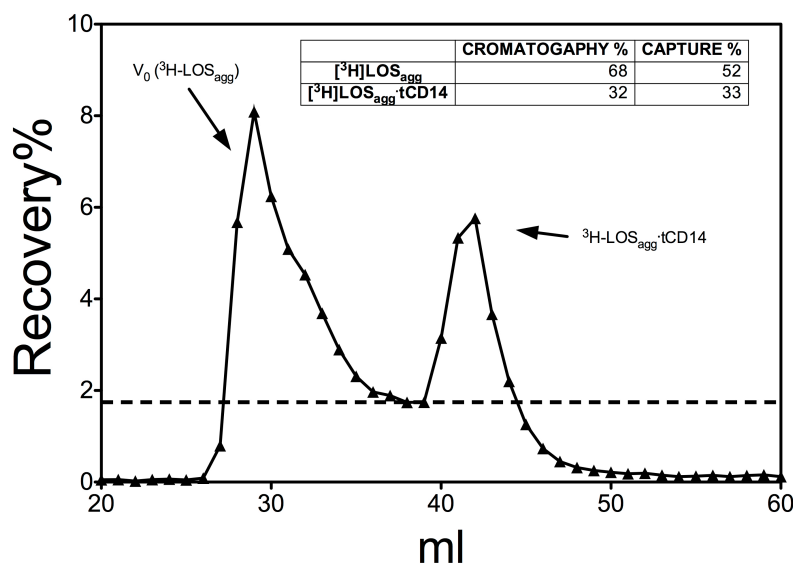


**Figure 22.** Comparison between gel-sieving results and co-capture assay. tCD14-His<sub>6</sub> (1,6 nM) was pre-incubated + LBP (4 pM) for 30' at 37°C. [<sup>3</sup>H]LOS<sub>agg</sub> (0.8 nM) was then added and samples were incubated for an additional 30 min at 37 °C. Reaction mixture was divided in two equivalent parts and analyzed with gel-sieving chromatography and co-capture assay. Co-capture results are presented as percentage of total radioactivity recovered. Gel sieving data in the table are represented as percentage of the total area of the chromatogram.

From the two last experiments it seems clear that [<sup>3</sup>H]LOS:tCD14 is selectively capture from beads while [<sup>3</sup>H]LOS<sub>agg</sub> peak is almost unchanged. Comparison of peaks areas in gel sieving chromatography and of bound and unbound percentage in co-capture analysis highlight a striking similarity.

We took advantage of this simpler and faster co-capture assay to quantify the inhibition of LOS-CD14 complex formation by our synthetic

### 3. Results and discussions

compounds (Fig. 22). Molecules 2, 5 and 7 showed a dose-dependent inhibition of the transfer of  $[^3\text{H}]\text{LOS}$  monomers from  $[^3\text{H}]\text{LOS}_{\text{agg}}$  to tCD14-His<sub>6</sub>, with a calculated IC<sub>50</sub> of 0.8, 2, and 0.4  $\mu\text{M}$  for molecules 2, 5, and 7, respectively. In contrast, molecule 4, even at 10  $\mu\text{M}$ , produced little inhibition of the transfer of  $[^3\text{H}]\text{LOS}$  monomers from  $[^3\text{H}]\text{LOS}_{\text{agg}}$  to tCD14-His<sub>6</sub> (Fig. 23).

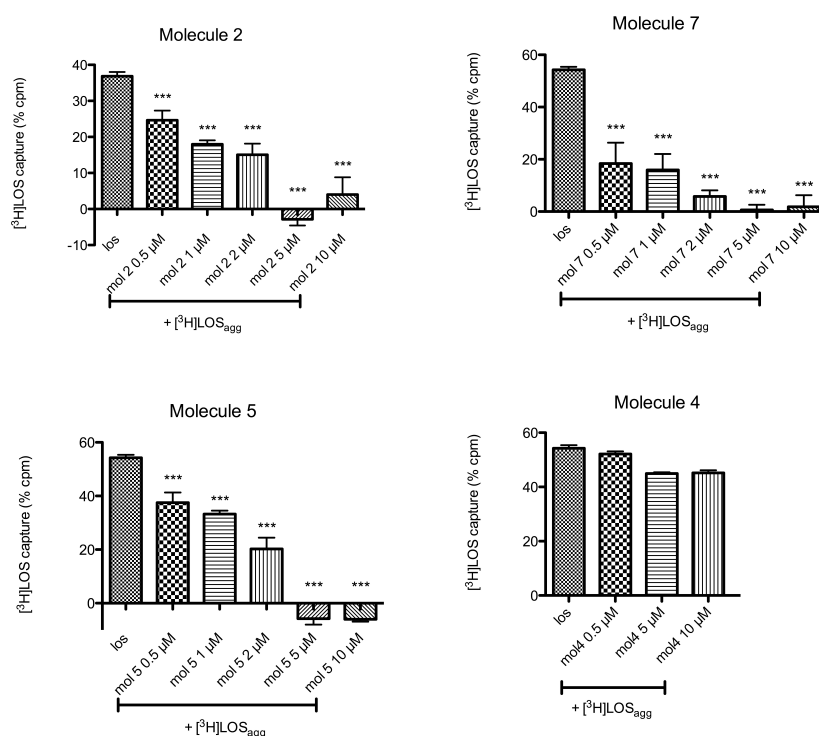


**Figure 23.** Dose-dependent inhibition of the net transfer of  $[^3\text{H}]\text{LOS}$  monomers from  $[^3\text{H}]\text{LOS}_{\text{agg}}$  to tCD14-His<sub>6</sub> by molecules 2-7 as assayed by co-capture of  $[^3\text{H}]\text{LOS}$  to HISLINK resin. tCD14-His<sub>6</sub> (1.6 nM) was pre-incubated + LBP (4 pM) for 30' at 37°C  $\pm$  increasing concentrations of the indicated synthetic compounds.  $[^3\text{H}]\text{LOS}_{\text{agg}}$  (0.8 nM) was then added and samples were incubated for an additional 30 min at 37 °C. Results shown are the mean  $\pm$  SEM of  $\geq 3$  independent experiments, each in duplicate. Non-specific binding, measured as  $[^3\text{H}]\text{LOS}$  binding in absence of tCD14-His<sub>6</sub>, was subtracted from each sample. \*\*\*indicates conditions in which pre-incubation of tCD14-His<sub>6</sub> with the added

### 3. Results and discussions

synthetic molecule resulted in a statistically significant ( $p < 0.01$  (ANOVA; Dunnett's test)) reduction in co-capture of [ $^3\text{H}$ ]LOS (i.e., reduced net formation of [ $^3\text{H}$ ]LOS.tCD14-His<sub>6</sub>).

The ability of molecule 2 to inhibit net transfer/binding of LOS to sCD14 could be more easily explained by an ability of molecule 2 (and related molecules 5 and 7) to bind to CD14 and thus reduce the interaction of LOS with CD14. To test more directly the possible interaction of molecule 2 with sCD14, we made use of STD NMR to probe intermolecular interactions between molecule 2 and sCD14 and to determine sites in molecule 2 that interact with sCD14. STD NMR experiments performed on the sample that contained both molecule 2 and sCD14 clearly showed saturation transfer from sCD14 to molecule 2, most strongly at 0.88 and 1.30 ppm and weakly at 3.13 ppm when the protein resonances were saturated by RF irradiation (Fig. 24D). Identical STD NMR experiments performed on the control sample that contained only sCD14 showed no resonances at these chemical shift positions except for the broad peaks of background signals (Fig. 24E). Excellent cancellation in the STD spectra of the strong solvent peaks present in the samples (Figs. 24B-E) confirmed the good quality of the STD data. The STD peaks detected at 0.88 and 1.30 ppm are derived from the lipid chain -CH<sub>3</sub> and -CH<sub>2</sub> groups, respectively (Fig. 24A). The weak STD peak at 3.13 ppm is likely derived from the lipid chain -OCH<sub>2</sub> group near the polar end of the compound. These findings thus indicate direct binding via the lipid chains of molecule 2 to sCD14.

### 3. Results and discussions

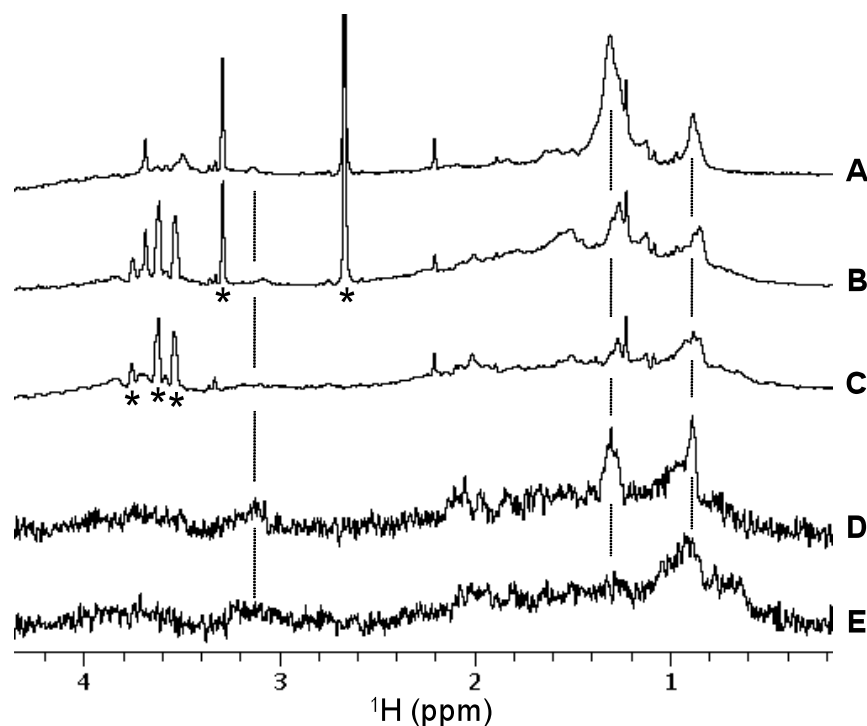


**Figure 24.** Saturation transfer difference NMR analysis of interaction between molecule **2** and sCD14. (A-C) 1D  $^1\text{H}$  NMR spectra of 19 mM compound **2** (sample A), 19 mM compound **2** plus 0.5 mM sCD14 (sample B), and 0.5 mM sCD14 (sample C), respectively. (D) STD NMR spectrum obtained on sample B. (E) STD NMR spectrum collected on the control sample C. The stars indicate  $^1\text{H}$  peaks derived from solvents (DMSO at 2.66 ppm, methanol at 3.29 ppm) and/or buffer components (*e.g.* glycerol from sCD14 initial stock at 3.5-3.8ppm).

#### 3.2.2. Discussion

Previous experimental observations on molecule **2** and similar glycolipids or benzylammonium lipids suggested that the anti-endotoxic activity of these molecules is due to an interference with the TLR4 pathway. The lipid A-stimulated cytokine production by dendritic cells and macrophages is inhibited by compound **2** and an antagonistic effect

### 3. Results and discussions

on TLR4-dependent but not on TLR2- or TLR9-dependent cell activation was observed in selectively transfected HEK293 cells. The main aim of this work was to better understand the mechanism of action of cationic glycolipid **2**, as a representative prototype of this class of compounds. For this purpose, we tested the effect of molecule **2** on the sequential extraction and transfer of [<sup>3</sup>H]LOS monomers from [<sup>3</sup>H]LOS<sub>agg</sub> to LBP, CD14, and MD-2(·TLR4<sub>ECD</sub>), reactions that are key to efficient delivery of activating E to MD-2/TLR4. Our findings demonstrate that molecule **2**, and structurally related molecules **5** and **7**, affect this multi-step pathway in a relatively selective manner, acting mainly to inhibit transfer to and/or stable occupation of CD14 by E ([<sup>3</sup>H]LOS) monomers. Similar inhibitory effects of molecule **2** were seen when the transfer of [<sup>3</sup>H]LOS from either [<sup>3</sup>H]LOS aggregates or from monomeric [<sup>3</sup>H]LOS·sCD14 was examined (Figs. 11, 10, and 15), indicating that an additional effect of molecule **2** on interactions between LBP and E-rich interfaces was unlikely and not necessary for the inhibitory action of molecule **2**. Remarkably, shuttling of E monomers from CD14 to MD-2 is unaffected by molecule **2**. The apparently selective targeting of CD14 by these diacylated compounds is reminiscent of the previously described ability of CD14, but not MD-2, to interact stably with other diacylated compounds such as phospholipids and lipopeptides. The targeting of CD14 by molecules **2**, **5** and **7** is consistent with their ability to inhibit CD14-dependent TLR4 activation by endotoxin (lipid A/LPS) but not CD14-independent cell activation by TLR2 and TLR9 agonists. Moreover, as predicted from our biochemical studies, molecule **2** does not block TLR4 activation when endotoxin (LOS) is presented as a pre-formed LOS·sCD14 complex that needs only to transfer LOS to MD-2 to induce TLR4 activation (data not shown).

### 3. Results and discussions

Whether or not the selective inhibition of LOS binding to CD14, but not to MD-2, reflects a higher affinity of these diacylated compounds for CD14 vs. MD-2 or rather a higher affinity and more stable association of LOS with MD-2 than with CD14 cannot be judged. The inability of molecule **2** to inhibit transfer of [<sup>3</sup>H]LOS to MD-2 from [<sup>3</sup>H]LOS-CD14 (Figs. 13, 14 and 15) underscores the efficiency of that transfer reaction and strongly suggests that molecule **2** and related compounds must have time to occupy CD14 and thereby exclude E from CD14 to exert their maximum inhibitory effects. The STD NMR data reported in this paper clearly show that molecule **2** is a ligand of CD14 and that the lipid chains of molecule **2** have a major role in its interaction with CD14. Work is in progress to determine the thermodynamic parameters of binding and affinity (included stoichiometry of binding) between compounds **2**, **5**, **7** and CD14 and the structural basis of the apparently lower reactivity of molecule **4** with CD14. The experiments reported here suggest that the affinity of compound **2** for CD14 is probably ca. 1000-fold lower than that of LBP-treated E aggregates or monomeric E·CD14 for CD14. The functional properties described suggest that molecules **2**, **5** and **7** could be considered lead compounds in the development of new anti-endotoxic agents selectively targeting CD14. The broader role of CD14 (vs. MD-2) in other biological recognition/response pathways may further expand the potential applications of these compounds.



### 3. Results and discussions

#### ***3.3.A synthetic TLR-4 active glycolipid disulfate targets the human MD-2 receptor***

Despite recent crystallographic data on TLR4 trimeric active complex and seminal works of Albright<sup>97</sup> on endotoxin epitopes involved in CD14 binding, is not possible yet to have an unique rationalization on TLR4 ligands structural requirements.

The majority of antisepsis agents designed to be TLR4 antagonists, such as Eritoran, are comprised of a  $\beta(1\rightarrow6)$ -N-acetylglucosamine disaccharide scaffold with two phosphates in 1 and 4' positions and four lipid chains instead of the six present in lipid A. Comparison of the crystal structure of the [TLR4-MD-2-LPS]<sub>2</sub> complex and that of TLR4-MD-2. Eritoran indicates that the size of the MD-2 pocket is the same whether hexaacylated agonists or tetraacylated antagonists are bound. The MD-2 cavity volume can readily accommodate the four lipid chains of antagonists and additional space for lipid binding is generated, at least in the case of hexaacylated E. coli LPS, by displacing the glucosamine backbone upward by about 5 Å. This shift of the anomeric phosphate and resulting rearrangement of the lipid A acyl chains may be essential for the interaction of activating LPS-MD-2 from one TLR4-MD-2-LPS ternary complex to TLR4 from a second ternary complex, leading to formation of the [TLR4-MD-2-LPS]<sub>2</sub> dimer.

According to this model, underacylated lipid A variants (tetra- and pentacyl) would occupy the MD-2 binding pocket without triggering receptor dimerization, thus having low endotoxic and in some cases anti-endotoxic (antagonist) activity. Structure-activity studies strongly suggest that the number and the length of lipid chains plays a pivotal role in the switch from endotoxic (agonist) to anti-endotoxic

### 3. Results and discussions

(antagonist) activity. This has been observed not only for lipid A variants based on the natural  $\beta(1\rightarrow6)$ diglucosamine backbone, but also in synthetic lipid A mimetic based on a monosaccharide scaffold as in the case of the monophosphoryl aminoalkyl glucosaminide phosphates (AGPs).

The presence of a  $\beta(1\rightarrow6)$ diglucosamine or an aminoalkyl glucosamine or other noncarbohydrate backbones bearing two correctly oriented anionic groups (phosphate or carboxylate isosters) and a variable number of lipid chains seem to be the minimal structural requirements to have TLR4-active compounds.

Molecules synthesized and discussed in the previous sections are unique examples of monosaccharides able to interfere with TLR4 activation. One of the more interesting features of those compounds is their selectivity for CD14 and no evident effect on MD2. CD14 and MD2 have very similar binding sites and up to now structural features of TLR4 ligands are studied in relation to their effects on TLR4 receptor complex, so there are still very few specific information regarding differences on MD2/CD14 binding. Endotoxin transfer from CD14 to MD2 is supposed to be a process involving a different affinity of the ligand for MD2, hence LPS moves to lower energy complex with MD2. Considering that a monomer (molecule 2) is targeted to CD14 and natural ligands (dimers) stably binds to MD2, we direct the synthesis toward a symmetric dimer to evaluate the possibility of its interaction with MD2.

The glycolipid disulfate 1 (GD1) is a lipid A mimetic with a disaccharide scaffold formed by two glucopyranose units bridged through a succinamide linker connecting the C-6 and C-6' positions of sugars (Fig. 25). GD1 backbone differs from natural  $\beta(1'-6)$ -GlcNAc-GlcNAc disaccharide, having an increased conformational mobility due to the

### 3. Results and discussions

presence of the four-atom succinamide linker and also the orientation of the two sulfate groups in 4 and 4' position is different from that of the 4 and 4' phosphates in lipid A. The occurrence of carbohydrate sulfates in nature (heparines and heparan sulfates) inspired the use of sulfate groups as mono-charged, isosteric analogues of the phosphates that is, at the best of our knowledge, unprecedented in lipid A mimetics. The lipid chains are four linear tetradecyl chains connected to the glucose scaffold through unnatural ether bonds. The C-14 ether chains are good mimetic of lipid A chains and were used in previous TLR4-active compounds developed by our group. The ether bond instead of the more labile ester has been selected to improve chemical and enzymatic stability and increase the drug-like properties of the molecule.

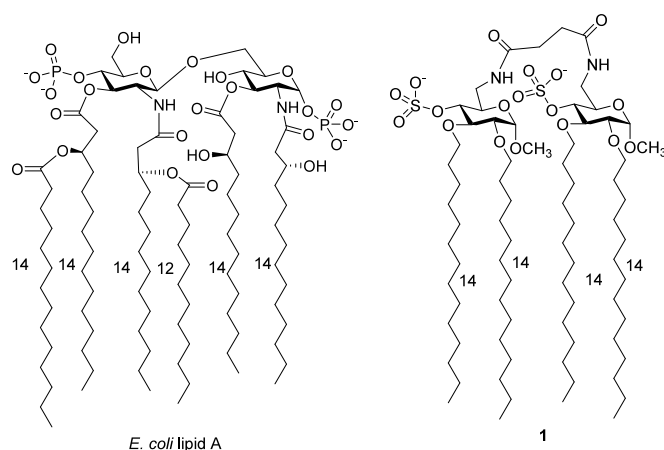


**Figure 25.** Structure of lipid A from E.Coli and of *N-N'* bis (methyl 6-anhydrous-6-amino-4-O-sulfate-2,3-di-O-tetradecil- $\alpha$ -D-glucopyranosil) succinimide

### 3. Results and discussions

#### ***3.3.1. Cellular and biochemical characterization of GD1 interaction with hMD2***

GD1 was then tested with stably transfected HEK-TLR4 cells (from ref) for its ability to interfere with endotoxin-stimulated TLR4 activation. HEK-TLR4 cells respond to bacterial LPS through a TLR4-dependent activation only when accessory receptors CD14 and MD-2 are supplied in addition to endotoxin stimulus. This kind of cells was used instead of HEK-Blue™ because this cellular model allows a better control of assay conditions. These cells produced the inflammatory cytokine IL-8 when stimulated with bacterial lipooligosaccharides (LOS) in form of aggregates in solution together with CD14 and MD-2. When HEK-TLR4 cells were exposed to increasing concentrations of GD1 in the presence of both sCD14 and MD-2, a dose-dependent IL-8 production was observed (Fig. 26).

### 3. Results and discussions

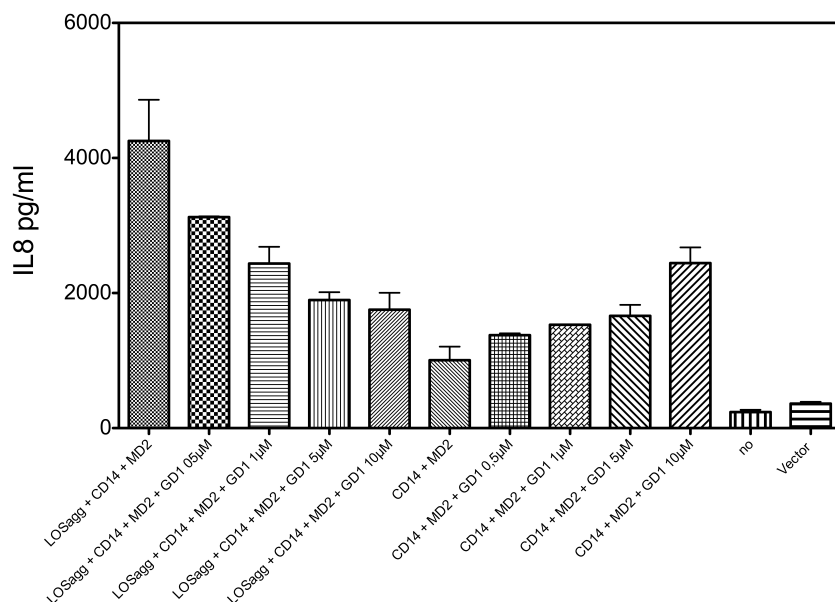


**Figure 26.** TLR4-dependent activation of HEK/TLR4 cells by GD1 in the presence of MD-2 and sCD14. Cell activation was measured as extracellular accumulation of IL-8 after overnight incubation of HEK/TLR4 ±increasing concentrations of GD1 as described in Materials and Methods.

Compound GD1 was also able to inhibit in a concentration-dependent manner the production of LOS-stimulated IL-8 in the presence of MD-2 and sCD14 (Fig. 26). When compared to bacterial LOS, GD1 is less potent in inducing IL-8 production (Fig. 26). Nevertheless, its agonistic activity is very likely TLR4-dependent because no interleukin production was observed when exposing HEK parental cells that do not express TLR4 to GD1 (Fig. 27).

### 3. Results and discussions

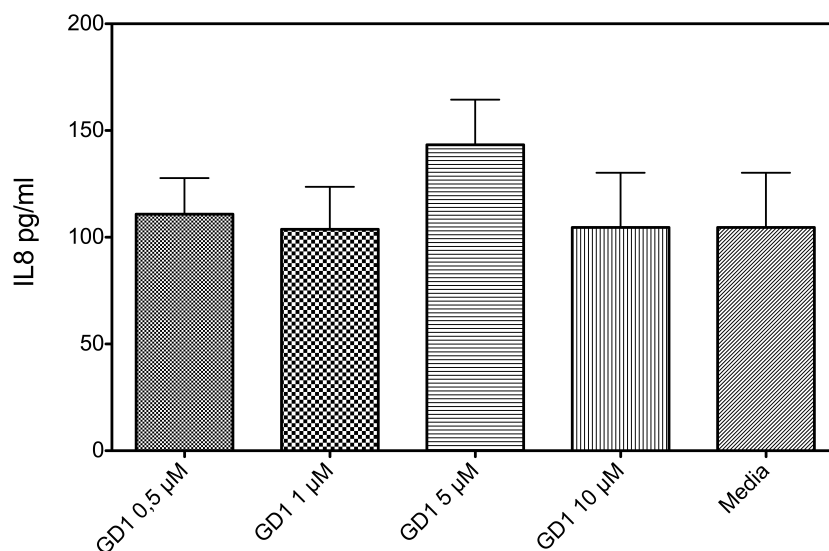


**Figure 27.** TLR4 independent activation of parental HEK293 cells by GD1. Cell activation was measured as extracellular accumulation of IL-8 after overnight incubation of HEK293 ±increasing concentrations of GD1 as described in Materials and Methods.

Previous experiment allow an overview of GD1 effect on TLR4 pathway activation, but remain unclear the precise step influenced by GD1. As described in the introduction section (section 1.3.1.7.3), endotoxin binds to CD14 then is transferred to MD2 and the E:MD2 complex allow TLR4 dimerization. Using different endotoxin donors we investigated the ability of GD1 to specifically interact with a precise step of TLR4 activation. As shown in figure 28 A, there is a dose dependent inhibition of LOS transfer from CD14 to MD2 and this result is comparable to data in figure 26. Instead when preformed LOS:MD2 is used in the assay as endotoxin donor there is no reduction of IL8 production (Fig. 28 B). Those data suggests an interference of GD1 on endotoxin shuttling from CD14 to MD2.

### 3. Results and discussions

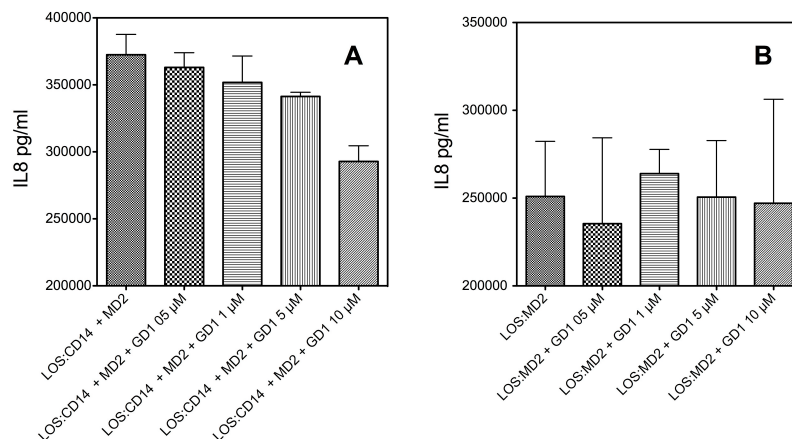


**Figure 28.** Inhibition of TLR4-dependent activation of HEK/TLR4 cells by GD1. Cell activation was measured as extracellular accumulation of IL-8 after overnight incubation of HEK/TLR4  $\pm$  increasing concentrations of GD1 and LOS:CD14 in presence of md2 or LOS:MD2 alone as described in Materials and Methods.

To better define the mechanism of the inhibitory action of molecule GD1 on LPS (lipid A)-triggered TLR4 activation, we tested the ability of this compound to inhibit LBP/CD14-dependent transfer of endotoxin ( $[^3\text{H}]$ LOS) monomers from  $[^3\text{H}]$ LOS aggregates to MD-2/TLR4, resulting in reduced formation of a  $[^3\text{H}]$ LOS·MD-2·TLR4<sub>ECD</sub><sub>2</sub> (Mr ~190,000) complex. For this purpose, sCD14 was pre-incubated with LBP in the presence or absence of molecule GD1 (10 mM), and then incubated with  $[^3\text{H}]$ LOSagg followed by conditioned medium containing preformed MD-2·TLR4<sub>ECD</sub> heterodimer. Size-exclusion chromatography of the reaction mixture (Fig. 29) showed that, in the absence of molecule GD1, virtually all  $[^3\text{H}]$ LOS aggregates (LOSagg) were converted to later eluting species (i.e., smaller  $[^3\text{H}]$ LOS-containing complexes) corresponding to  $[^3\text{H}]$ LOS·sCD14 (Mr~60,000) and  $[^3\text{H}]$ LOS·MD-2·TLR4<sub>ECD</sub><sub>2</sub> (Mr~190,000). The generation of  $[^3\text{H}]$ LOS·sCD14 reflects extraction and

### 3. Results and discussions

transfer of [ $^3\text{H}$ ]LOS monomers from [ $^3\text{H}$ ]LOSagg to sCD14 by the combined action of LBP and sCD14. Formation of [[ $^3\text{H}$ ]LOSMD-2·TLR4ECD] $_2$  reflects transfer of [ $^3\text{H}$ ]LOS monomers from [ $^3\text{H}$ ]LOSsCD14 to MD-2·TLR4<sub>ECD</sub>. Thus, the chromatographic profile of [ $^3\text{H}$ ]LOSagg incubated first with LBP and sCD14 and then with conditioned medium containing sMD-2·TLR4<sub>ECD</sub> suggests that, under these experimental conditions, there is nearly complete extraction and transfer of [ $^3\text{H}$ ]LOS monomers from [ $^3\text{H}$ ]LOSagg to [ $^3\text{H}$ ]LOSsCD14 followed by transfer of [ $^3\text{H}$ ]LOS monomers from about half of the [ $^3\text{H}$ ]LOSsCD14 formed to MD-2·TLR4<sub>ECD</sub>. In contrast, in the presence of 10 mM molecule GD1, accumulation of [[ $^3\text{H}$ ]LOSMD-2·TLR4<sub>ECD</sub>] $_2$  was markedly reduced while the peak corresponding to the [ $^3\text{H}$ ]LOSsCD14 resulted almost unvaried (Fig. 29). The inhibition of accumulation of [[ $^3\text{H}$ ]LOSMD-2·TLR4<sub>ECD</sub>] $_2$  and not of [ $^3\text{H}$ ]LOSsCD14 once more suggests that molecule GD1 very likely interferes in the process of LOS transfer from [ $^3\text{H}$ ]LOSsCD14 to the MD-2 receptor or to the MD-2·TLR4<sub>ECD</sub> complex.



### 3. Results and discussions

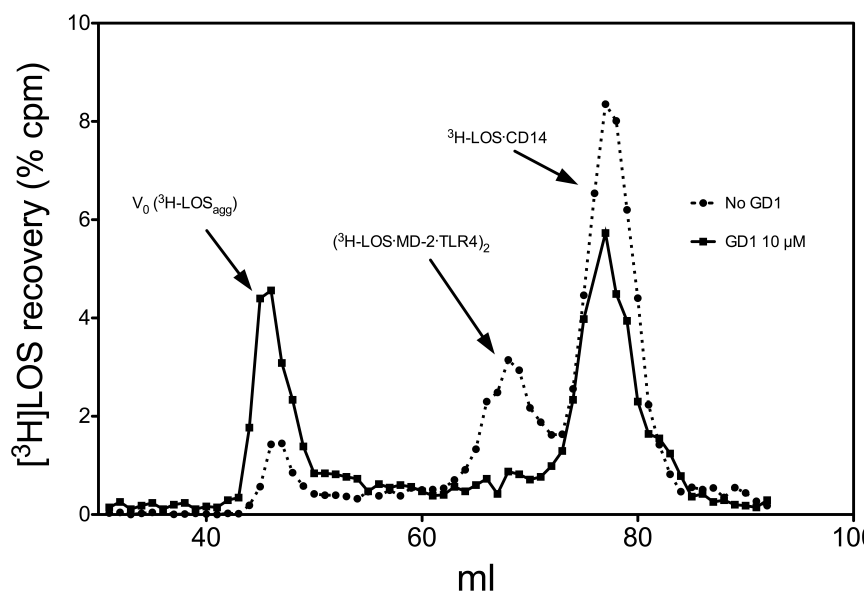


**Figure 29.** GD1 inhibits conversion of  $[^3\text{H}]\text{LOS}_{\text{agg}}$  to  $[^3\text{H}]\text{LOS}\cdot\text{sCD14}$  and  $[^3\text{H}]\text{LOS}\cdot\text{MD-2}\cdot\text{TLR4}_2$ . sCD14 (0.8 nM) was pre-incubated  $\pm$  GD1 (10  $\mu\text{M}$ ) for 30 min at 37 °C in the presence of LBP (4 pM). Subsequently,  $[^3\text{H}]\text{LOS}_{\text{agg}}$  (0.8 nM) was added and this mixture was incubated for 30 min at 37 °C. After the second incubation, conditioned HEK293T cell medium containing preformed reactive MD-2·TLR4<sub>ECD</sub> heterodimer (ca. 0.2 nM, final concentration) was added and incubated again for 15 min at 37 °C. This reaction mixture was applied to Sephacryl S200 as described under Experimental Procedures to measure conversion of  $[^3\text{H}]\text{LOS}_{\text{agg}}$  (void volume) to  $[^3\text{H}]\text{LOS}\cdot\text{sCD14}$  ( $M_r \sim 60,000$ ) and  $[^3\text{H}]\text{LOS}\cdot\text{MD-2}\cdot\text{TLR4}_2$  ( $M_r \sim 190,000$ ). The chromatographic profiles shown are representative of  $\geq 4$  experiments. Overall recoveries of  $[^3\text{H}]\text{LOS}$  were  $\geq 70\%$ .

It was therefore decided to verify directly the hypothesis that molecule GD1 could inhibit the endotoxin transfer from the complex with CD14 to that with MD-2. It was designed an experiment in which the transfer of the radiolabelled endotoxin monomer ( $[^3\text{H}]\text{LOS}$ ) from the  $[^3\text{H}]\text{LOS}\cdot\text{sCD14}$  to the  $[^3\text{H}]\text{LOS}\cdot\text{MD-2}$  complex in which an His-tagged MD-2 is used, can be monitored by capturing the  $[^3\text{H}]\text{LOS}\cdot\text{MD-2}$  complex

### 3. Results and discussions

with a nickel-coated HISLINK resin (Fig. 30). As described in material and methods section His-tagged MD-2 was pre-incubated at 37 °C for 30' ± increasing concentrations of GD1, then preformed [<sup>3</sup>H]LOS-sCD14 complex was added and followed by another incubation at 37 °C for 30'. Transfer of radiolabeled LOS ([<sup>3</sup>H]LOS) from sCD14 to MD-2-His6 was observed by capturing the latter complex with HISLINK resin after incubation (Fig. 30). The incubation of [<sup>3</sup>H]LOS-sCD14 with MD-2-His6 followed by resin capture yielded a good radioactivity recovery on resin, indicating that LOS is transferred from CD14 to MD-2. In the presence of increasing concentrations of molecule GD1 in incubation medium, the bound radioactivity levels decreased proportionally, thus clearly suggesting direct effect of molecule GD1 in inhibiting the LOS transfer from CD14 to MD-2.

### 3. Results and discussions

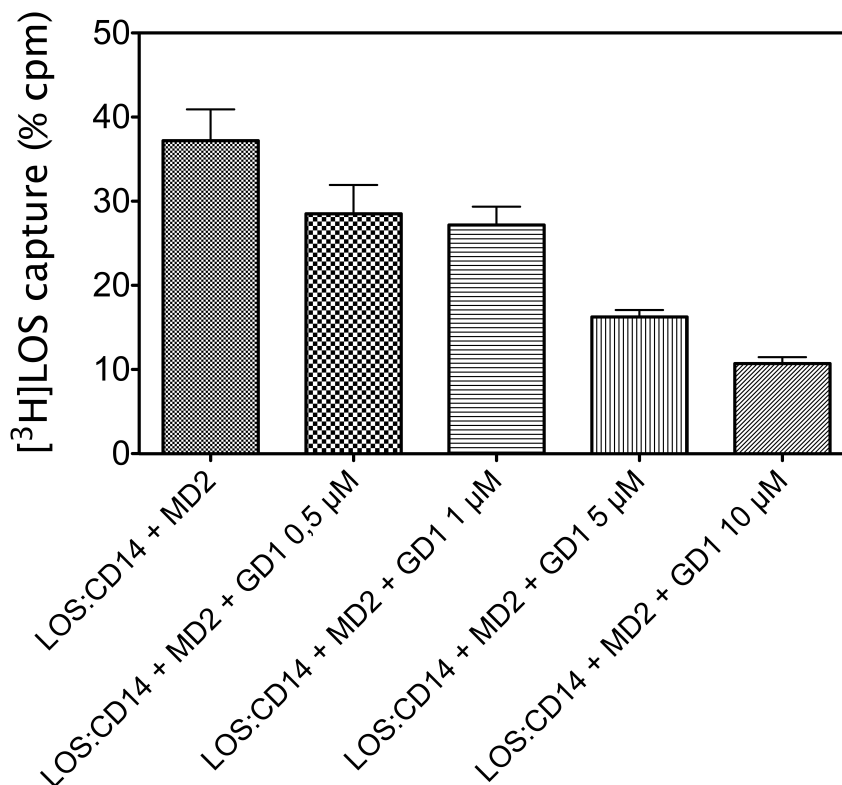


**Figure 30.** GD1 selectively inhibits transfer of [<sup>3</sup>H]LOS monomer to MD-2. His-tagged sMD2 (1.6 nM) was pre-incubated for 30' at 37°C with 10 uM GD1, followed by addition of [<sup>3</sup>H]LOS-sCD14 (0.8 nM) and further incubation for 30 min at 37 °C. Transfer of [<sup>3</sup>H]LOS to MD-2 was assayed by co-capture of [<sup>3</sup>H]LOS to the HISLINK resin as described under Experimental Procedures. Capture of [<sup>3</sup>H]LOS-sCD14 (no His-tag) before and after incubation in medium without His-tagged protein was < 4% and subtracted from each of the experimental samples shown. Data shown are representative of 3 experiments, each in duplicate, and are expressed as mean ± SEM.

Also if both the previous experiments and the striking evidence given from gel sieving analysis demonstrate a MD2 dependent mode of action for GD1 it is possible that the compound interfere with LOS:CD14 complex disrupting it, thus misleading the interpretation of the

### 3. Results and discussions

experiments. To clarify this possibility we performed a preincubation of CD14 with the compound in presence of LBP followed by another incubation with LOSagg and analyzed the reaction mixture with a co-capture assay (more detailed description of the procedure in section 2.4). Figure 31 demonstrate that GD1 has no effect on endotoxin binding to CD14 and further confirm that this compound acts inhibiting the transfer of monomeric endotoxin to MD2.

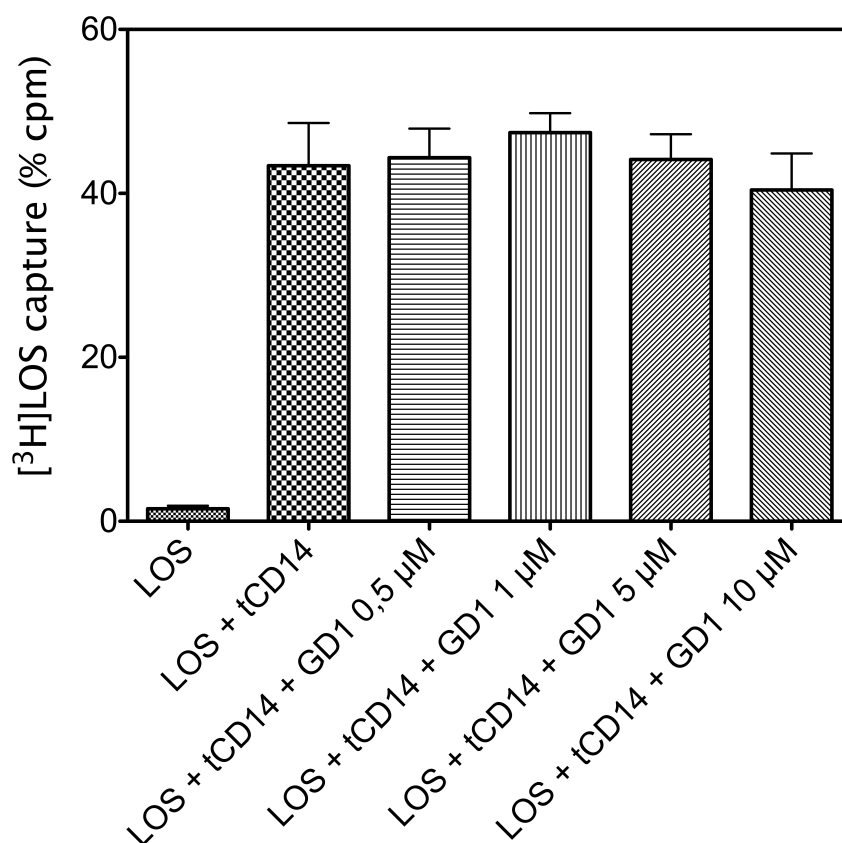


**Figure 31.** GD1 do not inhibits transfer of [<sup>3</sup>H]LOS monomer to tCD14. His-tagged tCD14 (1.6 nM) was pre-incubated for 30' at 37°C with 10 uM GD1, followed by addition of [<sup>3</sup>H]LOSagg (0.8 nM) and further incubation for 30 min at 37 °C. Transfer of [<sup>3</sup>H]LOS to His-tagged tCD14 was assayed by co-capture of [<sup>3</sup>H]LOS to the HISLINK resin as described

### 3. Results and discussions

under Experimental Procedures. Capture of [<sup>3</sup>H]LOSagg in absence of His-tagged tCD14 was < 4% and subtracted from each of the experimental samples shown. Data shown are representative of 3 experiments, each in duplicate, and are expressed as mean ± SEM.

Reduction of LOS:MD2 captured complexes highlight the final inhibitory effect of GD1 but from those data is not possible to understand if the compound occupies MD2 binding site avoiding incoming endotoxin to enter or dynamically compete with the latter displacing it from preformed LOS:MD2 complexes.

Preformed LOS:MD2 is a stable complex and is further stabilized by interaction with TLR4 so we expected that LOS bound to MD2 could not be displaced from GD1. To answer this question we incubated [<sup>3</sup>H]LOS:MD2-His6 with increasing concentrations of GD1 and captured MD2 with HISLINK resin. Bound percentages in figure 32 do not significantly change in presence of GD1.

### 3. Results and discussions

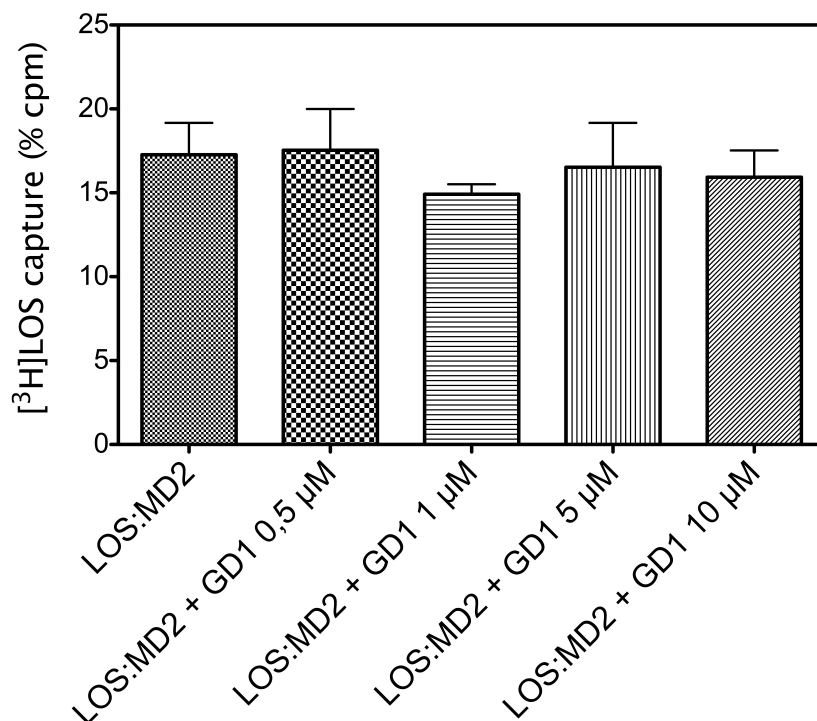


**Figure 32.** GD1 do not inhibit displacement of [<sup>3</sup>H]LOS monomer from preformed [<sup>3</sup>H]LOS.MD2 complexes. His-tagged MD2 (1.6 nM) was pre-incubated for 30' at 37°C with 10 μM GD1, followed by addition of [<sup>3</sup>H]LOSagg (0.8 nM) and further incubation for 30 min at 37 °C. Transfer of [<sup>3</sup>H]LOS to His-tagged tCD14 was assayed by co-capture of [<sup>3</sup>H]LOS to the HISLINK resin as described under Experimental Procedures. Capture of [<sup>3</sup>H]LOSagg in absence of His-tagged tCD14 was < 4% and subtracted from each of the experimental samples shown. Data shown are representative of 3 experiments, each in duplicate, and are expressed as mean ± SEM.

### 3. Results and discussions

#### 3.3.2. Discussion

Taken together, the experiments presented indicate that the disaccharide disulfate 1 (GD1) is active in interfering with the TLR4-dependent cytokine production in HEK cells. When administered alone, GD1 triggers TLR4 activation and IL-8 production, while when co-administered with bacterial LOS has a dose-dependent antagonistic effect and inhibits cytokine production. This behaviour suggest a role of GD1 as partial agonist of the TLR4 receptor. GD1 is a mild agonist and giving aTLR4 stimulation milder than bacterial LOS, so it could be a good candidate as vaccine adjuvant. On the other and, GD1 inhibits the LOS-triggered TLR4 activation suggesting the use of GD1 as lead for the development of anti-endotoxic molecules.

#### ***3.4. Heme and a metabolic derivative, coproheme, modulate the TLR4 pathway differently through different molecular targets***

Several TLR4 antagonists were developed (see section 3.1), all of them with different structures but always related with some features of Lipid A. Recent discoveries suggest that TLR4 could bind a wide array of endogenous ligands most of them with unknown structures. Those ligands are involved in different pathologies and chronic inflammatory diseases like neuropatic pain and arteriosclerosis. Study and develop of variants of those compounds could be useful to expand the library of structural epitopes interacting with MD2 or CD14. A recent paper investigated the molecular mechanism whereby heme activates macrophages and it was observed that heme induces the secretion of

### 3. Results and discussions

TNF- $\alpha$  by activating TLR4 (see section 1.4.1.2). We synthesized a highly carboxylated variant of heme, coproheme, and decided to study its properties in inhibiting the LPS-stimulated interleukin production in HEK-TLR4 cells. As with the previous compounds, biochemical studies on the interaction of coproheme with isolated receptors of the TLR4 pathway (namely LBP, CD14, MD-2 and TLR4) will be performed. In parallel, we would try to characterize the biological activity of heme considering the previous observations.

#### ***3.4.1. Biochemical and cellular characterization of heme and coproheme effects on TLR4 receptor complex***

HEK-TLR4 cells were treated with increasing concentrations of heme in culture media with or without CD14, MD2 and LBP (see section 2.4 for further technical informations). A dose-dependent production of IL-8 was induced by heme and the level of interleukin produced did not change when MD-2 and CD14 receptors were added to the medium (Fig. 33). The levels of interleukin secreted upon heme exposure, were anyway much lower than that induced by stimulating cells with LPS provided in three different forms: as LOS aggregates, as LOS.CD14 and LOS.MD-2 complexes.



### 3. Results and discussions

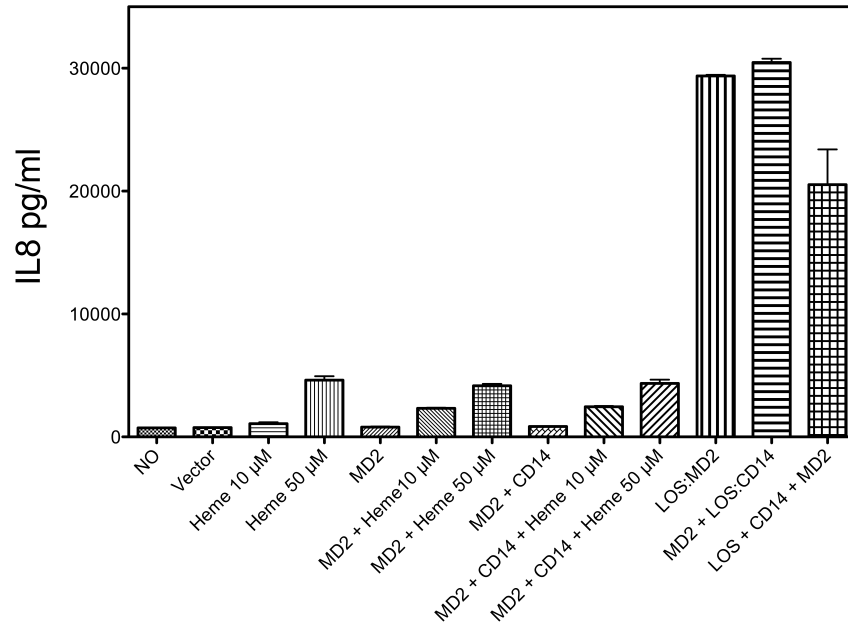


**Figure 33.** TLR4-dependent activation of TLR4-HEK293 cells by heme in the presence and absence of MD-2 and sCD14. Cell activation was measured as extracellular accumulation of IL-8 after overnight incubation of HEK/TLR4  $\pm$  increasing concentrations of heme as described in Materials and Methods.

It was then checked if this increase of cytokine production was a response to a stress condition generated by heme or was related to a specific action on TLR4. Exposure to heme up to a concentration of 70 mM did not cause any IL-8 production in HEK parental cells lacking TLR4 (Fig 34), thus confirming that the stimulus driven by heme relies on the presence of TLR4.

### 3. Results and discussions

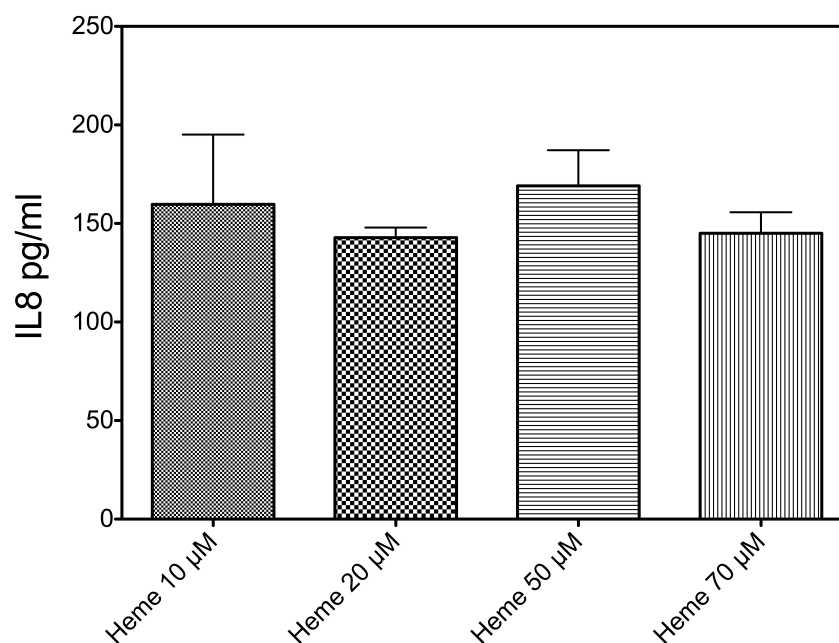


**Figure 34.** Response of HEK parental cells in presence of heme.

Previous experimental observations suggested that LPS and heme, despite both interacting with TLR4, likely target different binding sites of the receptor. The IL-8 production of HEK-TLR4 cells stimulated by the exposure to the preformed endotoxin.MD-2 complex, was then monitored in the presence of increasing quantities of heme. No significant inhibition of endotoxin-derived stimulus was observed when HEK-TLR4 cells are preincubated with heme (50  $\mu\text{M}$ ) both by supplying endotoxin in the form of LOS-CD14 and LOS-MD-2 complexes (Fig. 35). The above experiments are in accordance with literature data and point out that heme elicits TLR4-dependent cytokine production but TLR4 activation is achieved through a molecular mechanism different from that associated to endotoxin stimulation.

### 3. Results and discussions

It often happened in older papers that being very easy endotoxin contamination, results on TLR4 agonism were often misled by tiny amount of LPS in the sample. In the case of heme this hypothesis could be discharged because activation occurs in the absence of MD2 and CD14.

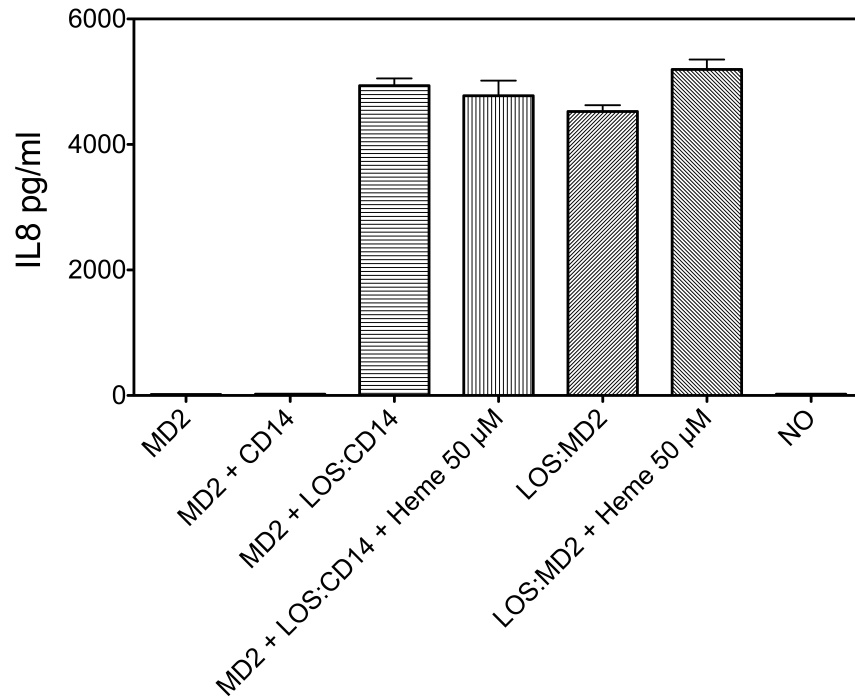


**Figure 35.** Inhibition of TLR4-dependent activation of HEK/TLR4 cells by heme. Cell activation was measured as extracellular accumulation of IL-8 after overnight incubation of HEK/TLR4  $\pm$ heme 50  $\mu$ M and LOS:CD14 in presence of md2 or LOS:MD2 alone as described in Materials and Methods.

The capacity of coproheme to induce a dose-dependent cytokine secretion in HEK cells was then investigated. In contrast with what observed in the case of heme, exposure to coproheme up to a concentration of 70 mM did not stimulate any IL-8 production from HEK-TLR4 cells (Fig. 36). The experiments done on heme were parallelized with coproheme, and the capacity of coproheme to modulate an LPS-triggered cell response was then investigated. As

### 3. Results and discussions

shown in the Fig.3, the exposure to coproheme did not alter the IL-8 production in HEK cells, when the stimulus was provided by administering the LOS.MD-2 preformed complex. In contrast, an inhibition of the interleukin secretion is observed when the endotoxin is supplied as preformed complex with CD14 (Fig. 36). In the canonical sequence of reactions associated to endotoxin recognition and TLR4 activation in innate immunity cells, the formation of E-CD14 complex is normally followed by endotoxin transfer to MD-2 with formation of E.MD-2 complex. The above experiments indicate that coproheme inhibits the endotoxin-triggered TLR4 activation whether inhibiting the [<sup>3</sup>H]LOS transfer from CD14 to MD-2 and/or by promoting displacement of bound [<sup>3</sup>H]LOS from MD-2.

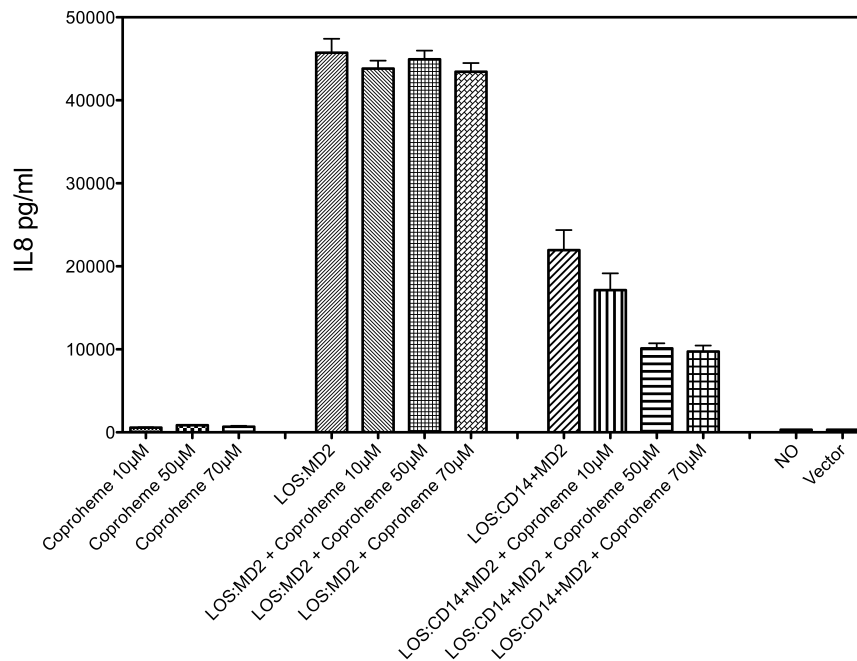


**Figure 36.** Inhibition of TLR4-dependent activation of HEK/TLR4 cells by coproheme. Cell activation was measured as extracellular

### 3. Results and discussions

accumulation of IL-8 after overnight incubation of HEK/TLR4  $\pm$  increasing concentrations of coproheme and  $\pm$  LOS:CD14 in presence of md2 or LOS:MD2 alone as described in Materials and Methods.

To better define the mechanism of the inhibitory action of coproheme on LPS-triggered TLR4 activation it was decided to follow the same experimental setting used for GD1 and molecule 1. It was tested the effect of coproheme on LBP/CD14-dependent transfer of endotoxin ( $[^3\text{H}]\text{LOS}$ ) from  $[^3\text{H}]\text{LOS}$  aggregates to the MD-2/TLR4 complex, by monitoring the formation of a  $[[^3\text{H}]\text{LOS}\cdot\text{MD-2}\cdot\text{TLR4}_{\text{ECD}}]_2$  ( $M_r \sim 190,000$ ) complex. For this purpose, sCD14 was pre-incubated with LBP in the presence or absence of coproheme (50  $\mu\text{M}$ ), and then incubated with  $[^3\text{H}]\text{LOS}_{\text{agg}}$  followed by conditioned medium containing preformed MD-2 $\cdot$ TLR4 $_{\text{ECD}}$  heterodimer. Size-exclusion chromatography of the reaction mixture (Fig. 37) showed that, in the absence of coproheme, virtually all  $[^3\text{H}]\text{LOS}$  aggregates ( $\text{LOS}_{\text{agg}}$ ) were converted to later eluting species (i.e., smaller  $[^3\text{H}]\text{LOS}$ -containing complexes) corresponding to  $[^3\text{H}]\text{LOS}\cdot\text{sCD14}$  ( $M_r \sim 60,000$ ) and  $[[^3\text{H}]\text{LOS}\cdot\text{MD-2}\cdot\text{TLR4}_{\text{ECD}}]_2$  ( $M_r \sim 190,000$ ). The generation of  $[^3\text{H}]\text{LOS}\cdot\text{sCD14}$  reflects extraction and transfer of  $[^3\text{H}]\text{LOS}$  monomers from  $[^3\text{H}]\text{LOS}_{\text{agg}}$  to sCD14 by the combined action of LBP and sCD14. Formation of  $[[^3\text{H}]\text{LOS}\cdot\text{MD-2}\cdot\text{TLR4}_{\text{ECD}}]_2$  reflects transfer of  $[^3\text{H}]\text{LOS}$  monomers from  $[^3\text{H}]\text{LOS}\cdot\text{sCD14}$  to MD-2 $\cdot$ TLR4 $_{\text{ECD}}$ .<sup>22</sup> Thus, the chromatographic profile of  $[^3\text{H}]\text{LOS}_{\text{agg}}$  incubated first with LBP and sCD14 and then with conditioned medium containing sMD-2 $\cdot$ TLR4 $_{\text{ECD}}$  suggests that, under these experimental conditions, there is nearly complete extraction and transfer of  $[^3\text{H}]\text{LOS}$  monomers from  $[^3\text{H}]\text{LOS}_{\text{agg}}$  to  $[^3\text{H}]\text{LOS}\cdot\text{sCD14}$  followed by transfer of  $[^3\text{H}]\text{LOS}$  monomers from about half of the  $[^3\text{H}]\text{LOS}\cdot\text{sCD14}$  formed to MD-2 $\cdot$ TLR4 $_{\text{ECD}}$ . In contrast, in the presence of 50  $\mu\text{M}$  coproheme, accumulation of  $[[^3\text{H}]\text{LOS}\cdot\text{MD-2}\cdot\text{TLR4}_{\text{ECD}}]_2$  was markedly reduced while

### 3. Results and discussions

the complex  $[^3\text{H}]\text{LOS}\cdot\text{sCD14}$  was formed in a similar amount than in the absence of the molecule (Fig. 37). The inhibition of accumulation of  $[[^3\text{H}]\text{LOS}\cdot\text{MD-2}\cdot\text{TLR4}_{\text{ECD}}]_2$  and the formation of  $[^3\text{H}]\text{LOS}\cdot\text{sCD14}$  suggested a primary effect of coproheme on transfer of  $[^3\text{H}]\text{LOS}$  monomers from  $[^3\text{H}]\text{LOS}\cdot\text{sCD14}$  to MD-2.

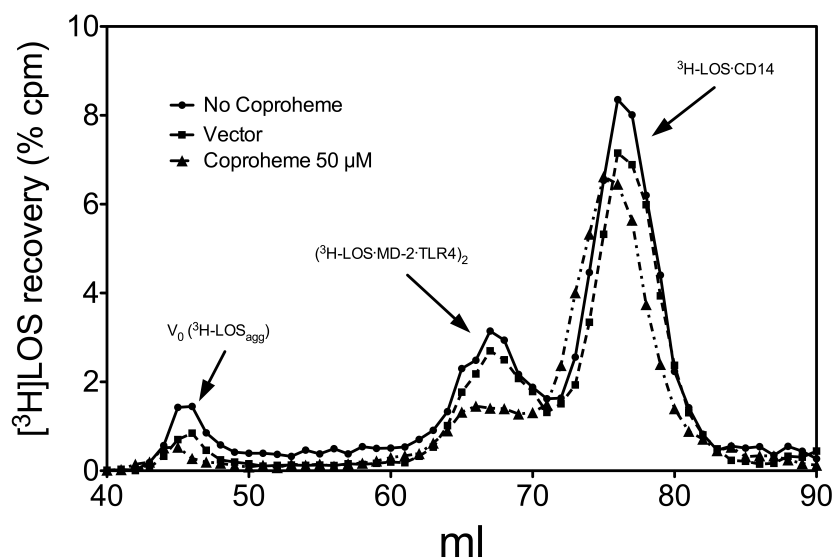


**Figure 37.** Coproheme inhibits conversion of  $[^3\text{H}]\text{LOS}\cdot\text{sCD14}$  to  $[^3\text{H}]\text{LOS}\cdot\text{MD2}$  and  $[[^3\text{H}]\text{LOS}\cdot\text{MD-2}\cdot\text{TLR4}]_2$ . sCD14 (0.8 nM) was pre-incubated  $\pm$  coproheme (50  $\mu\text{M}$ ) for 30 min at 37  $^\circ\text{C}$  in the presence of LBP (4 pM). Subsequently,  $[^3\text{H}]\text{LOS}_{\text{agg}}$  (0.8 nM) was added and this mixture was incubated for 30 min at 37 $^\circ\text{C}$ . After the second incubation, conditioned HEK293T cell medium containing preformed reactive MD-2 $\cdot$ TLR4 $_{\text{ECD}}$  heterodimer (ca. 0.2 nM, final concentration) was added and incubated again for 15 min at 37  $^\circ\text{C}$ . This reaction mixture was applied to Sephacryl S200 as described under Experimental Procedures to measure conversion of  $[^3\text{H}]\text{LOS}_{\text{agg}}$  (void volume) to  $[^3\text{H}]\text{LOS}\cdot\text{sCD14}$  ( $M_r \sim 60,000$ ) and  $[[^3\text{H}]\text{LOS}\cdot\text{MD-2}\cdot\text{TLR4}]_2$  ( $M_r \sim 190,000$ ). The chromatographic profiles shown are representative of  $\geq 4$  experiments. Overall recoveries of  $[^3\text{H}]\text{LOS}$  were  $\geq 70\%$ .

### 3. Results and discussions

To test this hypothesis more directly, MD2 containing media was preincubated with coproheme (50  $\mu\text{M}$ ) then subsequently the reaction mixture was incubated with  $[^3\text{H}]\text{LOS}\cdot\text{sCD14}$  to allow  $[^3\text{H}]\text{LOS}\cdot\text{MD2}$  complex formation. As shown in figure 38, coproheme caused an evident reduction in the formation of  $[^3\text{H}]\text{LOS}\cdot\text{MD-2}$ , while the peak corresponding to  $[^3\text{H}]\text{LOS}\cdot\text{sCD14}$  was unvaried.

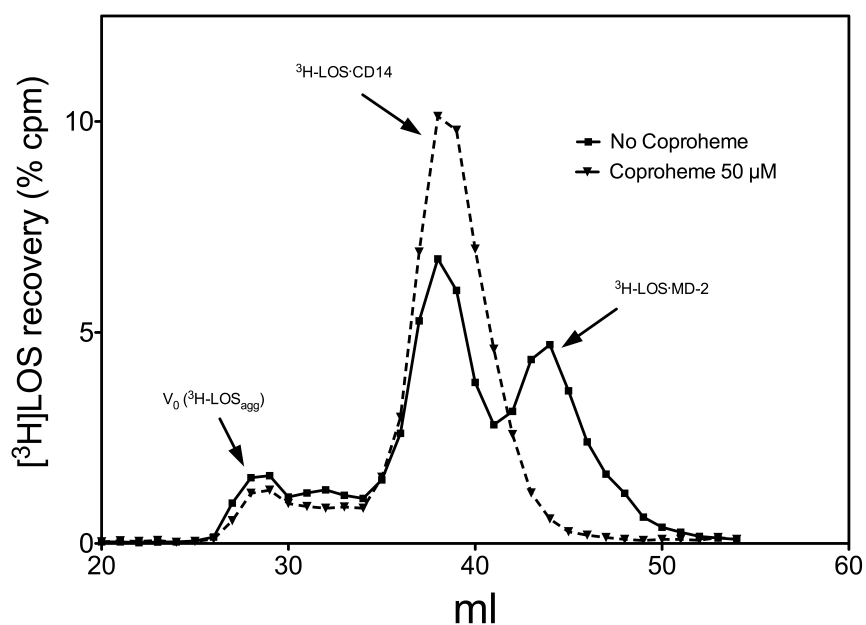


**Figure 38.** Inhibition by coproheme of  $[^3\text{H}]\text{LOS}$  monomers transfer from  $[^3\text{H}]\text{LOS}\cdot\text{CD14}$  to MD2. MD2 (0.8 nM) was pre-incubated with coproheme (50  $\mu\text{M}$ ) for 30 min at 37 °C in PBS, pH 7.4, 0.1% HSA.  $[^3\text{H}]\text{LOS}\cdot\text{CD14}$  (0.8 nM) was then added to the reaction mixture followed by an incubation for 30 min at 37° C and reaction products were analyzed using Sephacryl S200 chromatography. The chromatographic profiles shown are representative of  $\geq 3$  experiments. Overall recoveries of  $[^3\text{H}]\text{LOS}$  were  $\geq 70\%$ .

### 3. Results and discussions

Previous experiment indicate that coproheme very likely inhibits the transfer of [<sup>3</sup>H]LOS from CD14 to MD-2. Further evidence of this mechanism of action was collected by experiments complementary to that described above, and based on the formation of complexes of [<sup>3</sup>H]LOS and histidine-tagged receptors followed by complex capture with a Ni-chelating resin and quantification of bound radioactivity. We therefore preincubated His tagged MD-2 (MD-2-His<sub>6</sub>) with or without increasing concentrations of coproheme (5-50 μM), then performed [<sup>3</sup>H]LOS·sCD14 was added to the reaction mixture. [<sup>3</sup>H]LOS·MD-2-His<sub>6</sub> formation was assessed with an HISLINK co-capture assay (Fig. 39). This assay showed a marked diminution of [<sup>3</sup>H]LOS bound to MD-2-His<sub>6</sub> induced by incubation with coproheme and this effect was dose-dependent. In contrast, the incubation with heme (Fig. 40) did not alter the quantity of [<sup>3</sup>H]LOS·MD-2-His<sub>6</sub> recovered indicating again that this molecule does not interfere with the formation of endotoxin.MD-2 complex.



### 3. Results and discussions

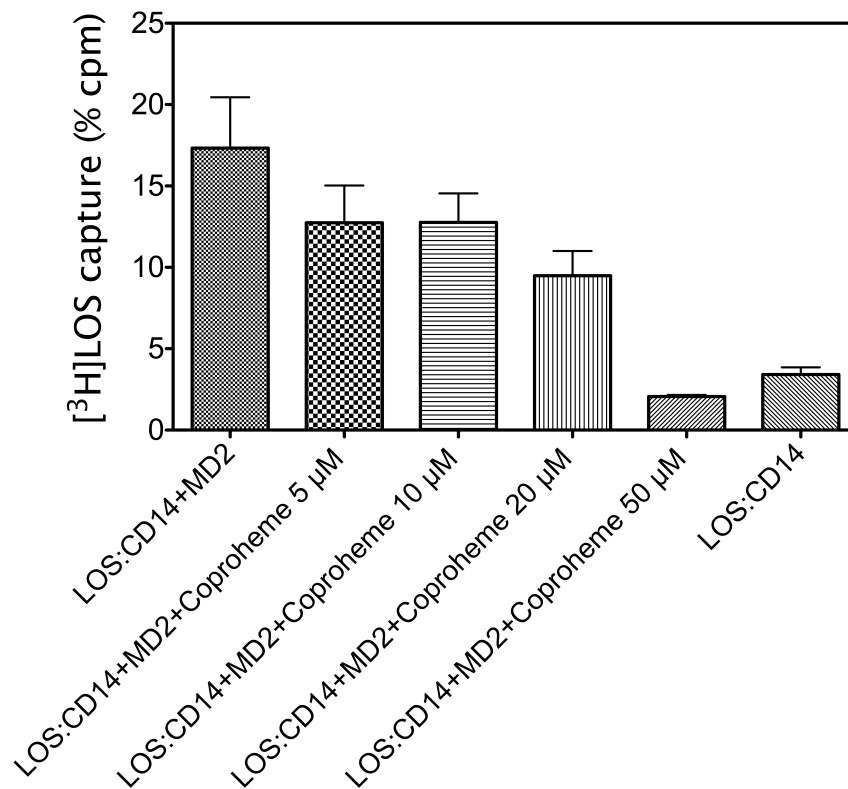


**Figure 39.** Coproheme selectively inhibits transfer of [<sup>3</sup>H]LOS monomer from sCD14 to MD2. His-tagged sMD2 (1.6 nM) was pre-incubated for 30' at 37°C ± increasing concentrations of coproheme, followed by addition of [<sup>3</sup>H]LOS·sCD14 (0.8 nM) and further incubation for 30 min at 37 °C. Transfer of [<sup>3</sup>H]LOS to His-tagged MD-2 was assayed by co-capture of [<sup>3</sup>H]LOS to the HISLINK resin as described under Experimental Procedures. Capture of [<sup>3</sup>H]LOS·sCD14 (no His-tag) before and after incubation in medium without His-tagged protein was < 4% and subtracted from each of the experimental samples shown. Data shown are representative of 3 experiments, each in duplicate, and are expressed as mean ± SEM.

### 3. Results and discussions

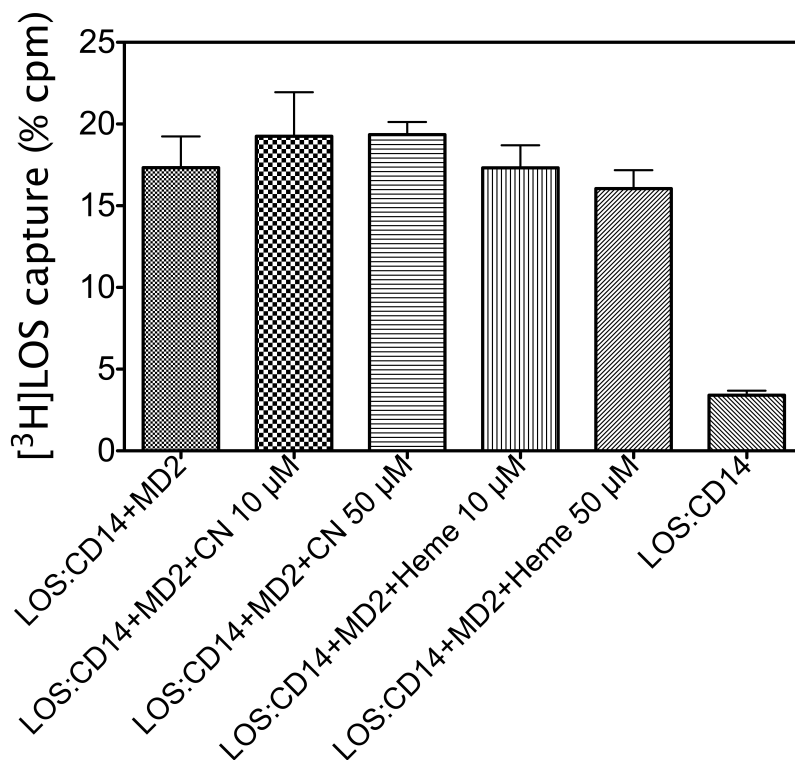


**Figure 40.** Heme and non-metalled coproheme (CN) do not inhibit transfer of [<sup>3</sup>H]LOS monomer from sCD14 to MD2. His-tagged sMD2 (1.6 nM) was pre-incubated for 30' at 37°C with 50 µM heme and non-metalled coproheme, followed by addition of [<sup>3</sup>H]LOS-sCD14 (0.8 nM) and further incubation for 30 min at 37 °C. Transfer of [<sup>3</sup>H]LOS to His-tagged MD-2 was assayed by co-capture of [<sup>3</sup>H]LOS to the HISLINK resin as described under Experimental Procedures. Capture of [<sup>3</sup>H]LOS-sCD14 (no His-tag) before and after incubation in medium without His-tagged protein was < 4% and subtracted from each of the experimental samples shown. Data shown are representative of 3 experiments, each in duplicate, and are expressed as mean ± SEM.

#### 3.4.2. Discussion

In conclusion, while heme is likely to target directly TLR4, giving a moderate activation of this receptor and inducing TLR4-mediated

### 3. Results and discussions

cytokine production, coproheme has an antagonistic activity on the extracellular TLR4 activation pathway and this effect seems to be due to an inhibition of EMD-2 complex formation. The different behavior of heme and coproheme described in this work could suggest some preliminary considerations and parallels with the role of these biomolecules in physiological and pathological events. Teleologically, it makes sense that heme is an inflammatory molecule because it is generally present in organism associated with proteins and free heme is a “danger” signal triggering a multitude of defense responses of the organism, among that the activation of TLR4-mediated innate immunity. The highly oxidated and hydrosoluble coproheme is on the contrary present in body fluids of healthy organisms as product of heme catabolic oxidation to be excreted. It is therefore reasonable that coproheme does not elicit any TLR4-mediated inflammatory response. The coproheme property of inhibiting the TLR4 activation targeting the endotoxin loading on MD-2 is an interesting preliminary indication for the development and study of similar heme variants with antiendotoxic activity.

#### ***3.5. Synthetic endotoxin aggregates for the study of TLR4 activation mechanisms***

Magnetic nanoparticles are a kind of important functional material. Due to their small size and superparamagnetic behavior, these magnetic nanoparticles exhibit different material properties from their bulk solutions. Magnetic nanoparticles have already been used widely in commercial domains, such as dynamic loudspeakers and computer hard drives. Magnetic nanoparticles with appropriately modified surface

### 3. Results and discussions

characteristics can be used to (a) facilitate the separation of biomolecules, (b) to sort specific cell types from a cell population, and (c) to deliver drugs to a target organ in the body. The application of small particles in in vitro Diagnostics has been practised for nearly 40 years. This is due to a number of beneficial factors including a large surface area to volume ratio, and the possibility of ubiquitous tissue accessibility. In the last decade increased investigations and developments were observed in the field of nanosized magnetic particles, the term nanoparticle being used to cover particulate systems that are less than 1 $\mu$ m in size, and normally below 500 nm. Nanoparticles that possess magnetic properties offer exciting new opportunities including improving the quality of magnetic resonance imaging (MRI), hyperthermic treatment for malignant cells, site-specific drug delivery and also the recent research interest of manipulating cell membranes. Iron oxide magnetic nanoparticles tend to be either paramagnetic or superparamagnetic, with particles approximately 20 nm being classed as the latter. In most cases superparamagnetic particles (usually Fe<sub>2</sub>O<sub>3</sub> and Fe<sub>3</sub>O<sub>4</sub>) are of interest for in-vivo applications, as they do not retain any magnetism after removal of the magnetic field. This is important as large domain magnetic and paramagnetic materials aggregate after exposure to a magnetic field (Bonnemaitet al1998, Wang et al2001). Previous sections mainly focalized on synthesis and biological characterization of small compounds interacting with TLR4. In those sections the main interest was to evaluate the importance of chemical structures in their interaction with TLR4. The role of those compounds is to interfere with TLR4 activation both inhibiting or triggering this condition. In this section it was decided to focus the attention on LPS presentation to TLR4 receptor complex and supramolecular requirements for TLR4

### 3. Results and discussions

activation.

As stated in the introductory section, endotoxin interaction with TLR4 complex is still a matter of debate. Most discussed is the role of endotoxin aggregates in binding and activating this receptor. Some papers<sup>98</sup> suggests that aggregates are the active form of LPS thus reassessing the importance of those multimeric structures in TLR4 activation. Other papers<sup>99-102</sup>, in contrast, suggests that LPS, to activate TLR4, has to be presented in monomeric form by LBP. We think that a more detailed study on pure endotoxin aggregates will help the clarification of LBP function and mechanism of action and will be extremely usefull for a deeper explanation of mechanism underlying TLR4 activation. Endotoxin aggregates are well studied and characterized structures<sup>98</sup> and obviously exists in solution in equilibrium with endotoxin monomers. Preparation of pure and stable aggregates without the monomeric components could be useful for studies on endotoxin interaction with TLR4 as for therapeutic purposes. In a recent paper endotoxin aggregates were prepared<sup>103</sup> with serial dialysis steps with dedicated membranes, but this approach has a very low level yield and aggregates prepared are stable only in a very broad range of concentrations. As preliminary experiments for LPS presentation in innovative nanostructures it was decided to design hydrophobic nanoparticles (HNPs) coated with LPS. To perform the coating hydrophobic interactions between the alkyl chains of LPS and the oleic acid portion of the nanoparticles will be used (Fig. 41). This structure should be a mimic of a natural micell but with an higher stability both to a broader concentration range than to different physical treatments (e.g. aerosol for therapeutical uses).

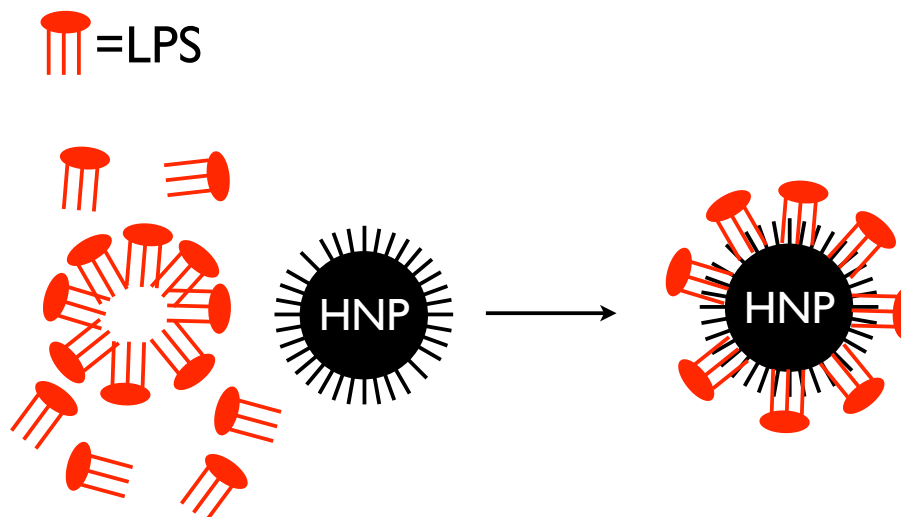


**Figure 41.** Schematic exemplification of the coating process

It was decided to use as a scaffold composed of a Fe<sub>3</sub>O<sub>4</sub> nanoparticle coated with oleic acid. This highly hydrophobic structure should allow the interaction between lipid chains of LPS and exposed oleic acid.

### ***3.5.1. Development of a protocol for synthetic endotoxin aggregates production***

Magnetic nanoparticles (MNPs) were synthesized as described in (ref<sup>104</sup>) from research group of Prof. Davide Prospero.

MNPs were then coated with LPS in a biphasic (Hexane/Aqueous buffer) reaction mixture. Being reasonably that LPS-coated MNPs became soluble in aqueous buffer, with this procedure it was expected to give an additional driving force for the reaction because LPS-coated MNPs will become hydrated in the aqueous phase thus increasing entropy and lipid chains of LPS are involved in energetically favored interactions

### 3. Results and discussions

with oleic acids. Different protocols were used prior to develop the definitive one described in material and methods section.

It was decided to follow a previous protocol used for SDS coating of similar hydrophobic NPs<sup>105</sup> (fig 42).

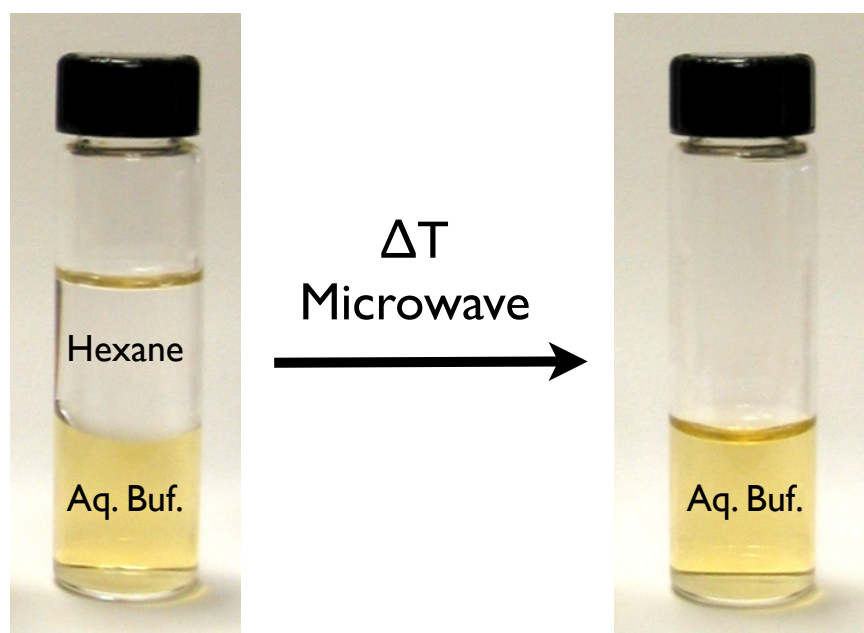


**Figure 42.** Two phase (hexane/aqueous buffer) system for HNPs coating with LPS

Using milliq-water as aqueous phase (Fig. 43, Table 1) and following radioactivity in supernatants and pellets is it not possible to detect a stable signal correlated with beads, hence there is no detectable coating of hydrophobic NPs (since now HNPs).

### 3. Results and discussions

**Table 1**

PURIF	BOUND %	SUP %
1.00	4.40	90.45
2.00	0.65	3.11
3.00	0.15	0.58
4.00	0.05	0.12

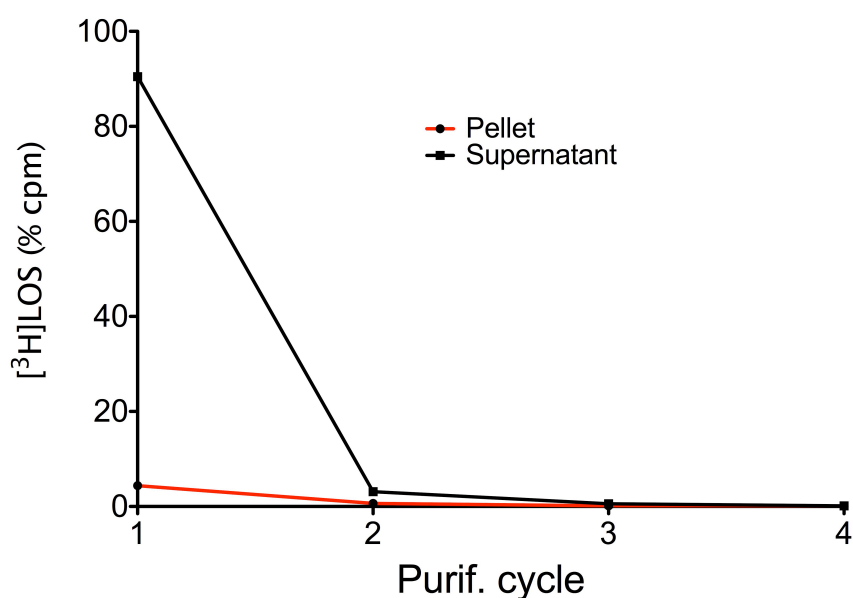


**Figure 43.** [<sup>3</sup>H]LOS recovery for each purification step using coating protocol n.1. After coating protocol described above the reaction mixture was repeatedly purified as described in material and method section.

LPS in very low ionic strength buffers is very difficult solubilized and in those experimental conditions preferentially interact with plasticware, thus drastically reducing LPS available for HNPs coating. In spite of those observations it was decided to use phosphate buffer as aqueous phase (Fig. 44, Table 2).



### 3. Results and discussions

**Table 2**

PURIFY. CYCLE	BOUND %	SUP %
1.00	13.53	58.76
2.00	4.44	8.01
3.00	0.45	0.82

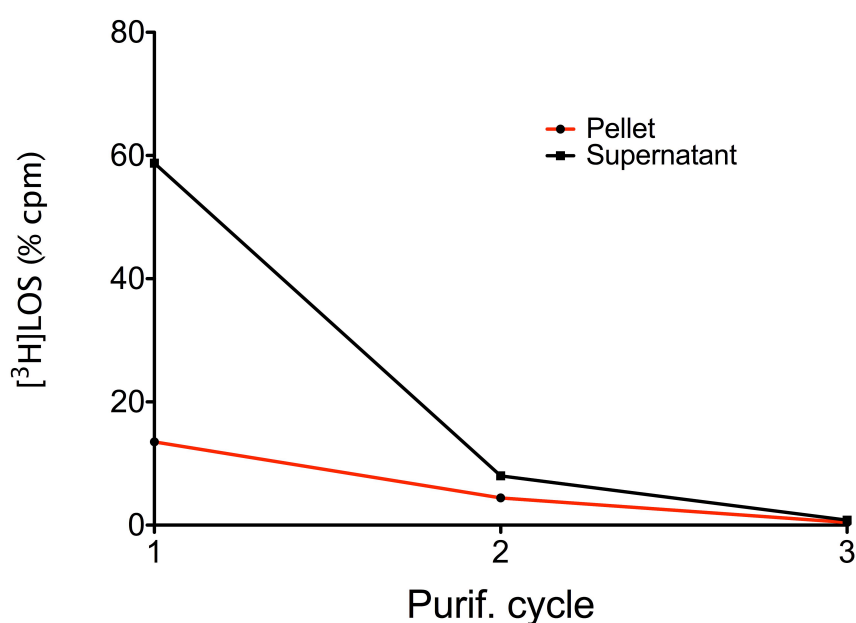


**Figure 44.** [ $^3\text{H}$ ]LOS recovery for each purification step using coating protocol n.2. After coating protocol described above the reaction mixture was repeatedly purified as described in material and method section.

Also using phosphate buffer radioactivity levels, connected to HNPs, are undetectable after three purification steps. LPS in presence of divalent cations, always presents in the endotoxin stocks, form stable aggregates, hence exposing the hydrophilic core, while acyl chains remain buried inside the micelles being no more available for interaction with HNPs.

### 3. Results and discussions

To loose those micelles the next preparation is done using 5 mM EDTA in TRIS buffer with or without Human Serum Albumin (HSA) to improve LPS solubilization (Fig 45, Table 3).

- 1) 40 ng LOS/ 50 uL Tris EDTA + 240 ng NP/40 uL Hexane
- 2) 40 ng LOS/ 50 uL Tris EDTA + 0,1% HSA 240 ng NP/40 uL Hexane

**Table 3**

PREP 1			
	Bound %	Sup %	recovery %
1	65.14	34.86	10.01
2	91.28	8.72	7.59
3	96.63	3.37	4.04
Prep 2			
	Bound %	Sup %	recovery %
1	41.44	58.56	57.82
2	68.95	31.05	21.08
3	56.68	43.32	12.65

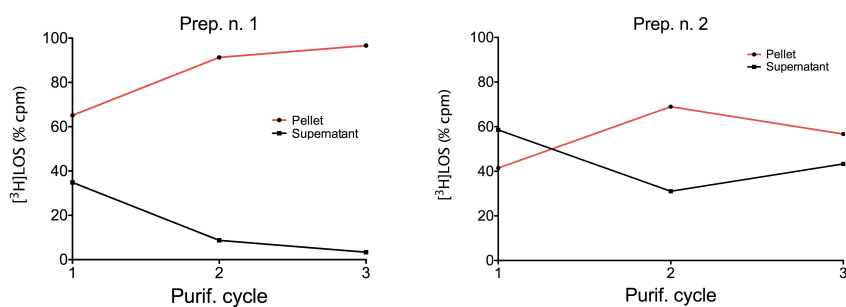


**Figure 45.**  $[^3\text{H}]$ LOS recovery for each purification step using coating protocol n.3 (preparations 1 and 2). After coating protocol described above the reaction mixture was repeatedly purified as described in material and method section.

### 3. Results and discussions

From results absence of divalent cations improve HNPs coating and HSA seems to allow the formation of unstable complexes between HNPs and LPS.

As a previous assessment of LPS coated HNPs stability the same preparation is repeated and a fourth purification cycle done after 15 days (Fig 46, Table 4).

**Table 4**

PREP 2	Bound %	Sup %	recovery %
1	79.96	20.04	51.70
2	92.01	7.99	26.46
4	98.27	1.73	17.08

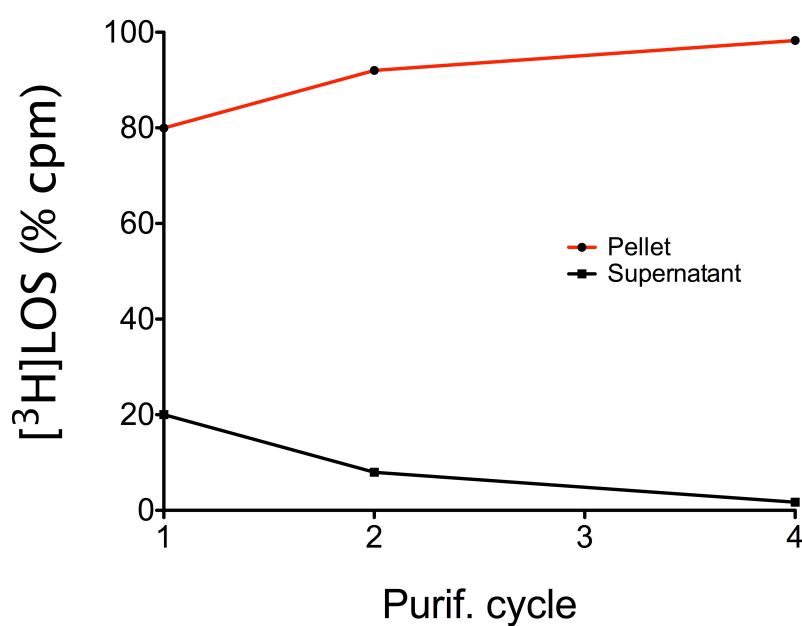


**Figure 46.**  $[^3\text{H}]$ LOS recovery for each purification step using coating protocol n.4. After coating protocol described above the reaction

### 3. Results and discussions

mixture was repeatedly purified as described in material and method section.

Radioactivity connected to HNPs do not significantly decrease after two weeks suggesting that LPS-HNPs complexes are stable over this period of time.

#### 3.5.2. Discussion

As shown in the previous section this protocol allow a small scale production of LPS-HNPs complex to use in in-vitro or in-vivo assay. Complexes formed with this protocol are stable enough for further experimental characterization. Protocol described in this section is the first attempt to create a stable and reproducible mimic of LPS micells that can be valuable for basic and applied studies.

## **4. Conclusion and future perspectives**

### **4.1. Conclusions**

Data presented in this thesis suggest a new class of compounds that selectively interact with different components of TLR4 receptor complex. Monosaccharides presented in section 3 are active both in vitro as in murine models inhibiting LPS-dependent activation of TLR4. Correlation between structure and activity lead to some preliminary observations on structural requirements for their activity. All active compounds present a protonable group in position C6 that is suppose to interact with a cluster of charged residues in the outer part of the binding cleft of CD14 and MD2. Lipid chains were considered necessary for the activity of all the molecules considering that binding pockets of CD14 and MD2 presents an extensive hydrophobic area that strongly interact with all known ligands. Surprisingly carbohydrate scaffold seems not to be an important feature because mol 7, based on a rigid aromatic ring, is very active in competing with LPS. Compounds seems to be very selective for TLR4 and do not influence cell viability nor metabolic rate. The latter parameter was assed pretreating cells with the molecules then measuring the activation derived upon TNF-alfa exposure.

In section 3.3 is presented the synthesys and characterization of a partial agonist of TLR4, GD1. This compound seems to elicit a specific, MD2-dependent, partial agonistic effect on TLR4 pathway. Surprisingly this compound show no interaction with CD14 thus suggesting a different interaction pattern, in comparison to LPS, with the whole TLR4

#### 4. Conclusions and future perspectives

receptor complex. We consider GD1 a good lead compound for the development of a more extensive library based on observations reported in this dissertation. As stated in the introductory section develop of partial agonist of TLR4 is important for several therapeutic uses, like vaccine adjuvants or potential anti cancer treatments.

To expand the knowledge of structural requirements for TLR4 interactions we extensively studied the effect of two natural compounds, Fe-coproporphyrin and heme. Both those compounds seems to interact with an alternative, not LPS comparable, pathway with TLR4. While Fe-coproporphyrin target protein was discovered, target of heme is still under study. In the last section (3.5) we then provide an affordable and reproducible protocol for LPS coating of functionalized NPs. We think that production of those structures is important for clarifying interaction of LPS with MD2 and TLR4 and could be useful as a selective delivery system of LPS, or LPS mimics, for potential therapeutic uses. So far all studies on TLR4 active compounds were done with cellular or murine models leading to indirect informations about the mechanism of action. For the purposes of this dissertation we developed reliable and scalable assays using purified components of the receptor complex. Those assays revealed to be a powerful techniques for screening of libraries and fast assessment of the target protein amongst MD2, CD14 or TLR4 itself. All experiments were carried out in single test tubes but the assay format could be easily modified to create an HTP-like screening system for bigger libraries or for testing several natural mutations of LPS. A simplified and controlled assays environment, coupled to cellular testing, allows also the rapid identification of the important structural features of ligand screened thus accelerating the development of second generation libraries. We are at present developing new assays based on Ni-chelating capture

#### 4. Conclusions and future perspectives

technique for the development of a LPS-quantification test alternative to the LAL assay, with hopefully an higher sensitivity and better robustness than the latter.

### 4.2. Future perspective

Based in the data obtained so far we are in the process of having the computer model simulation of the docking between the compounds and CD14 or MD2. This model will allow to to better define structural requirement for binding of GD1 or antagonistic compounds to their target proteins and residues of the proteins involved in the interaction. In parallel the same experiments will be done not in-silico forming the complexes compound:receptors and analyzing their mass with a mass spectrometry equipment. Those experiments will provide valuable data on stoichiometry of the complexes and more precise calculations of the binding constants. Binding constants will be also analyzed with isothermal calorimetry for comparison of those results with data from in-silico simulations. Once those informations will be available we will synthesize a new generation library of antagonists and GD1. As described for compound 2, also GD1 is actually undergoing the process of NMR characterization for its interaction with MD2. Regarding HNPs coated with LPS we are scaling up the process to have more material for in-vivo and in-vitro experiments aimed to clarify HNPs-LPS activity.

BIBLIOGRAPHY

- (1) Medzhitov, R.; Janeway, C. *New England Journal of Medicine* **2000**.
- (2) Beutler, B. *Molecular immunology* **2004**.
- (3) Medzhitov, R. *Nature* **2007**.
- (4) Rankin, J. A. *AACN Clin Issues* **2004**, 15, 3.
- (5) Wenzel, S. E. *Prostaglandins Leukot Essent Fatty Acids* **2003**, 69, 145.
- (6) Kumagai, Y.; Takeuchi, O.; Akira, S. *Journal of Infection and Chemotherapy* **2008**.
- (7) Kimbrell, D.; Beutler, B. *Nature Reviews Genetics* **2001**.
- (8) Imler, J.; Hoffmann, J. *Trends in Cell Biology* **2001**.
- (9) Gadjeva, M.; Takahashi, K.; Thiel, S. *Mol Immunol* **2004**, 41, 113.
- (10) Gadjeva, M.; Thiel, S.; Jensenius, J. C. *Curr Opin Immunol* **2001**, 13, 74.
- (11) Proell, M.; Riedl, S. J.; Fritz, J. H.; Rojas, A. M.; Schwarzenbacher, R. *PLoS One* **2008**, 3, e2119.
- (12) Jin, M.; Lee, J. *Immunity* **2008**.
- (13) Jin, M.; Kim, S.; Heo, J.; Lee, M.; Kim, H.; Paik, S. *Cell* **2007**.
- (14) Keith, F. J.; Gay, N. J. *EMBO J* **1990**, 9, 4299.
- (15) Kubota, K.; Keith, F. J.; Gay, N. J. *Biochem J* **1993**, 296 (Pt 2), 497.



## Bibliography

- (16) Modlin, R. L. *Ann Allergy Asthma Immunol* **2002**, *88*, 543.
- (17) Bauer, S.; Kirschning, C. J.; Hacker, H.; Redecke, V.; Hausmann, S.; Akira, S.; Wagner, H.; Lipford, G. B. *Proc Natl Acad Sci U S A* **2001**, *98*, 9237.
- (18) West, A.; Koblansky, A.; Ghosh, S. *Annual Reviews* **2006**.
- (19) Vollmer, J. *Int Rev Immunol* **2006**, *25*, 155.
- (20) Krieg, A. M.; Vollmer, J. *Immunol Rev* **2007**, *220*, 251.
- (21) Wetzler, L. M. *Vaccine* **2003**, *21 Suppl 2*, S55.
- (22) Takeuchi, O.; Hoshino, K.; Akira, S. *J Immunol* **2000**, *165*, 5392.
- (23) Ozinsky, A.; Underhill, D. M.; Fontenot, J. D.; Hajjar, A. M.; Smith, K. D.; Wilson, C. B.; Schroeder, L.; Aderem, A. *Proc Natl Acad Sci U S A* **2000**, *97*, 13766.
- (24) Flo, T. H.; Ryan, L.; Latz, E.; Takeuchi, O.; Monks, B. G.; Lien, E.; Halaas, O.; Akira, S.; Skjak-Braek, G.; Golenbock, D. T.; Espevik, T. *J Biol Chem* **2002**, *277*, 35489.
- (25) Perera, P. Y.; Mayadas, T. N.; Takeuchi, O.; Akira, S.; Zaks-Zilberman, M.; Goyert, S. M.; Vogel, S. N. *J Immunol* **2001**, *166*, 574.
- (26) Massari, P.; Henneke, P.; Ho, Y.; Latz, E.; Golenbock, D. T.; Wetzler, L. M. *J Immunol* **2002**, *168*, 1533.
- (27) Kataoka, K.; Muta, T.; Yamazaki, S.; Takeshige, K. *J Biol Chem* **2002**, *277*, 36825.

## Bibliography

- (28) Alexopoulou, L.; Holt, A. C.; Medzhitov, R.; Flavell, R. A. *Nature* **2001**, *413*, 732.
- (29) Andrejeva, J.; Childs, K. S.; Young, D. F.; Carlos, T. S.; Stock, N.; Goodbourn, S.; Randall, R. E. *Proc Natl Acad Sci U S A* **2004**, *101*, 17264.
- (30) Kawai, T.; Takahashi, K.; Sato, S.; Coban, C.; Kumar, H.; Kato, H.; Ishii, K. J.; Takeuchi, O.; Akira, S. *Nat Immunol* **2005**, *6*, 981.
- (31) Hayashi, F.; Smith, K. D.; Ozinsky, A.; Hawn, T. R.; Yi, E. C.; Goodlett, D. R.; Eng, J. K.; Akira, S.; Underhill, D. M.; Aderem, A. *Nature* **2001**, *410*, 1099.
- (32) Mizel, S. B.; Honko, A. N.; Moors, M. A.; Smith, P. S.; West, A. P. *J Immunol* **2003**, *170*, 6217.
- (33) Franchi, L.; McDonald, C.; Kanneganti, T. D.; Amer, A.; Nunez, G. *J Immunol* **2006**, *177*, 3507.
- (34) Hemmi, H.; Yoshida, T.; Kumazaki, T.; Nemoto, N.; Hasegawa, J.; Nishioka, F.; Kyogoku, Y.; Yokosawa, H.; Kobayashi, Y. *Biochemistry* **2002**, *41*, 10657.
- (35) Diebold, S. S.; Kaisho, T.; Hemmi, H.; Akira, S.; Reis e Sousa, C. *Science* **2004**, *303*, 1529.
- (36) Krug, A.; French, A. R.; Barchet, W.; Fischer, J. A.; Dzionek, A.; Pingel, J. T.; Orihuela, M. M.; Akira, S.; Yokoyama, W. M.; Colonna, M. *Immunity* **2004**, *21*, 107.
- (37) Barton, B. E. *Expert Opin Ther Targets* **2006**, *10*, 459.
- (38) Zhang, D.; Zhang, G.; Hayden, M. S.; Greenblatt, M. B.; Bussey, C.; Flavell, R. A.; Ghosh, S. *Science* **2004**, *303*, 1522.

## Bibliography

- (39) Jiang, Q.; Akashi, S.; Miyake, K.; Petty, H. *J Immunol* **2000**.
- (40) Clark, A. G.; Szumski, F. M.; Bell, K. A.; Keith, L. E.; Houtz, S.; Merriwether, D. A. *Genet Res* **1990**, *56*, 49.
- (41) Schumann, R. *Research in immunology(Paris)* **1992**.
- (42) Kirschning, C.; Au-Young, J.; Lamping, N.; Reuter, D. *Genomics* **1997**.
- (43) Tobias, P.; Soldau, K.; Iovine, N.; Elsbach, P.; Weiss, J. *Journal of Biological Chemistry* **1997**.
- (44) Schumann, R.; Rietschel, E.; Loppnow, H. *Medical microbiology and immunology* **1994**.
- (45) Jahr, T.; Sundan, A.; Lichenstein, H.; Espevik, T. *Scandinavian Journal of Immunology* **1995**.
- (46) Bernheiden, M.; Heinrich, J.; Minigo, G.; Schutt, C. *Journal of Endotoxin Research* **2001**.
- (47) Landmann, R.; Müller, B.; Zimmerli, W. *Microbes and Infection* **2000**.
- (48) Muroi, M.; Ohnishi, T.; Tanamoto, K. *Journal of Biological Chemistry* **2002**.
- (49) Kim, J.; Jin, M.; Lee, C.; Paik, S.; Lee, H. *Journal of Biological Chemistry* **2005**.
- (50) Jack, R. *books.google.com* **2000**.
- (51) Wright, S.; Ramos, R.; Tobias, P.; Ulevitch, R. *Science* **1990**.

## Bibliography

- (52) Hold, G. L.; Rabkin, C. S.; Gammon, M. D.; Berry, S. H.; Smith, M. G.; Lissowska, J.; Risch, H. A.; Chow, W. H.; Mowat, N. A.; Vaughan, T. L.; El-Omar, E. M. *Eur J Cancer Prev* **2009**, *18*, 117.
- (53) Schroder, N.; Morath, S.; Alexander, C.; Hamann, L. *Journal of Biological Chemistry* **2003**.
- (54) Gengenbacher, D.; Salm, H.; Vogt, A.; Schneider, H. *Bone Marrow Transplant* **1998**, *22 Suppl 1*, S48.
- (55) Triantafilou, K.; Triantafilou, M.; Dedrick, R. *Nature Immunology* **2001**.
- (56) Gruber, A.; Mancek, M.; Wagner, H.; Kirschning, C. *Journal of Biological Chemistry* **2004**.
- (57) Fitzgerald, K. A.; Rowe, D. C.; Golenbock, D. T. *Microbes Infect* **2004**, *6*, 1361.
- (58) Gioannini, T. L.; Teghanemt, A.; Zhang, D.; Coussens, N. P.; Dockstader, W.; Ramaswamy, S.; Weiss, J. P. *Proc Natl Acad Sci USA* **2004**, *101*, 4186.
- (59) Ohto, U.; Fukase, K.; Miyake, K.; Satow, Y. *Science* **2007**, *316*, 1632.
- (60) Teghanemt, A.; Re, F.; Prohinar, P.; Widstrom, R.; Gioannini, T. L.; Weiss, J. P. *The Journal of biological chemistry* **2008**, *283*, 1257.
- (61) Walsh, C.; Gangloff, M.; Monie, T.; Smyth, T.; Wei, B. *The Journal of Immunology* **2008**.
- (62) Medzhitov, R.; Preston-Hurlburt, P.; Janeway, C. A., Jr. *Nature* **1997**, *388*, 394.
- (63) Kajava, A. V. *J Mol Biol* **1998**, *277*, 519.

## Bibliography

- (64) Hajjar, A. M.; Ernst, R. K.; Tsai, J. H.; Wilson, C. B.; Miller, S. I. *Nat Immunol* **2002**, *3*, 354.
- (65) Choe, J.; Kelker, M. S.; Wilson, I. A. *Science* **2005**, *309*, 581.
- (66) Kim, H. M.; Park, B. S.; Kim, J.-I.; Kim, S. E.; Lee, J.; Oh, S. C.; Enkhbayar, P.; Matsushima, N.; Lee, H.; Yoo, O. J.; Lee, J.-O. *Cell* **2007**, *130*, 906.
- (67) Kopp, E.; Medzhitov, R. *Current Opinion in Immunology* **1999**.
- (68) Rietschel, E. T.; Kirikae, T.; Schade, F. U.; Mamat, U.; Schmidt, G.; Loppnow, H.; Ulmer, A. J.; Zahringer, U.; Seydel, U.; Di Padova, F.; et al. *FASEB J* **1994**, *8*, 217.
- (69) Raetz, C. R.; Whitfield, C. *Annu Rev Biochem* **2002**, *71*, 635.
- (70) Bhattacharya, I.; Gautam, H.; Das, H. R. *Glycoconj J* **2002**, *19*, 395.
- (71) Evrard, B.; Balestrino, D.; Dosgilbert, A.; Bouya-Gachancard, J. L.; Charbonnel, N.; Forestier, C.; Tridon, A. *Infect Immun* **2009**.
- (72) Rioux, S.; Begin, C.; Dubreuil, J. D.; Jacques, M. *Curr Microbiol* **1997**, *35*, 139.
- (73) Kim, H.; Park, B.; Kim, J.; Kim, S.; Lee, J.; Oh, S. *Cell* **2007**.
- (74) Park, B.; Song, D.; Kim, H.; Choi, B.; Lee, H.; Lee, J. *Nature* **2009**.

## Bibliography

- (75) Henricson, B. E.; Manthey, C. L.; Perera, P. Y.; Hamilton, T. A.; Vogel, S. N. *Infect Immun* **1993**, *61*, 2325.
- (76) Hagen, S. R.; Thompson, J. D.; Snyder, D. S.; Myers, K. R. *J Chromatogr A* **1997**, *767*, 53.
- (77) Galanos, C.; Luderitz, O.; Freudenberg, M.; Brade, L.; Schade, U.; Rietschel, E. T.; Kusumoto, S.; Shiba, T. *Eur J Biochem* **1986**, *160*, 55.
- (78) Wollenweber, H. W.; Broady, K. W.; Luderitz, O.; Rietschel, E. T. *Eur J Biochem* **1982**, *124*, 191.
- (79) Dawson, J. H. *Science* **1988**, *240*, 433.
- (80) Pfeifer, K.; Kim, K. S.; Kogan, S.; Guarente, L. *Cell* **1989**, *56*, 291.
- (81) Lathrop, J. T.; Timko, M. P. *Science* **1993**, *259*, 522.
- (82) Letarte, P. B.; Lieberman, K.; Nagatani, K.; Haworth, R. A.; Odell, G. B.; Duff, T. A. *J Neurosurg* **1993**, *79*, 252.
- (83) Nath, K. A.; Shah, V.; Haggard, J. J.; Croatt, A. J.; Smith, L. A.; Hebbel, R. P.; Katusic, Z. S. *Am J Physiol Regul Integr Comp Physiol* **2000**, *279*, R1949.
- (84) Wagener, F. A.; da Silva, J. L.; Farley, T.; de Witte, T.; Kappas, A.; Abraham, N. G. *J Pharmacol Exp Ther* **1999**, *291*, 416.
- (85) Figueiredo, R. T.; Fernandez, P. L.; Mourao-Sa, D. S.; Porto, B. N.; Dutra, F. F.; Alves, L. S.; Oliveira, M. F.; Oliveira, P. L.; Graca-Souza, A. V.; Bozza, M. T. *J Biol Chem* **2007**, *282*, 20221.
- (86) Shiozaki, M.; Doi, H.; Tanaka, D.; Shimozato, T. *Tetrahedron* **2006**.

## Bibliography

- (87) Shiozaki, M.; Iwano, Y.; Doi, H.; Tanaka, D.; Shimozato, T. *Carbohydrate Research* **2006**.
- (88) Burns, M. R.; Jenkins, S. A.; Kimbrell, M. R.; Balakrishna, R.; Nguyen, T. B.; Abbo, B. G.; David, S. A. *J Med Chem* **2007**, *50*, 877.
- (89) Ii, M.; Matsunaga, N.; Hazeki, K.; Nakamura, K. *Molecular Pharmacology* **2006**.
- (90) Peri, F.; Marinzi, C.; Barath, M.; Granucci, F.; Urbano, M. *Bioorganic & Medicinal Chemistry* **2006**.
- (91) Peri, F.; Granucci, F.; Costa, B.; Zanoni, I.; Marinzi, C. *ANGEWANDTE CHEMIE* **2007**.
- (92) Bettoni, I.; Comelli, F.; Rossini, C.; Granucci, F.; Giagnoni, G.; Peri, F.; Costa, B. *Glia* **2008**, *56*, 1312.
- (93) Peri, F.; Granucci, F.; Costa, B.; Zanoni, I.; Marinzi, C.; Nicotra, F. *Angew Chem Int Ed Engl* **2007**, *46*, 3308.
- (94) Piazza, M.; Rossini, C.; Della Fiorentina, S.; Pozzi, C.; Comelli, F.; Bettoni, I.; Fusi, P.; Costa, B.; Peri, F. *J Med Chem* **2009**, *52*, 1209.
- (95) Mancek-Keber, M.; Jerala, R. *The FASEB Journal* **2006**, *20*, 1836.
- (96) Jerala, R. *International Journal of Medical Microbiology* **2007**.
- (97) Albright, S.; Chen, B.; Holbrook, K.; Jain, N. *Biochemical and Biophysical Research Communications* **2008**.
- (98) Mueller, M.; Lindner, B.; Kusumoto, S.; Fukase, K.; Schromm, A. B.; Seydel, U. *J Biol Chem* **2004**, *279*, 26307.

## Bibliography

- (99) Prohinar, P.; Re, F.; Widstrom, R.; Zhang, D.; Teghanemt, A.; Weiss, J. P.; Gioannini, T. L. *J Biol Chem* **2007**, *282*, 1010.
- (100) Teghanemt, A.; Prohinar, P.; Gioannini, T.; Weiss, J. *Journal of Biological Chemistry* **2007**.
- (101) Gioannini, T.; Teghanemt, A.; Zarembek, K.; Weiss, J. *Journal of Endotoxin Research* **2003**.
- (102) Gioannini, T.; Teghanemt, A.; Zhang, D.; Levis, E. *Journal of Endotoxin Research* **2005**.
- (103) Muller, M.; Scheel, O.; Lindner, B.; Gutschmann, T. *Journal of Endotoxin Research* **2003**.
- (104) Prospero, D.; Polito, L.; Morasso, C.; Monti, D. *Mixed Metal Nanomaterials* **2009**.
- (105) Cui, Z.; Shi, K.; Cui, Y.; Binks, B. *Colloids and Surfaces A: Physicochemical and ...* **2008**.



## Table of Contents

<b>Introduction 1</b> .....	<b>1</b>
<b>Innate immunity 1.1</b> .....	<b>1</b>
<b>Inflammation 1.2</b> .....	<b>2</b>
<b>Receptors 1.3</b> .....	<b>5</b>
TLRs 1.3.1.....	9
TLR1, TLR2, and TLR6 1.3.1.1 .....	11
TLR3 1.3.1.2.....	13
TLR5 1.3.1.3.....	14
TLR7 and TLR8 1.3.1.4 .....	15
TLR9 1.3.1.5.....	16
TLR11 1.3.1.6.....	17
TLR4 1.3.1.7.....	17
LBP 1.3.1.7.1.....	18
CD14 1.3.1.7.2.....	18
MD2 1.3.1.7.3 .....	24
TLR4 1.3.1.7.4.....	29
<b>TLR4 ligands 1.4</b> .....	<b>32</b>
Natural ligands 1.4.1 .....	32
LPS 1.4.1.1 .....	32
Heme 1.4.1.2.....	42
Synthetic ligands 1.4.2.....	44
Eritoran 1.4.2.1 .....	45
Polycationic sulfonamides 1.4.2.2 .....	48
TAK-242 1.4.2.3 .....	49
Monomeric antagonists 1.4.2.4.....	50

Table of contents

<b>Materials and methods 2</b> .....	<b>53</b>
<b>Introduction to materials and methods section 2.1</b> .....	<b>53</b>
<b>Chemical section 2.2</b> .....	<b>54</b>
General section 2.2.1 .....	54
Antagonists synthesis 2.2.2.....	55
Synthetic pathway of compound 7 2.2.2.1.....	55
Synthesis pathway of compounds 1, 2, 5, 6 2.2.2.2.....	63
Agonist synthesis 2.2.3.....	81
Hydrophobic nanoparticles coating 2.2.4.....	90
<b>Biology section 2.3</b> .....	<b>90</b>
<b>Results and discussion 3</b> .....	<b>100</b>
<b>Library development 3.1</b> .....	<b>100</b>
Inhibition of LPS-dependent TLR4 activation 3.1.1 .....	101
Discussion 3.1.2.....	111
<b>Specific interaction between synthetic ligands and CD14 3.2</b> .	<b>112</b>
Biochemical characterization of synthetic ligands with CD14 3.2.1	
.....	113
Discussion 3.2.2.....	132
<b>A synthetic TLR-4 active glycolipid disulfate targets the human MD-2 receptor 3.3</b> .....	<b>135</b>
Cellular and biochemical characterization of GD1 interaction with hMD2 3.3.1.....	138
Discussion 3.3.2.....	149
<b>Heme and a metabolic derivative, coproheme, modulate the TLR4 pathway differently through different molecular targets 3.4</b> .....	<b>149</b>

## Table of contents

Biochemical and cellular characterization of heme and coproheme effects on TLR4 receptor complex 3.4.1 .....	150
Discussion 3.4.2.....	160
<b>Synthetic endotoxin aggregates for the study of TLR4 activation mechanisms 3.5.....</b>	<b>161</b>
Development of a protocol for synthetic endotoxin aggregates production 3.5.1 .....	162
Discussion 3.5.2.....	170
<b>Conclusion and future perspectives 4.....</b>	<b>171</b>
<b>Conclusions 4.1 .....</b>	<b>171</b>
<b>Future perspectives 4.2 .....</b>	<b>173</b>

## RINGRAZIAMENTI

Mihaela. Nessuno ci prepara a incontrare persone come te, sarebbe banale riempirti di complimenti e ripeterti quanto sei stupenda. Vorrei solo poterti ricoprire di sguardi e abbracci per sempre. Non so' perche' tu mi abbia sposato ma sono sicuro che e' stato il regalo piu' emozionante e meraviglioso che tu potessi farmi. Passare ogni giorno con te mi rende semplicemente felice.

Vanna e Piero. Piu' passano gli anni e piu' capisco quanto sono stato fortunato, credo che avrei fatto davvero poco senza di voi e forse non sono mai riuscito a dirvi che vi voglio bene.

Teresa e Tino. Cosa dire, siete speciali.

Mari e Segra. Vi associo nel ringraziarvi perche' entrambi siete importanti. Ma soprattutto non saprei pensare a due amici migliori: mi avete fatto ridere (soprattutto), arrabbiare (pochissimo) e mi avete insegnato moltissimo.

Marco. L'incontro migliore che si possa fare, ovunque e sempre.

Nella. Beh, non potevo pensare a una persona migliore da avere vicino in questi tre anni di dottorato. Grazie anche solo perche' mi sopporti.

Theresa and Jerry. Somebody said that she was searching for a mentor and she found a family, I think for me it is the same . I have not enough words to tell you everything, so just imagine.

Clara. Nonostante tu sia una delle persone piu' strane che si possano incontrare: "e' stato un piacere, torna presto a trovarci"

Anna. Grazie per le risate e l'aiuto, spesso sei un vero esempio (spesso, non sempre)

Elena, Tato e tutti i bioinfo. Rallegrereste la giornata di un morto. A me sembra un complimento.

Athmane. In a place where I was a foreigner you was like a (big....older....old) brother for me.

Tommi and Polona. Thank you so much for everything. I think meeting you was a true luck.

Jamie&Justin. You have to write a book: "Ten hints to be like us" (probably in a better English). I'll buy one for sure.

Ramona. Simply a good person. I like that.

Keri, Greg, Sonya, DeSheng. Thank you for being you.

Maya, Laura, Laura, Valentina e tutte le persone che, meglio o peggio, ho conosciuto durante questi tre anni. Spero di essere riuscito a rubare qualcosa a tutti voi, ho passato dei bellissimi momento con tutti, grazie.

Francesco. Avrei dovuto apprezzarti di piu' prima. Sei una strana miniera piena di sorprese.

Mihaela. La prima e l'ultima perche' sei per per me quello che c'e' tra l'inizio e la fine.